UNIVERSITY OF CALIFORNIA,
IRVINE

Ultra–Faint Dwarf Galaxies:
Investigating the Evolution of Our Universe & Those Who Study It

DISSERTATION

submitted in partial satisfaction of the requirements
for the degree of

DOCTOR OF PHILOSOPHY

in Physics

by

Maria Kathleen Rodriguez Wimberly

Dissertation Committee:
Professor Michael Cooper, Chair
Professor James Bullock
Professor Manoj Kaplinghat

2022

DEDICATION

To my hubby,
kris.w
You've waited a long time for this.
(No, you're not allowed to retire yet.)

TABLE OF CONTENTS

LIST OF FIGURES

LIST OF TABLES

ACKNOWLEDGMENTS

Foremost I want to express endless gratitude to my hubby for truly being an equal partner — for all the nights you stayed up working alongside me, for all the dishes you washed, coffees you made, babies you bathed and countless questions you answered. Thank you for being the best career coach, editor and comic relief. I am excited for the decades we will spend making one another laugh as Mr. & Dr. Wimberly.

I cannot thank my advisor, Mike Cooper, enough for first off selecting to be my Cal–Bridge UC Mentor and now for the immense support and faith in the probably too many things I attempted to accomplish during these past 7 years. Thank you for guiding me through science and career opportunities, and for immensely boosting my confidence through your belief in me.

To my baby girls — I am grateful to Zion Khamil for making my working mom dreams come true and for doing so in the cutest, sweetest way possible and for her inexplicalbe ability to take away all my daily stressors with one perfect toddler giggle. Qora Karmen Ryanne, my little pandemic–thesis baby beast, thank you for forcing me to slow down, focus on our health and for being such a good snuggler especially when I am stressed.

I would like to thank my committee members, James Bullock and Manoj Kaplinghat, for their great support and continued interest in my success during my graduate career. I would also like to thank Alex Rudolph for having nominated me to join the Astronomical Society of the Pacific's Board, for hiring me as Cal–Bridge's Director of Peer Mentorship and for being such a supportive mentor. Additionally, I thank my co–authors not listed above for immensely contributing to this work including Sean Fillingham, Mike Boylan–Kolchin, Shea Garrison–Kimmel, Devontae Baxter, Alex Ji, Laura Sales, Josh Simon, Carol Hood, Rachel Scherr, and Chris Pfund. I thank Tyler Kelley, Dan Weisz, Mary Jenkins, Alex Riley, Marcel Pawlowski, Dan Kelson, Franklin Dollar, Mu–Chun Chen and Steph Sallum for helpful discussions regarding these projects. Thank you to my fellow astro–moms who have supported my journey — Aomawa Shields, Vivian U, Laura Tucker and Stacy Copp. I would also like to thank my peers (i.e. friends) who have been so wonderful, supportive and collaborative, especially Arianna Long, Francisco Mercado, Tae Baxter, Stephanie Stawinski, Anna Yu, Sal Fu, Ivanna Escala and Kaley Brauer.

Lastly, thank you to all 5 of my sisters, my mom and dad and the $\sim$ 100 other wonderful folk I consider my immediate family for being my motivation to fight for my passion, happiness and humility. Your endless love and support and genuine curiosity about space continually inspire me to work hard and try to spread this nerdy joy.

A portion of this dissertation has been published in the Oxford University Press. Specifically Chapter 2 was published in the Monthly Notces of the Royal Astronomical Society (MNRAS) 483, 3 (Rodriguez Wimberly et al., 2019(Chapter 3 has been submitted to MNRAS and is under review at the time of this submission with publication expected in mid–2022. This work was supported in part by NSF grants AST–1518257, AST–1518291, AST–1517226, AST–1910346, and AST–1815475. Additional support was provided to MKRW's co–authors from NSF CAREER grants AST–1752913, and 1945310, NASA grants ATP 80NSSC20K0566, NNX17AG29G,

GO–12914, AR–13888, AR–13896, GO–14191, AR–14282, AR–14289, AR–14554, and AR–15006 from the Space Telescope Science Institute, which is operated by the Association of Universities for Research in Astronomy, Inc., under NASA contract NAS 5–26555. Co–author support was also provided from HST–AR–15006, HST–AR–15809, HST–GO–15658, HST–GO–15901, HST–GO–15902, HST–AR–16159, and HST–GO–16226 from the Space Telescope Science Institute, which is operated by AURA, Inc., under NASA contract NAS5–26555. MKRW acknowledges support from the National Science Foundation Graduate Research Fellowship. This material is based upon work supported by the National Science Foundation Graduate Research Fellowship Program under Grant No. DGE–1321846. This research also utilized `astropy`, a community–developed core Python package for Astronomy [11, 10]. Additionally, the Python packages `NumPy` [102], `iPython` [206], `SciPy` [123], and `matplotlib` [107] and scikit–learn [205] were utilized for the majority of our data analysis and presentation. This work has made use of data from the European Space Agency (ESA) mission *Gaia* (`https://www.cosmos.esa.int/gaia`), processed by the *Gaia* Data Processing and Analysis Consortium (DPAC, `https://www.cosmos.esa.int/web/gaia/dpac/consortium`). Funding for the DPAC has been provided by national institutions, in particular the institutions participating in the *Gaia* Multilateral Agreement.

CURRICULUM VITAE

Maria Kathleen Rodriguez Wimberly

mkrodriguezwimberly.github.io
katy.r.wimberly@gmail.edu
ORCID: 0000–0003–1848–5571
Twitter: @astronomouse_

EDUCATION

Ph.D. Candidate Physics & Astronomy — January 2022
University of California, Irvine (UCI)
Thesis Advisor: Prof. Michael Cooper

M.S. Physics — June 2019
University of California, Irvine (UCI)
GPA: 3.34 out of possible 4.00

M.S. Physics — May 2016
Transfered to PhD Program
California State University, Long Beach (CSULB)
GPA: 4.00 out of possible 4.00

B.S. Physics — May 2015
California State University, Long Beach (CSULB)
Minor: Math
Overall GPA: 3.15 out of possible 4.00
Major GPA: 3.20 out of possible 4.00

A.A. — June 2009
Mount San Antonio College, Walnut, CA
Majors: Fine Arts, Natural Sciences & Math, Social & Behavioral Sciences
GPA: 3.32 out of possible 4.00

PUBLICATIONS

Sizing from the Smallest Scales: *The Mass of the Milky Way*
Rodriguez Wimberly, M.K., et al. 2021, submitted to MNRAS, (arXiv: 2109.00633)

Characterizing the Infall Times and Quenching Timescales of the Milky Way Satellites with Gaia Proper Motions
Fillingham, S.P. **et al.** 2019, MNRAS, under review (arXiv: 1906..04180)

Suppressing Star Formation on the Smallest Scales: *What Role Does Environment Play*?
Rodriguez Wimberly, M.K., et al. 2019, MNRAS, 483, 4031

SETI Observations of Exoplanets with the Allen Telescope Array
Harp, G.R., **et al.** 2016, AJ, 152.6 (2016b): 181

HONORS, AWARDS, PRIZES

NSF MPS Ascend Postdoctoral Fellow	2022 – 2024
Eugene Cota–Robles Fellow	2016 – 2021
AAS National Osterbrock Fellow	2020 – 2021
NSF Graduate Research Fellow	2016 – 2021
UCI Latino Excellence & Achievement Award	2020
UCI Physics & Astronomy Department Award for Outstanding Contributions	2019
UCI Graduate Division Tom Angell Mentor Fellowship	2019
CSU–UC Cal–Bridge Scholar	2014 – 2017
Doctoral Diversity Initiative Fellow	2016
Diversity Recruitment Fellowship	2016
Nevin Graduate Endowment Fellowship	2016
LSAMP PROUD Scholar Award	2015
CSULB Physical Sciences and Mathematics Scholar	2014
CSULB Physics Department Scholarship	2014
Louis Stokes' Alliance for Minority Participation Academic Year Fellow	2013 – 2014
CSULB Physics Department Scholarship	2013

OBSERVING EXPERIENCE

Keck Observatory
DEIMOS: 15 nights

UCO/Lick Observatory Robert P. Kraft Observational Astronomy Workshop
October 2015, Lick Observatory, Mt. Hamilton, CA

TEACHING EXPERIENCE

ASTR100L: Intro to Astronomy Lab
(Stand Alone) Course Instructor, CSULB Fall 2015 & Spring 2016

TECHNICAL SKILLS

Python IRAF MySQL LaTex Aladin DS9 Unix Fortran95
Certified LabVIEW Associate Developer Mathematica Atomic & Magnetic Force Microscopy

INVITED TALKS

Ultra Faint Dwarf Galaxies: October 2021
Quenching, Predictions & Evolutionary History
Cosmology and Astronomy Seminar at UC Daviss

Ultra Faint Dwarf Galaxies: October 2021
Quenching, Predictions & Evolutionary History
CCAPP Little Galaxies Meeting at The Ohio State Universitys

Ultra Faint Dwarf Galaxies: September 2021
Quenching, Predictions & Evolutionary History
Lunchtime Seminar at Carnegie Observatoriess

Ultra Faint Dwarf Galaxies: February 2020
Smallest Scales Quenching & Predictions
Lunchtime Seminar at Carnegie Observatoriess

Astronomical Society of the Pacific 130*th Annual Meeting* September 2018
Plenary Speaker on Imposter Syndrome
Plenary Session — Barriers to Equity, Inclusion, and Diversity in Astronomy

RECENT CONTRIBUTED PRESENTATIONS

Studying the Smallest Satellites: October 2020
Star Formation Quenching & The Milky Way's Halo Mass
Talk Given at Galaxy Formation & Evolution
in the Era of the Roman Space Telescopes

Studying the Small Scales: September 2020
Star Formation Quenching & The Milky Way's Halo Mass
Poster Presentation at the Space Telescope Science Institute's
2020 Spring Symposium — The Local Group: Assembly & Evolutions

Ultra Faint Dwarf Galaxies: September 2020
Smallest Scales Quenching & Predictions
Science by Diverse Scientists: A Cal–Bridge Physics & Astronomy Seminar

HIGHLIGHTED SERVICE ACTIVITIES

Cal–Bridge Mentorship Committee Co–Chair 2020 – Current

Cal–Bridge Director of Peer Mentoring Program 2019 – Current
Creator & Organizer of Peer Mentoring Program for Cal–Bridge Scholars

Astronomical Society of the Pacific Board of Directors Member 2019 – Current
Diversity Committee Co–Chair

APS–IDEA Network: *UCI Team Member* 2020 – 2021
Network creating equitable, inclusive and diverse communities

UCI Physics & Astronomy Community Excellence 2018 – 2020
Co–Creator of Peer Mentoring Programs for 1st Year Physics Graduate Student
Group Sessions & 1–on–1 Mentoring with Trained Peer Mentors
Our Website: `uci-pace.github.io`

WORK EXPERIENCE

UCI Competitive Edge Program 2017 & 2018
Graduate Student Peer Mentor

UCI Competitive Edge Program 2016
Graduate Student Researcher

CSLUB Physics Dept. 2015 – 2016
Teaching Assistant — Astronomy Lab Instructor

UCI Summer Internship Program 2015
Cal–Bridge Student Researcher

US Army Reserves 2003–2015
Staff Sergeant, Saxophonist, Human Resources Manager

CSLUB Physics Dept. 2013 – 2015
Learning Assistant

SETI Institute REU 2014
CAMPARE Student Researcher

LSAMP Academic Year Fellowship 2013 – 2014
Student Researcher

University of Texas, Brownsville Physics REU 2012
Student Researcher

CSULB Physics Dept. 2012
Winter Research Student Researcher

Dept. of Defense Army Civilian 2009 – 2012
300th Army Band Unit Administrator

Anbeten Productions 2006 – 2009
Design Assistant/Consultant

Disneyland Attractions Dept. 2007 – 2009
Innoventions Supervisor, Project Lead & Performer

Mt. San Antonio College Theatre Dept. 2006
Asst. Costumer

Disneyland Entertainment Dept. 2003 – 2006
Costumer & Atmosphere Character

DIVERSITY, OUTREACH, & COMMUNITY

DreamWakers Speaker 2017 – Current
Virtual chats with grade school science classrooms.

UCI Competitive Edge Workshop Leader 2020
Created and Lead Workshop on Impostor Phenomena

APS Conference for Undergraduate Women in Physics at UCI 2020
Local Organizing Committee
Assisted in proposal, promotion, recruitment, and programming
Co–Leader of ASCEND@UCI Mini Conference
Our Website: `https://sites.uci.edu/cuwip2020/ascend-at-uci/`

Astronomical Society of the Pacific Junior Board Fellow 2017 – 2019
First ever Junior Board Fellow on the ASP Board of Directors
Serving on the Diversity Committee

Bruin Brains Research Conference — Keynote Speaker 2019
TRIO Programming at Salt Lake Community College, UT

Expand Your Horizons Event — Keynote Speaker 2019
Annual Workshop for 6–10th Grade Girls Interested in STEM
Salt Lake Community College, UT

UCI Physics & Astronomy Inclusive Excellence Committee 2017 – 2019
Department Committee to Improve Climate and Diversity
A Graduate Student Representative

UCI Physics & Astronomy Physics Graduate Caucus 2017 – 2019
Department Organization to Improve Graduates' Experience
Mentorship Chair— Creating and Reviving Peer Mentor Programs

UCI Physics & Astronomy Admission Task Force 2018 – 2019
Department Committee to Improve Diversity in Admissions
A Graduate Student Representative

UCI Astronomy Outreach 2016 – 2019
Telescope Volunteer for Elementary–level Classroom Night Sky Viewing Parties

Astronomy Outreach for Underrepresented Youth 2016 – 2019
K–12 Classroom Visits for underrepresented groups ranging from
ethnic minorities to Autistic and Downs Syndrome students.

Letters to a Pre–Scientist Scientist Pen Pal 2015 – 2019
Pen Pal during each Academic Year with a grade school student
interested in space science.

UCI DECADE Learning Community –Invited Workshop Leader 2018
Created and Lead Workshop on Facing Impostor Phenomena

Reclaiming STEM Science Communication Workshop — Invited Speaker 2018
Presented "Building Your Social Media Brand"

UCI Physics & Astronomy Stride! *Mentoring* 2018
Lead a Grad–Undergrad Mentoring Summer Program
Mentoring & Activities Focused on Graduate Applications & Transition

UCSC Osterbrock Sierra Conference Planning Comittee, Co–I 2017
Lead Professional Development Planning & Execution

SPS CSULB Chapter Secretary 2013 – 2015
Assist in outreach program & event planning & execution
Assist in chapter and physics department event planning and execution

CSULB Science Outreach 2013 – 2014
Volunteer for Mexican American Engineers & Scientists CSULB Chapter's
2013 & 2014 Science Extravaganzas as both small group & workshop leader

PAST CONTRIBUTED PRESENTATIONS

Ultrafaint Dwarf Galaxies: August 2019
The Suppression of Their Star Formation & Their Orbits
Talk given at GalFRESCA UCI

Suppressing Star Formation on the Smallest Scales: September 2018
What Role Does Environment Play?
Poster Presentation given at Keck Science Meeting 2018

Suppressing Star Formation on the Smallest Scales: August 2018
What Role Does Environment Play?
Talk given at UCSC Galaxy Workshop 2018, Santa Cruz

Suppressing Star Formation on the Smallest Scales: August 2017
What Role Does Environment Play?
Talk given at GalFRESCA 2017, CalTech

Constraining Quenching Timescales at $z > 1.5$ August 2016
Poster Presentation at UCI Summer Research Symposium

Constraining Quenching Timescales at $z > 1.5$ January 2016
Poster Presentation at AAS 2016 Meeting

Constraining Quenching Timescales at $z > 1.5$ October 2015
Talk given at APS Far West Meeting 2015

Quenching Time: *A study on galaxy evolution & formation.* September 2015
Talk given at Cal Poly Pomona's 2015 CAMPARE Research Symposium

Quenching Time: *A study on galaxy evolution & formation.* September 2015
Talk given at UC Irvines's 2015 Summer Research Symposium

Analysis of SETI's Radio Signal Observations & Classification Tests June 2015
Talk given at the national Astrobiology Science Conference, Chicago, IL

Surface Morphology of Ferromagnetic Nanostructures October 2014
Poster presentation given at CSULB's Student Research Symposium

Analysis of SETI's Radio Signal Observations & Classification Tests September 2014
Talk given at Cal Poly Pomona's 2014 CAMPARE Research Symposium

Analysis of SETI's Radio Signal Observations and Classification Tests August 2014
Talk given to the SETI Institute, Mountain View, CA for SETI/NSF REU

Volume Meter October 2013
Poster presentation given at CSULB's Student Research Symposium

The Variability of Vega January 2013
Poster presentation for the 2013 Conference for Undergraduate Women in Physics

The Variability of Vega August 2012
Poster presentation & talk at the University of Texas, Brownsville

ABSTRACT OF THE DISSERTATION

Ultra–Faint Dwarf Galaxies:
Investigating the Evolution of Our Universe & Those Who Study It

By

Maria Kathleen Rodriguez Wimberly

Doctor of Philosophy in Physics

University of California, Irvine, 2022

Professor Michael Cooper, Chair

The beginning of our Universe continues to elude us with many unanswered questions, some involving evolutionary histories of the most ancient galaxies — ultra–faint dwarfs (UFDs). Recent optical observation and cosmological simulation advancements have opened new opportunities to study these evolutionary histories. The predominantly ancient stellar populations observed in UFDs suggest their star formation was suppressed by reionization. However, most of the well–studied UFDs are within the central half of the Milky Way (MW) dark matter halo, such that they are consistent with an early accreted population and potentially quenched via environmental processes. To study this possibility, we utilize *N*–body cosmological simulations, the ELVIS suite, to constrain the distribution of infall times for subhalos likely to host UFDs. For the MW's UFDs, we find that environment is highly unlikely to play a dominant role in quenching their star formation. Further in UFD exploration, we use this population as a tool to constrain a fundamental Galactic property — dark matter halo mass. As the MW and its satellite system become more entrenched in near–field cosmology, the need for an accurate estimate of the halo mass is increasingly critical. Using new 6D phase–space information for the MW satellite population calculated from *Gaia*'s early third data release of stellar proper motions to compare to subhalo properties drawn from the Phat ELVIS simulations, we constrain the MW dark matter halo mass to be ~ 1–1.2×10^{12} $M_\odot$. This preferred dark matter halo mass for the MW is largely insensitive to the exclusion of systems associated

with the Large Magellanic Cloud (LMC), changes in galaxy formation thresholds, and variations in observational completeness. Turning focus inward, current work in progress analyzes, for the first time, chemical abundances in the UFD LMC satellite, Hydrus I. Through abundance trends, we will begin to explore how large scale environments, such as the LMC's dark matter halo, have impacted UFD evolutionary histories. These mostly yet–to–be–explored evolutionary histories of UFD satellites help to refine which are pristine relics of the first galaxies and can serve as the most optimal cosmic sites to search for signatures of the first stars ever formed.

Alongside astrophysics research I have established and led Peer Mentorship programming within my graduate department and a state–wide bridge scholarship program, Cal–Bridge. These peer mentorship activities provide students space to create community around equity through normalizing common struggles, individual holistic success, and determining how to improve their academic experience. While peer mentorship programs are often unsupported within STEM, there is a growing body of research showing how impact–full these programs are. Within my programs, evaluation results show peer mentorship increased growth mindset and recognition of mentor network importance, and has clarified career paths. This type of programming creates leadership opportunities and assists participants in defining and raising confidence in their academic identities. Peer Mentorship empowers participants to have career autonomy while creating supportive, inclusive and equitable communities.

Chapter 1

Introduction

1.1 Preface

Throughout my graduate career I have had the fortunate opportunity to write scientific communication style articles for the Astronomical Society of the Pacific's Mercury Magazine [4]. These articles present my research and related astrophysics topics in a manner where any reader interested in astronomy can enjoy the content. While Chapters 2 — 4 are written for astronomers specifically, this introductory chapter is written for any astronomy fan.

1.2 Historical Background

Only 100 years ago (April 26, 1920) Harlow Shapely, Harvard astronomer, and Herber Curtis, Lick Observatory astronomer, argued during the Great Debate whether the Milky Way (MW) was just one of many galaxies or the entire Universe [1]. Many say Shapely, who believed the MW to be the whole Universe won. Though shortly after the debate, Edwin Hubble, Mt. Wilson Observatory astronomer, studied Cepheid variable stars to prove Curtis' main argument to be correct — there

are in fact many many galaxies other than the Milky Way [106]. Since then with telescopes such as the Hubble Space Telescope, we have discovered countless more galaxies. A few tens of these galaxies are close enough to the MW that they are gravitationally bound (i.e. satellite galaxies).[1] What we use to think was a lonely corner of space, we now see as a bustling neighborhood with a diversity of satellites galaxies. Some of the MW's satellite galaxies can be found by simply looking up on a clear night in the Southern Hemisphere. The Large and Small Magellanic Clouds have been a part of human culture for centuries. In Australia, one Aboriginal belief sees the Clouds as a hungry elderly couple as a way to teach respect and sharing of food for those in need [158]. The overwhelming majority of the MW's satellites though are not cultural icons and cannot be seen with the unaided eye.

More MW satellites were not discovered until 1938 when Harlow Shapley found faint and wide spread stellar associations in photographic plates which we now know are the Sculptor and Fornax dwarf spheroidal satellite galaxies [232, 233]. Since then we have discovered over 50 other MW satellite galaxies [235] — a few massive satellites galaxies (i.e. the Large and Small Magellanic Clouds); faint dwarf spheroidal galaxies, such as Sculptor and Fornax; and the tiniest galaxies ever found. These tiniest galaxies (i.e. ultra–faint dwarf galaxies, UFDs) were discovered in the Sloan Digital Sky Survey's (SDSS) vast amount of data spurring a digital revolution [279, 280]. Digital surveys such as SDSS, the Dark Energy Survey and the upcoming Legacy Survey of Space and Time at the Vera Rubin Observatory, automatically cover huge areas of the night sky capturing every photon within their telescope's power. The resulting data can then be searched through using big data and machine learning techniques. Since 2005, discovering UFDs through digital surveys has more than quadrupled our satellite count!

So, out of the millions of galaxies seen, we categorize less than 100 as ultra–faint dwarf galaxies. Why? Well, their name says it all — they are ultra–hard to see aka faint. They are vastly different from our own galaxy — their mass compared to the MW's is the same magnitude difference as

[1] This is the same idea as the Moon being gravitationally bound to the Earth but instead of two rocks orbiting each other, we're talking about entire galaxies dancing around one another!

the Earth compared to a large marble; the MW has spiral arms, whereas ultra–faints are irregularly shaped; and our Galaxy is continuing to birth new stars, while these dwarf galaxies generally have only ancient stars and are unable to make new ones.

1.3 Investigating Star Formation Suppression Timescales

Despite the obvious differences between the MW and UFDs, there's a lot we can learn about the MW's fate from these little galactic neighbors. The theory of galaxy evolution tells us how galaxies live their lives from their formation through what happens when they stop birthing new stars. Currently, we are trying to understand the mechanisms behind galactic evolution and in particular how they stop the process of creating new stars and changes that are inflicted upon a smaller galaxy as it moves through space interacting with larger galaxies.

When you think of an image of a galaxy, do you see a bright blue swirly mess of stars and dust, maybe even with some luminous pink spots mixed in? This vibrant chaotic picture is the prevailing image of a galaxy. Though astronomers know that through time there are increasingly less of these bright actively star forming galaxies! One of the monumental questions in the study of galaxy evolution is why is there this build up of passive, no–longer–star–forming galaxies over cosmic time? Maybe more pressing — is this our fate, too?

A perfect place to start searching for answers is our own cosmic backyard — the Local Group of galaxies. This Local Group consists of us, the Milky Way, and the "near–by" large Andromeda galaxy, plus all the smaller satellite galaxies of these two big galaxies and the field galaxies which hang out in between. In fact astronomers believe that most galaxies are a satellite to some larger galaxy or group of galaxies. Now, there does exist a minority population of galaxies doing a solo dance, these are the field galaxies. Field galaxies are smaller than the MW and outside our sphere

of gravitational influence.[2]

An intriguing distinction between the MW satellites and field galaxies is the fact that our satellites are of the dull, passive, no–long–star–forming variety while the solo field galaxies are vibrant and active. Is something about the MW causing this? Are we contributing to the build up of passive galaxies over cosmic time? Are we doomed to the same fate? Ya know, we are on a merger course with the more massive Andromeda galaxy! Fortunately, the study of why and how long it takes galaxies to stop forming new stars is an active area of astrophysical research. Investigating timescales is a way to categorize the mechanisms causing star formation to end.

These star formation quenching timescales also illuminate the mechanisms not responsible a galaxy's suppressed star formation! For instance, as will be discussed in Chapter 2, even though UFDs have been satellites of the MW for a considerable amount of time, they have not been satellites long enough for the MW to have suppressed their star formation leaving only the very ancient stars we observe today. This lends itself to the idea that these tiny galaxies are essentially cosmic artifacts that may have formed only 400 million years after the Big Bang. We currently measure the age of our universe to be 13.8 billion years old; so, 400 million years compared to the age of the universe is like 42 minutes compared to 24 hours. In this tiny blip of time after the Big Bang, the universe entered what's called the Reionization Age. This is when the very first stars and galaxies began to form. We think ultra–faint dwarfs may be the ancient fossils of the first galaxies to emerge from the Reionization Age.

This very beginning of our Universe continues to be largely elusive — even with our observational probes and the most state–of–the–art cosmological simulations, we are left with many unanswered questions on how our Universe came to be. From the challenge of understanding the early Universe, a new astronomical sub–field was born just two decades ago — near–field cosmology [82]. In this discipline, these near–by relics of the first stars and galaxies are studied to learn about the events of the early Universe such as how elements heavier than hydrogen were polluted throughout the

[2]One might even say we are social distancing with the field galaxies.

cosmos.

1.4 Determining Dark Matter Halo Mass

From our cosmically tiny blue marble of a planet, the Milky Way appears merely as a bright strip of stars set against the darker night sky. Every human culture on Earth has seen, known, and wondered about this pathway in the sky. Some cultures, such as the Cherokee, see the MW's band as a pathway to the afterlife while others, such as the Lakota, know it to be "The Place of Spirits" or Wanagi Yata [5]. For many modern astronomers, we see it as our mysterious home — a vast astronomical laboratory where we can take incredibly detailed observations across the full range of visible light and the rest of the electromagnetic spectrum. We now know that the largest and most massive component of the Milky Way is the dark matter halo we reside in. This massive halo can be thought of as a cloud of invisible material, called "dark matter," that gravitationally keeps the visible parts of our galaxy at the cloud's center and attracts nearby smaller galaxies into it — all via gravity.

Mass is truly a fundamental property of physical objects. Think of some of the most famous physics equations. Did you perhaps recall $F = ma$ or $e = mc^2$? Many of the fundamental equations rely on knowing the mass of the object in question. So, knowing precisely the mass of the Milky Way in its various components — such as dark matter content, stellar content, gas and dust content — allows us to learn more about the universe and how nature itself works! See our cosmic backyard, consisting primarily of the MW's satellite galaxies, is a rich playground in which to study many aspects of astrophysics largely due to our ability to conduct detailed observations of these nearest objects.

There are actually many ways to determine the mass of a galaxy. Often astronomers measure mass by observing then extrapolating the number of stars in a galaxy and the chemical make up of those

stars. This is a common way to 'measure' the stellar mass of a galaxy. Since we do not directly observe dark matter, we cannot take the same approach to determining the dark matter mass of a galaxy. Dark matter mass is often inferred through the distribution of rotational stellar velocities in a galaxy. See if galaxies were not surrounded by a dark matter halo, the rotational velocity of the stars in the outskirts of the galaxy would be much lower than the stars closer in to the center. What we see when looking at these rotational velocity curves for galaxies is that the stars in the outskirts actually have similar velocities as those centric stars! This increased velocity is due to an invisible mass we call dark matter! Now this is a great way to 'measure' dark matter mass when we can see an entire galaxy, but how is it possible to do this when you're sitting in the galaxy?!

Similarly to measuring stellar rotational velocities to then infer dark matter mass of an extragalactic galaxy, the MW's dark matter mass can be worked out from calculating the escape speed from counter–rotating stars in the Galaxy's outer halo [178]. Two other common, and recently popular, methods are to use a mathematical dark matter mass estimator equation involving the density, potential and anisotropy (directional variation) of the satellites — galaxies or globular clusters — surrounding our Galaxy [267, 84] and to compare phase space distributions in simulations and semi–analytic models to observed distributions to then infer the mass [156, 45, 64]. All three of these recent works utilize the incredibly precise proper motion measurements[3] from the second data release of the revolutionary telescope, *Gaia*! This one telescope has truly revived a centurial question.

Unfortunately, the results of these investigations prove this great question is not yet answered — only the limits are further refined. Prior to the second data release of Gaia's proper motions, the limits on the Milky Way's dark matter halo's mass were 0.8–4.5 $\times 10^{12}$ M_{Sun} [124, 208].[4] These limits have been refined through the 3 methods discussed earlier over 6 investigations to [64, 267]). While these are the extremes of the 6 results, it's important to note that not all 6 masses agree with

[3]The proper motion of a star is it's actual movement through space, not just how we see it move through the sky at night.

[4]Here M_{Sun} means solar masses, which is the mass of our Sun — 2×10^{30} kg.

each other within their respective errors — aka there's still a lot of science to do! Hooray! Chapter 3 describes a method of MW dark matter halo mass investigation using the latest (the early third) data release from *Gaia* and the most advanced dark matter only MW + neighbors simulations and further constrains our dark matter mass.

1.5 Detailing Chemical Abundances

Astrophysics maybe the only field of study in the world that deals simultaneously with the largest and smallest scales known to humans — for example, this work deals with masses from one trillion times more massive than the Sun all the way down to the mass of a hydrogen atom (roughtly 1700 septillionths of a kilogram or 1.7×10^{-27} kg). Hydrogen atoms and it's slew of tiny cousins, aka the other elements, detected in stars can illuminate many cataclysmic star forming events!

The relative amount of various elements can be determined through a star's spectra. In these stellar spectra there are absorption lines — light that has been absorbed by atoms and molecules which then leaves a dark feature in the white light spectrum of the star. Each atom and molecule has specific wavelengths of light that they absorb. The length of the atom's absorption line at the various wavelengths determine the amount of that atom in the star.

From these abundances, astronomers act as cosmic slueths using theories from stellar evolution, galaxy evolution and cosmology to piece together the evolutionary history of the galaxy the star resides in. Chapter 4 does exactly this for the UFD, Hydrus I where 2 stars are examined in this preliminary report.

1.6 Peer Mentorship

Alongside exploring the evolution of our Universe, this work also investigates those who study our Universe, specifically by looking into how students from historically underrepresented groups (HU students) are impacted by participation in peer mentorship programming. Such programs are often unsupported within STEM departments — not yet at least. There is a growing body of research showing how impactful peer mentorship programs are, especially for broadening participation of HU students. As detailed in Chapter 5, this type of programming effecticaly creates community and leadership opportunities among young, diverse scientists with their own strong academic identities. Peer Mentorship specifically aids in creating a thriving equitable community through normalizing common struggles and holistic success.

Chapter 2

The Suppression of Star Formation on the Smallest Scales: What Role Does Environment Play?

2.1 Introduction

The Local Group serves as a cosmic Rosetta Stone, offering the opportunity to study galaxy formation and evolution at a level of detail not possible at cosmological distances [29]. This is especially true at the smallest galactic scales — i.e. for very low–mass galaxies or what are often referred to as ultra–faint dwarfs (UFDs). Photometric observations of UFDs in the Local Group find universally old stellar populations, such that these systems have typically ceased forming stars by $z \sim 2$ (or a lookback time of $\sim$ 10.3 Gyr) [33, 270]. The prevalence of ancient stellar components in these extremely low–mass systems is commonly interpreted as evidence of quenching via reionization, where a photoionizing background increases the cooling time for low–density gas so as to quell the fuel supply for star formation in the lowest–mass halos [e.g. 65, 212, 251].

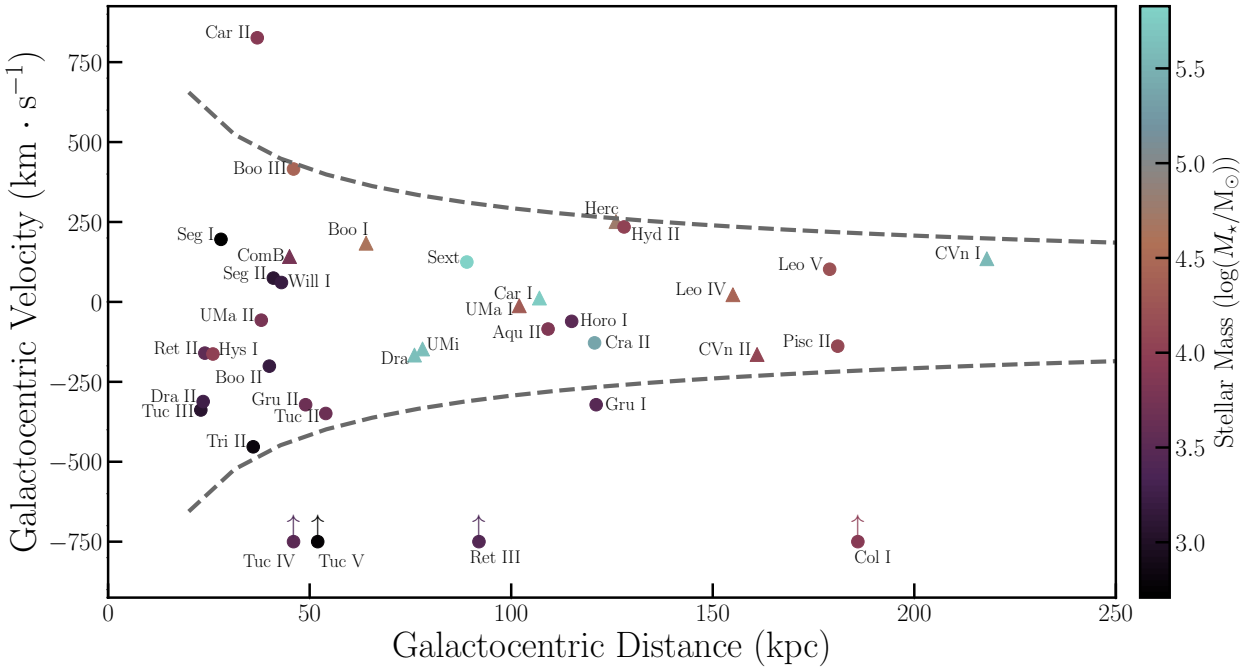

Figure 2.1: Galactocentric velocity versus distance for the sample of UFD satellites of the Milky Way. Points are color–coded according to stellar mass, assuming a V–band mass–to–light ratio of 1.2; the triangles denote those objects with a published SFH from Brown et al. 2014 [33] or Weisz et al. 2014a [270]. To account for unknown tangential motion, the observed line–of–sight velocities have been multiplied by a factor of $\sqrt{3}$. Those systems without published line–of–sight velocity measurements (Tuc IV, Tuc V, Ret III, and Col I) are plotted at $\sqrt{3} \cdot V_{\ell \mathrm{os}} = -750$ km s^{-1} with upward arrows representing the uncertainty in their $V_{\ell \mathrm{os}}$. Masses (i.e. luminosities), distances, and line–of–sight velocities for this sample are based on published values from [172], [13], [61], [146], [33], [270], [236], [239], [135], [132], [133], [134], [153], [260], [257], [40], [166], [146], [263], [143], and references therein.

While the measured star formation histories of UFDs are compatible with quenching via reionization, the most well–studied systems in the Local Group are located at relatively small galactocentric radii, which is also consistent with a population that was accreted at early cosmic time [215, 197]. As such, the old stellar populations identified in UFDs orbiting the Milky Way and M31 may instead be the result of environmental processes that suppressed star formation following infall onto the host halo. For example, recent measurements of the proper motion for the Segue I dwarf [17] suggest that it was accreted by the Milky Way halo roughly 9.4 Gyr ago [85], such that rapid environmental quenching would produce an ancient and metal–poor stellar population as observed today [81, 268]. Undoubtedly, observations of isolated UFDs (i.e. beyond the reach of environmental effects) would be an excellent way to differentiate between these two physical scenarios (quenching via reionization versus via environment). Current datasets, however, lack the depth to identify and characterize the stellar populations of UFDs in the local field.

To address the potential role of environment in quenching UFDs, given current observational datasets, we utilize a suite of *N*–body simulations to track the accretion and orbital history of the low–mass subhalos that host the UFD satellite population. In particular, we aim to quantify the likelihood that environmental effects can explain the universal ancient stellar populations in the lowest–mass galaxies. In §2.2, we provide a brief census of the UFD satellite population of the Milky Way along with a description of our simulation dataset and our primary analysis methods. In §3.4, we present our results regarding the role of environment in quenching UFDs. Finally, we conclude with a brief discussion and summary of our work in §2.4 and §2.5, respectively.

2.2 Data

2.2.1 UFD Galaxy Sample

Since the discovery of the first ultra–faint dwarfs using photometric data from the Sloan Digital Sky Survey [SDSS, 285], a large number of UFDs have been identified as satellites of the Milky Way [e.g. 279, 280, 287, 288, 16, 13, 61]. Deep imaging of M31 has likewise uncovered a population of UFDs orbiting M31, with similarly old stellar populations [e.g. 167, 270, 240]. Throughout this work, we focus our analysis on the ultra–faint satellite population of the Milky Way, selecting all systems with $L_V < 5 \times 10^5\ L_\odot$ ($M_V > -9.3$) as UFDs. Figure 2.1 shows the position and line–of–sight velocity of these systems relative to the Milky Way, with velocities scaled by a factor of $\sqrt{3}$ to crudely account for potential tangential motion.[1]

Of the 36 known UFD satellites of the Milky Way, there are published star–formation histories (SFHs) in the literature for 10 based on *Hubble Space Telescope* (*HST*) imaging from Brown et al. 2014 [33] or Weisz et al. 2014a [270] For all 10 of these systems, the reported mean stellar age is > 9 Gyr with 90% of the stars forming by $z \sim 2$. For the small number of objects included in both the Brown [33] or Weisz [270] samples, there is relatively good agreement between the measured SFHs. The exception is CVn II, for which Weisz et al. 2014 [270] find a tail of star formation extending to $z \sim 1$. The *HST*/WFPC2 imaging analyzed by Weisz et al. 2014, however, is shallower and covers a smaller area than the *HST*/ACS imaging utilized by Brown et al. 2014, such that greater photometric errors may be increasing the dispersion in the main sequence turn–off population and thereby yielding a broader SFH. Altogether, observations of the known UFD population orbiting the Milky Way suggest that these very low–mass systems have old stellar populations, with little star–formation activity since $z \sim 1 - 2$ [e.g. 195, 196, 56, 225, 226, 227, 32, 168, 20].

[1]This typically serves as a lower limit to the total velocity, with the recently measured motions for a subset of UFDs from Gaia Data Release 2 [234, 83] yielding higher total velocities than our $\sqrt{3}V_{los}$ estimate.

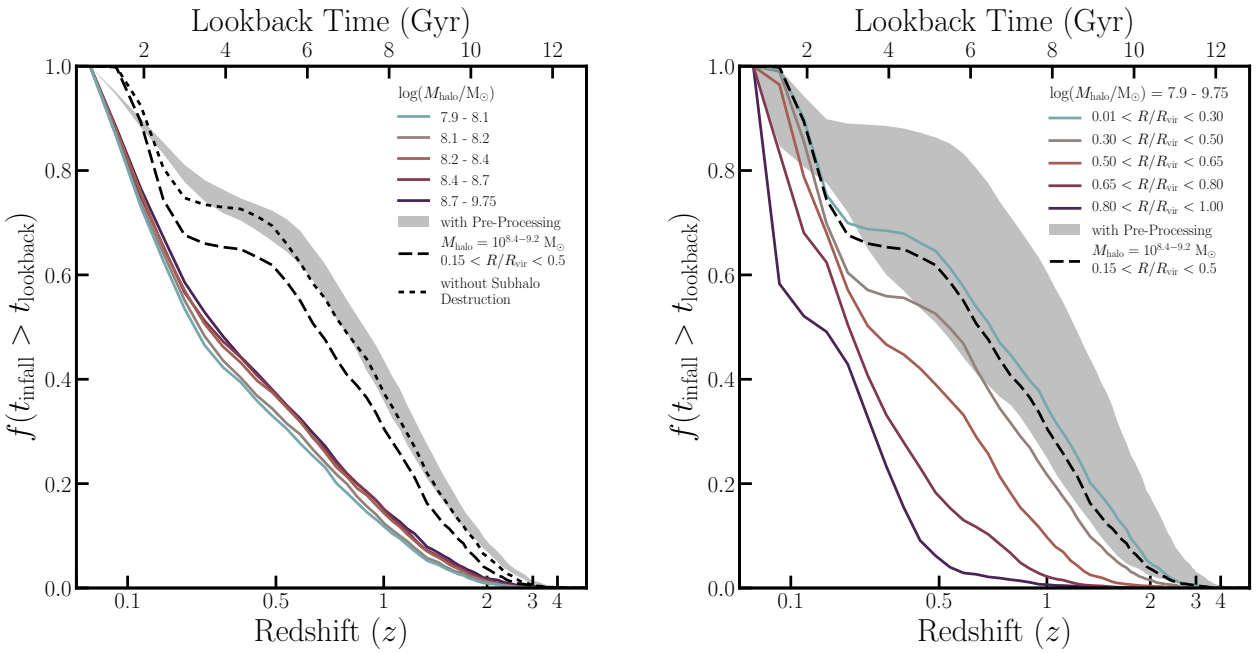

Figure 2.2: The cumulative distribution of infall times ($t_{\rm infall}$) as a function of redshift for subhalos likely to host the Milky Way UFD satellite population. In both panels, the black long–dashed line corresponds to the distribution of infall times for our fiducial selection criteria, where subhalos are restricted to $0.15 < R < 0.50\,R_{\rm vir}$ and $M_{\rm peak} = 10^{8.4-9.2}$ M$_\odot$. At *left*, we show the variation in infall times as a function of subhalo mass, for all subhalos within $R_{\rm vir}$ at $z = 0$. At *right*, we plot the infall time distribution across bins in host–centric distance for all subhalos with $M_{\rm peak} = 10^{7.9-9.75}$ M$_\odot$. Each bin in distance or mass contains an approximately equal number of subhalos ($N \sim 3050$). The dotted line illustrates the distribution of infall times for our fiducial sample without including the effects of subhalo disruption (i.e. using the original EVLIS catalogs versus the Fat ELVIS catalogs). Finally, the grey bands illustrate the corresponding distributions for infall onto a $\geq$ SMC–like host halo prior to the last infall onto a Milky Way–like host halo (see §2.2.2). While the distribution of infall times is largely independent of subhalo mass (and thus our assumed stellar mass–halo mass relation), it is strongly dependent upon host–centric (i.e. galactocentric) distance.

2.2.2 *N*–Body Cosmological Simulations

To investigate the role environmental mechanisms play in the quenching of UFDs, we utilize the Exploring the Local Volume In Simulations (ELVIS) suite of 36 high–resolution, cosmological zoom–in simulations of Milky Way–like halos [90]. Within the suite, 24 simulations are of isolated Milky Way–like halos and 12 are of Milky Way–and M31–like pairs. Each simulation occurs within a high–resolution uncontaminated volume spanning $2 - 5$ Mpc in size with a particle mass of 1.9×10^5 $M_\odot$ and a Plummer–equivalent force softening length of $\epsilon = 141$ physical parsecs. Within the high–resolution volumes, the halo catalogs are complete down to $M_{\rm halo} > 2 \times 10^7$ $M_\odot$, $V_{\rm max} > 8\,{\rm km\,s^{-1}}$, $M_{\rm peak} > 6{\times}10^7$ $M_\odot$, and $V_{\rm peak} > 12\,{\rm km\,s^{-1}}$ — thus sufficient to track the evolution of halos hosting Local Group dwarfs with stellar masses of $\sim 10^{3-5}$ $M_\odot$. ELVIS adopts a ΛCDM cosmological model based on *Wilkinson Microwave Anisotropy Probe* 7–year data [140, 147] with the following parameters: $\sigma_8 = 0.801$, $\Omega_{\rm m} = 0.266$, $\Omega_\Lambda = 0.734$, $n_{\rm s} = 0.963$, and $h = 0.71$.

As a dark matter–only simulation suite, ELVIS fails to capture the impact of the host baryonic component on the subhalo population. In short, the inclusion of a disk potential can substantially alter the subhalo distribution inside of the host virial radius by tidally disrupting subhalos [59, 30, 31, 91, 229]. This subhalo destruction preferentially occurs in objects with early infall times and/or more radial orbits. As such, the distribution of subhalo infall times for a dark matter–only simulation (such as ELVIS) will be biased towards earlier cosmic times, so as to overestimate the role of environmental mechanisms in quenching star formation at high z.

To account for the impact of the host baryonic component, following the work of [71], we implement a correction to the ELVIS subhalo population that will broadly capture the tidal effects of the host. Based on Figures 5 and A2 from [91], we model the ratio of subhalos in dark matter–only versus hydrodynamic simulations of Milky Way–like hosts as

$$N_{\rm DMO}/N_{\rm HYDRO} = 40\,e^{-22\,d_{\rm peri}/{\rm kpc}}\ ({\rm for}\ d_{\rm peri} < 50\ {\rm kpc}),$$

where $N_{\rm DMO}$ is the number of subhalos that survive to present–day in a dark matter–only simulation, $N_{\rm HYDRO}$ is the corresponding subhalo count for a hydrodynamic simulation, and $d_{\rm peri}$ is the host–centric distance at pericenter in kpc. This relationship between pericentric passage and the likelihood of subhalo disruption is supported by a larger number of dark matter–only simulations of Milky Way–like hosts, run with (and without) an evolving disk potential (Kelley et al. in prep).

To mimic the disruption of subhalos in ELVIS, we adopt $(N_{\rm DMO}/N_{\rm HYDRO})^{-1}$ as the likelihood that a subhalo survives to $z = 0$ as a function of pericentric distance; for $d_{\rm peri} \geq 50$ kpc, we assume no subhalo destruction (i.e. $N_{\rm HYDRO}/N_{\rm DMO} = 1$). Within the ELVIS halo catalogs, we then randomly destroy subhalos as a function of their pericentric distance given this probability of survival. In total, this removes approximately 25% of the subhalo population at the selected mass scale ($M_{\rm peak} = 10^{7.9-9.75}$ M$_\odot$). Throughout the remainder of this work, we refer to these modified halo populations as comprising the "Fat" ELVIS halo catalogs, given their inclusion of the destructive effects produced by the host's additional baryonic mass component. As hosts of the Milky Way's UFD population, we select subhalos from our Fat ELVIS catalogs at $z = 0$ within the host virial radius and within a mass range of $M_{\rm peak} = 10^{7.9-9.75}$ M$_\odot$, following the stellar mass–halo mass (SMHM) relation of [90]. This yields a population of 15, 269 subhalos across the 48 ELVIS host systems.

The ELVIS merger trees include 75 snapshots ranging from $z = 125$ to $z = 0$. Following [74], all halo properties are spline interpolated across the snapshots at a time resolution of 20 Myr, which enables more precise measurement of subhalo infall times and pericentric distances. To constrain the infall time ($t_{\rm infall}$) for each subhalo in our Fat ELVIS catalogs, we measure the redshift at which a subhalo was first and last accreted onto its host halo. In 51% of cases, the first infall is the only infall, such that $t_{\rm first} = t_{\rm last}$. To account for the potential role of pre–processing, we also track the first infall onto any host halo with $M_{\rm peak} \geq 10^{10.8}$ M$_\odot$ at $z = 0$. Following the SMHM relation of [90], this host selection corresponds to systems that are similar to the Small Magellanic Cloud (SMC) or more massive. In total, roughly 65% of subhalos in our chosen mass range ($M_{\rm peak} = 10^{7.9-9.75}$ M$_\odot$)

experience pre–processing, such that they are influenced by environment roughly 2.4 Gyr earlier on average [see also 274]. Throughout this work, we take the last infall onto the current host (i.e. onto a Milky Way–like host) as the infall time for a subhalo, unless otherwise stated. In general, our primary results are qualitatively independent of the adopted definition of infall time.

As shown in Figure 2.2, the distribution of subhalo infall times is very weakly dependent upon subhalo mass at $M_{\rm peak} < 10^{10}$ M$_\odot$, such that our results are largely independent of the assumed stellar mass–halo mass relation. In contrast, the typical infall time of a subhalo depends much more significantly on host–centric distance, with those systems located near the host biased towards early accretion. For our sample of low–mass halos, the inclusion of tidal effects shifts the distribution of subhalo infall times by ~ 0.7 Gyr earlier on average (see black dash–dotted line in Figure 2.2). Our fiducial subhalo population, selected to have $0.15 < R/R_{\rm vir} < 0.5$ and $10^{8.4} < M_{\rm peak}/{\rm M}_\odot < 10^{9.2}$, includes a total of $1,739$ subhalos. This sample is well–match to the Brown UFD sample [33] via both host–centric distance and stellar mass through the assumed SMHM relation.

2.2.3 Methods

We employ a simple statistical method to quantify the probability that environmental mechanisms may be responsible for suppressing star formation in a given population of subhalos (i.e. UFDs). From the parent subhalo population, chosen to match a particular observed galaxy sample, we select (with replacement) a sample of N random subhalos. If all N subhalos are accreted onto their host halo (for the last time) at or before a given redshift, then for that redshift the entire set of subhalos is considered quenched. This process is replicated across 10,000 trials at each z, spanning from $z = 4$ to $z = 0$ at intervals of $\Delta z = 0.05$. The "environmental quenching probability" as a function of cosmic time (or z) is then calculated as the ratio of trails where all N systems quench relative to the total number of trials (i.e. 10,000). Throughout the remainder of this work, we explore the dependence of this environmental quenching probability on the sample size ($N = 6, 10, 20$), the

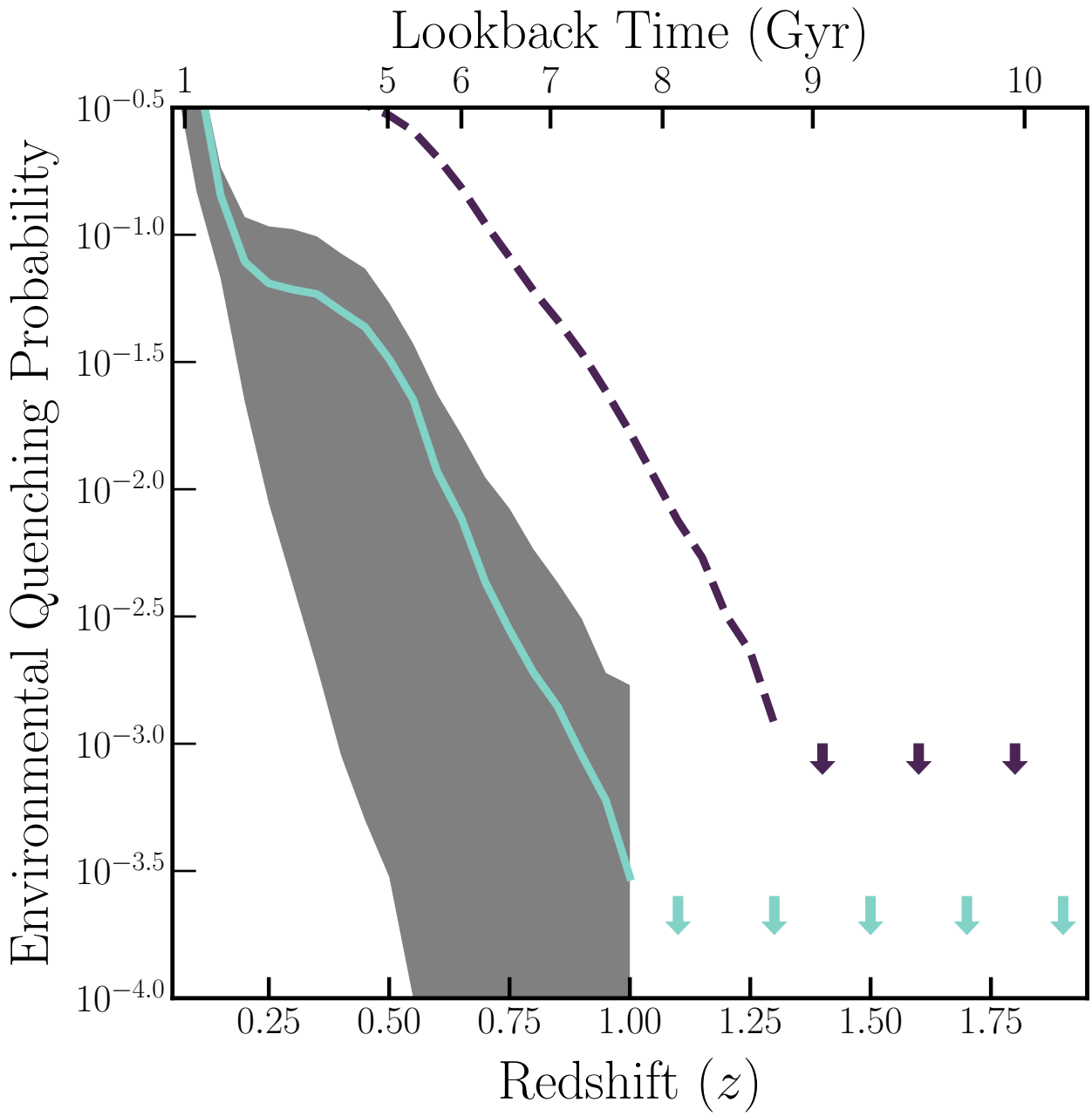

Figure 2.3: The probability that a random sample of 6 subhalos, selected as likely UFD hosts, were all accreted prior to a given redshift (z). The aqua line illustrates this "environmental quenching probability" as a function of redshift for our fiducial subhalo sample, while the grey shaded region illustrates the scatter associated with varying our selection of subhalos across the range $0.01 < R/R_{\rm vir} < 0.9$. The dashed plum line includes the role of pre–processing (infall onto a $\geq$ SMC–like host halo). The likelihood that environmental processes quenched the 6 UFDs from [33] is relatively small ($< 1\%$).

adopted infall time (e.g. allowing for pre–processing by lower–mass hosts), and the fraction of the sample required to be quenched at a given redshift.

2.3 Results

To determine if environmental effects were responsible for quenching the present–day lowest–mass satellites of the Milky Way, we utilize our fiducial Fat ELVIS subhalo population to constrain the likelihood that all 6 galaxies in the Brown UFD sample [33] were accreted at early cosmic times — such that environmental quenching could reproduce the observed SFHs of these systems. From our fiducial subhalo sample, we randomly draw (with replacement) 6 subhalos and evaluate — as a function of redshift — whether the entire sample of 6 was accreted by a given z. Repeating this exercise across 10,000 trials, we compute the likelihood that a sample of 6 randomly–chosen UFDs could be environmentally quenched as a function of cosmic time.

As shown in Figure 2.3, there is a vanishingly small probability that 6 random subhalos would all be accreted at high redshift (i.e. $z > 1$) or that the corresponding galaxies would be quenched by environmental process at such early cosmic time. At $z \sim 1$, after observations suggest that star formation halted in the UFD sample from Brown et al. 2014 [33], there is still an extremely low probability ($< 0.1\%$) that all 6 systems could be quenched via environmental effects. Allowing ~ 1 Gyr for a satellite to quench following infall [74], such that all 6 UFDs must be accreted by $z \sim 1.3$ to quench by $z \sim 1$, only further decreases the potential impact of environmental quenching (see Fig. 2.3). While allowing for pre–processing in hosts down to SMC–like scales increases the possible effectiveness of environmental effects (see dashed plum line in Fig. 2.3), the likelihood that environment quenched the UFDs in the Brown sample [33] is remarkably low ($< 1\%$ for $z_{\rm quench} > 2$). Overall, environmental mechanisms are unlikely to be responsible for the universally old stellar populations inferred for the Brown UFD sample [33].

Including both Brown et al. 2014 [33] and Weisz et al. 2014a [270], there are published SFHs for 10 UFDs, all indicating that star formation halted by $z \gtrsim 2$. Moreover, spectroscopic and/or photometric observations of (at least) a further 10 systems point to old (or metal–poor) stellar populations [e.g. 61, 146, 236, 239, 154, 257]. While these additional UFDs span a broader range of galactocentric distance, with some potentially pre–processed by the Magellanic Clouds [142, 13, 61, 286, 115, 223], the total sample of 20 UFDs creates a powerful dataset with which to examine the role of environment. As expected, if we expand the sample of UFDs to all of those with well–measured star–formation histories ($N = 10$) or yet larger to $N = 20$, it is even more difficult to explain the universally–ancient stellar populations observed in terms of an environmental effect. Figure 2.4 shows the probability that a sample of $N = 10$ (sage thin line) or $N = 20$ (sienna line) UFD satellites were quenched following infall onto the Milky Way halo as a function of cosmic time. We find that there is a $\lesssim 0.01\%$ probability that samples of this size were entirely accreted by $z = 2$. Even if we allow for late–time star formation in 25% of the UFD population (see grey shaded region in Fig. 2.4), we find that the current sample of known UFDs orbiting the Milky Way is unlikely to have been quenched by environment.

2.4 Discussion

2.4.1 Quenching on the Smallest Scales

Our analysis shows that the old stellar populations (and lack of significant star formation at $z \lesssim 2$) observed in the Milky Way's UFD satellites is unlikely to be reproduced via environmental quenching. Instead, the observed star–formation histories of local UFDs are much more likely to have been truncated via reionization. Building upon the analysis of [74, 73], Figure 2.5 presents a complete picture of the dominant physical processes driving late–time satellite quenching across more than 7 orders of magnitude in satellite stellar mass. In particular, we plot the current constraints

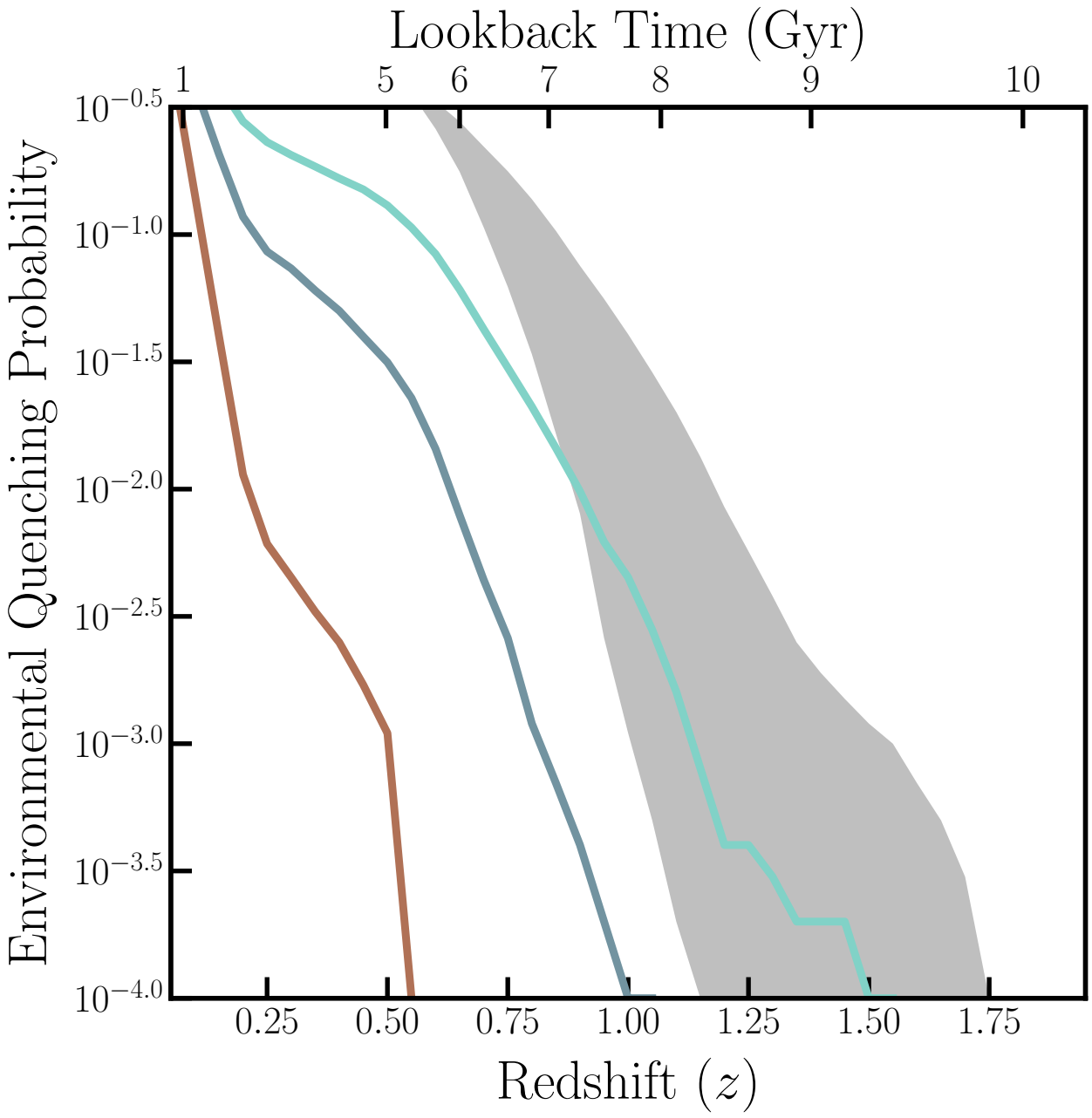

Figure 2.4: The probability that all (*solid lines*) or 75% (*shaded region*) of a random sample of N subhalos, selected as likely UFD hosts, were accreted prior to a given redshift. For a parent subhalo population with $0.01 < R/R_{\rm vir} < 0.9$ and $10^{7.9} < M_{\rm peak}/{\rm M}_{\odot} < 10^{9.75}$, the aqua, sage and sienna lines illustrate the environmental quenching probability as a function of redshift for subsamples of $N = 6, 10, 20$, representing our fiducial sample, the set of UFDs with SFHs, and the set of all UFDs with an estimated age, respectively. The grey shaded region illustrates the environmental quenching probability for samples of $N = 6$ to $N = 20$ UFDs, requiring that only 75% of the population was accreted by the given redshift.

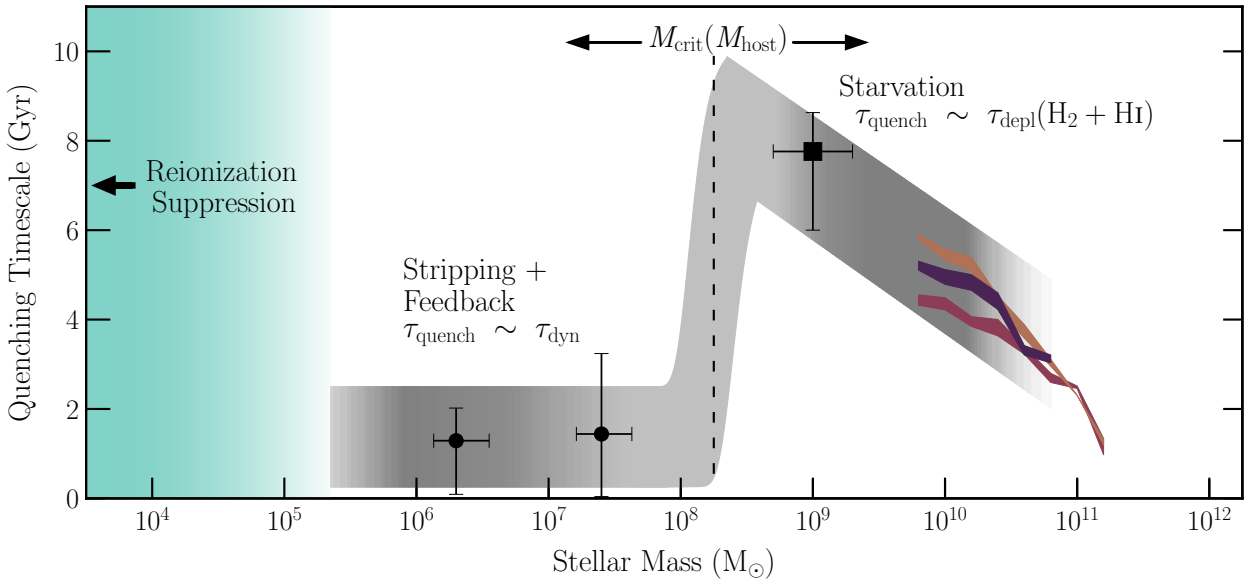

Figure 2.5: The dependence of the satellite quenching timescale on satellite stellar mass in massive host halos ($\gtrsim 10^{12}$ $\rm M_\odot$), as adapted from [74, 73]. The plum, sienna, and burgundy colored bands show the constraints from [275] for satellites in host halos of $M_{\rm host} \sim 10^{12-13}$ $\rm M_\odot$, 10^{13-14} $\rm M_\odot$, and 10^{14-15} $\rm M_\odot$, respectively. The black square and circles correspond to the typical quenching timescale for intermediate–and low–mass satellites from [278] and [74], respectively. The light grey shaded regions highlight the expected dominant quenching mechanism as a function of satellite mass, while the vertical dashed black line denotes the critical mass scale below which satellite quenching becomes increasingly efficient for a roughly Milky Way–like host. This critical mass, at which the dominant quenching mechanism changes, should increase with host halo mass. Finally, the aqua shaded region highlights the mass range where reionization is the most probable quenching mechanism.

on the satellite quenching timescale (measured relative to infall) as a function of satellite stellar mass; we caution that these measurements span a broad range of host halo masses (from $\sim 10^{12-15}$ $M_\odot$), but do describe a coherent physical scenario ([275, 278, 74, 73, 71], see also [57, 104, 55]).

As illustrated in Fig. 2.5, above a host–dependent critical mass scale, satellites are able to largely resist stripping forces, such that they are quenched on longer timescales consistent with starvation [148, 74]. Below this critical mass scale, which is roughly $M_\star \sim 10^8$ $M_\odot$ for Local Group–like hosts [278, 209], stripping is able to remove the fuel supply for star formation from infalling satellites, such that quenching occurs on roughly a dynamical time [74, 73, 276]. This critical mass scale increases with host halo mass, such that stripping is efficient at greater satellite masses in more massive host halos [e.g. 130, 244, 23]; meanwhile, there likely exists some limiting host mass (e.g. $M_{\rm halo} \sim 10^{11}$ $M_\odot$) for which stripping is inefficient on all mass scales and local environment is unable to quench satellites ($\tau_{\rm quench} \sim \tau_{\rm depl} > t_{\rm hubble}$). Finally, at the very lowest masses ($M_\star \lesssim 10^5$ $M_\odot$), reionization acts to suppress star formation, independent of environment (i.e. for both isolated and satellite systems). We illustrate this regime in Fig. 2.5 as the aqua shaded region.

Our results are consistent with recent hydrodynamical simulations of galaxy formation, which find that suppression of star formation by reionization is commonplace below a mass scale of $M_\star \lesssim 10^5$ $M_\odot$ [75, 114]. While reionization halts the infall of new gas in low–mass halos, residual star formation can be fueled by the galaxy's existing gas reservoir so as to produce star–formation histories similar to those observed for UFDs [193, 277]. Additionally, reignition of star formation after initial quenching via reionization may produce short and late periods of star formation [150, 283], such as that observed in Carina by [270]. Observations in the Local Volume also broadly suggest that the mass scale at which quenching via reionization dominates is approximately $M_\star \sim 10^5$ $M_\odot$ [e.g. 255]. In particular, Leo T has a stellar mass of $M_\star \sim 10^{5.5}$ $M_\odot$, with a significant neutral gas reservoir [222, 7] and a complex star–formation history, including significant activity at $z < 1$ [56, 48, 273]. At a distance of > 400 kpc from the Milky Way [111],

Leo T likely represents the tail of the star–forming field population, having a dark matter halo mass greater than that at which reionization suppresses gas cooling. Studies of stellar and gas kinematics in Leo T suggest a halo mass of $\sim 10^9$ $M_\odot$ [238, 222]. While Leo T supports a mass scale for reionization quenching of $M_\star \sim 10^5$ $M_\odot$ ($M_{\rm halo} \sim 10^9$ $M_\odot$), recent observations of low–mass satellites of M31 indicate that the relevant mass scale may be yet lower [$M_\star \sim 10^{4.5}$ $M_\odot$, 166, 169].

Taking $M_\star \sim 10^5$ $M_\odot$ ($M_{\rm halo} \sim 10^9$ $M_\odot$) as the scale at which reionization quenches star formation across all environments, we predict a population of $\gtrsim 250$ UFDs within $1 < R/R_{\rm vir} < 2$ of the Milky Way and M31, based on counts of halos with $M_{\rm halo} = 10^{7.9-9.75}$ $M_\odot$ in the Fat ELVIS catalogs across all 36 simulations.[2] All of these systems are expected to be dominated by ancient stellar populations. While some will have interacted with the Milky Way and/or M31, a relatively large fraction ($> 50\%$) of halos at these distances are true "field" systems, having never spent time as a subhalo. Future imaging surveys, such as the Large Synoptic Survey Telescope [**?**], are expected to discover much of this population in the coming decade, opening new avenues to study the suppression of star formation on the smallest scales. The total number of field UFDs will not only depend on the mass scale at which reionization quenches ongoing star formation at high z, but also the yet lower scale at which it is able to suppress all star formation [e.g. 37, 245].

2.4.2 The Curious Case of Eri II

If reionization truly quenches all low–mass galaxies, independent of environment, we would expect that isolated UFDs should host ancient stellar populations similar to those observed for known UFD satellites. The recent discovery of Eridanus II at a distance of $\gtrsim 350$ kpc from the Milky Way [13, 153] has offered the opportunity to probe the SFH of a "field" UFD in significant detail. At a galactocentric distance of ~ 1.2 $R_{\rm vir}$, however, Eri II cannot be considered an isolated system, unaffected by potential environmental effects. A significant fraction of systems at such distances

[2]On average, the 12 paired host simulations have slightly more halos in the $1 < R/R_{\rm vir} < 2$ range and a smaller fraction of these being backsplash halos.

are associated with "backsplash" halos [250, 90, 71], which previously passed within the host's (i.e. Milky Way's) virial radius before returning to the field.

While recent observations show no signs of late–time star formation ([153], but see also [142, 52]), Eri II — as a solitary system with an unknown orbital history — places limited constraints on the dominant mechanism responsible for suppressing star formation on the smallest scales. As shown in Figure 2.6, the current sample of Milky Way UFD satellites already places a stronger constraint on the role of environment. To test whether Eri II is likely to have been quenched by environment, we select subhalos from our Fat ELVIS catalogs, matching the mass ($8.9 < M_{\rm peak}/{\rm M}_\odot < 9.75$), host–centric line–of–sight velocity (-90 km s^{-1} $< V_{\ell{\rm os}} < -40$ km s^{-1}), and host–centric distance ($0.9 < R/R_{\rm vir} < 1.9$) of Eri II [153].[3] From the resulting sample of 274 subhalos, we compute the infall distribution as a function of cosmic time (see Fig. 2.6), which corresponds to the likelihood that environment played a role in quenching star formation in Eri II. We find that there is a $\sim 10\%$ chance that Eri II was quenched via an interaction with the Milky Way at $z \sim 1$. While Eri II is unlikely to have been quenched due to an interaction with the Milky Way at $z > 2$ (so as to produce a purely old stellar population), the measured SFHs for the existing sample of UFD satellites orbiting the Milky Way already argue more strongly against environment's role in suppressing star formation on the smallest scales.

2.5 Summary

Using the ELVIS suite of Milky Way–and Local Group–like N–body simulations to constrain the infall times for subhalos likely to host the ultra–faint satellite population of the Milky Way, we explore the potential role of environment in suppressing star formation on small scales. Our

[3]The adopted phase–space range was selected to encompass velocity and distance errors, as well as a possibly higher than originally assumed total velocity, following suit based on recently–derived velocities for UFDs from Gaia Data Release 2 [234, 83].

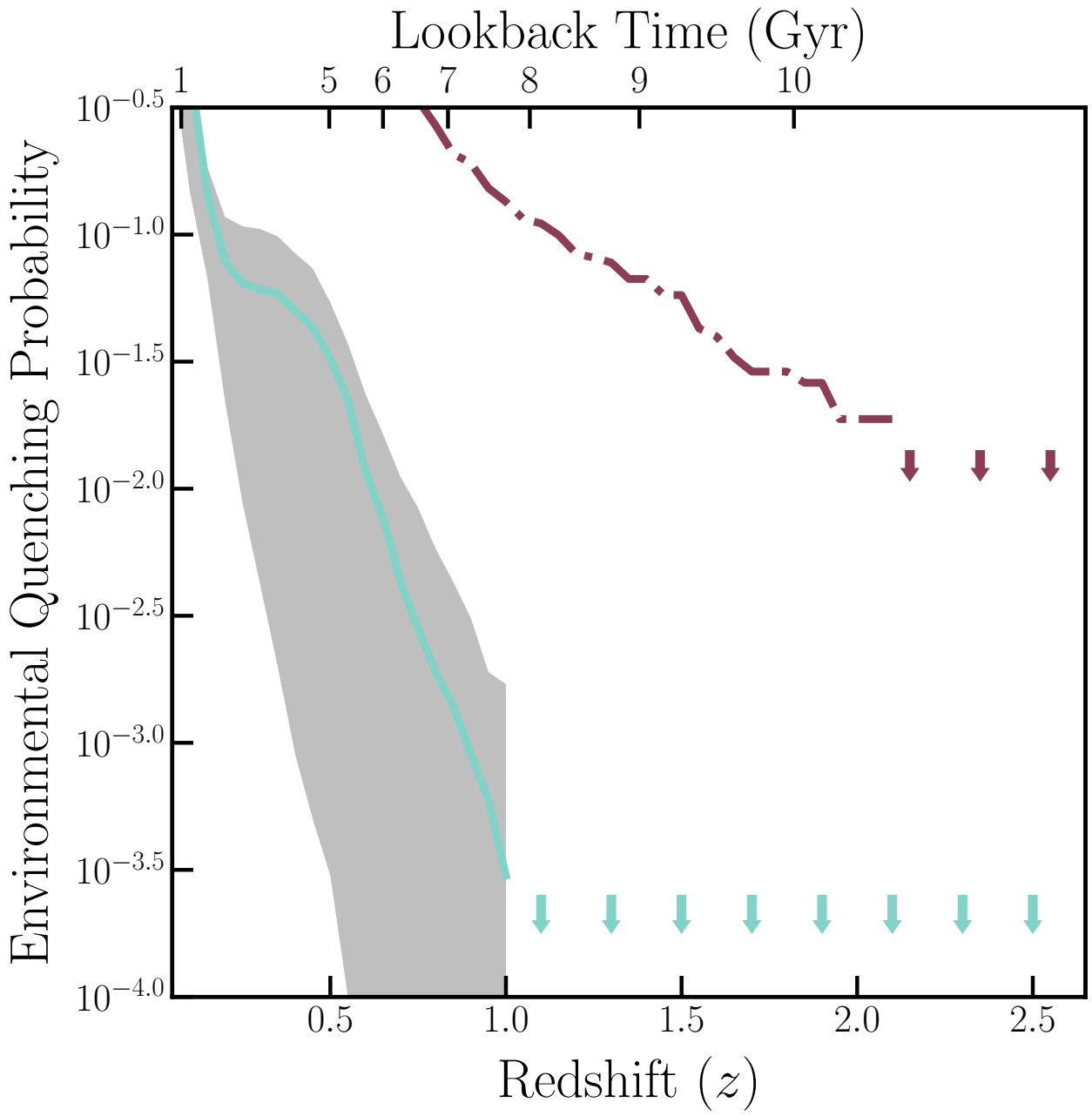

Figure 2.6: The probability that a randomly–selected Eri II–like halo was accreted by the Milky Way as a function of cosmic time (burgundy dash–dotted line). For comparison, we overplot the probability that a sample of 6 subhalos were accreted by the same redshift (from Fig. 2.3). While Eri II is unlikely to have been quenched by environment, the ancient stellar populations observed in current samples of UFD satellites argue more strongly against environment's role in suppressing star formation on the smallest scales.

principal results are as follows:

1. When incorporating the effects of subhalo tidal disruption due to the inclusion of the host's baryonic component, we find a shift in the typical infall time of ~ 0.7 Gyr for subhalos in the mass range of $M_{\rm halo} = 10^{7.9-9.75}$ $M_\odot$, such that subhalos are preferentially accreted at later cosmic time versus the same subhalos in a pure dark matter–only, N–body simulation.

2. For the 6 UFDs included in the Brown sample [33], we find that there is a $\lesssim 0.1\%$ probability that the Milky Way environment was solely responsible for quenching their star formation at $z > 1$.

3. For larger samples of UFDs, the likelihood that environment plays a dominant role in quenching decreases dramatically, such that there is a $< 0.01\%$ probability that environmental mechanisms are responsible for quenching all 10 UFDs included in the Brown and Weisz samples [33, 270].

4. Given the inability of environmental effects to reproduce the observed star–formation histories of observed UFDs, we conclude that reionization is the most likely mechanism by which star formation is suppressed on the smallest scales.

5. Finally, we predict that there is a population of $\gtrsim 250$ UFDs within $1 < R/R_{\rm vir} < 2$ of the Milky Way and M31, all with ancient stellar populations. Future imaging surveys, such as LSST, will be able to uncover much of this population.

Combined with results from [74] and [73], our results produce a coherent physical picture describing the dominant quenching mechanism across the entire range of satellite (and host) masses (see Fig. 2.5). At the very smallest scales, we argue that the suppression of star formation is largely independent of environment and set by the minimum halo mass at which reionization curtails gas accretion.

Chapter 3

Sizing from the Smallest Scales: The Mass of the Milky Way

3.1 Introduction

Several of the most pressing cosmological problems challenging the ΛCDM paradigm, namely the Too Big to Fail [TBTF, 25, 26] and the Missing Satellites problems [180, 137], depend heavily on the Milky Way's dark matter halo mass. One way to resolve the TBTF problem within ΛCDM is through the assumption of a less massive Milky Way, for which fewer massive satellites with high central densities are expected. Similarly, in conjunction with suppression of galaxy formation on the very smallest scales [e.g. 65, 251], the Missing Satellites problem can also be largely eliminated by lowering the assumed Milky Way dark matter halo mass (and thus the predicted number of satellite systems). As such, the Milky Way's dark matter halo mass is a critical parameter in testing ΛCDM and models of galaxy formation on small scales [see discussion in 36].

Alternative resolutions to both the TBTF and Missing Satellites problems lie in the possibility that the Milky Way may be an outlier relative to the cosmic norm. For example, only $\sim$ 10%

of Milky Way–like systems are estimated to have satellites as massive as the Large and Small Magellanic Clouds [28, 38, 253, 228]. The Milky Way's satellite population is also remarkable in another characteristic — its Vast Polar Structure [VPOS, e.g. 160, 144, 204, 83, 202]. While our ability to observe such structures in systems beyond our very local Universe is still relatively new [110, 51, 50, 182], our observed flattened polar distribution of satellites, the VPOS, seems to be uncommon [177, 203, 201, 109, 35, 8, 230, 231]. Another unusual feature of our local system may be the high fraction of quenched (or passive) satellite galaxies. Extragalactic surveys, such as SAGA, have found that the majority of satellites around Milky Way–like systems are actively star forming — SAGA in fact finds 85% of low–mass satellites ($M_\star \sim 10^{7-8.5}$ $M_\odot$) are star–forming across 36 Milky Way–like systems [164, 93]. The radial distributions of the Milky Way satellites versus observed and simulated Milky Way analogues is also a contentious point which may place the Milky Way out of the cosmic norm. Some recent work highlights discrepancies in the 3D radial distributions of Milky Way satellites and various cosmological simulations, in particular that Milky Way satellites are more radially concentrated than their simulated counterparts ([179, 281, 284, 42], but see also [161, 224, 77, 22]). The dark matter halo mass of the Milky Way has strong implications on its ability to quench satellite galaxies and on the radial distribution of its satellite population. More broadly, our reliance upon the Milky Way as a Cosmic Rosetta Stone [29] requires a strong constraint on its dark matter halo mass.

Gaia has opened a new opportunity to study the distribution and dynamics of the Milky Way satellite population and to constrain the Milky Way's dark matter halo mass. Prior to the second data release (DR2) of proper motions from *Gaia*, the Milky Way's dark matter halo mass limits were $0.8 - 4.5 \times 10^{12}$ $M_\odot$ [e.g. 27, 208, 124]. Since *Gaia* DR2, this mass has been inferred in various ways — from calculating the escape speed from counter–rotating stars in the Galaxy's outer halo [178]; using a scale–free mass estimator involving the density, potential, and anisotropy (β) of the satellites — galaxies or globular clusters — surrounding the Milky Way [267, 84]; comparing phase–space distributions in simulations and semi–analytic models to observed distributions to then infer the mass [199, 64, 155, 45]; calculating the mass within 100 kpc via a distribution

function method then extrapolating total mass [58]. The results of these recent studies range from $M_{200} = 0.7^{+0.11}_{-0.08} - 1.55^{+0.64}_{-0.51} \times 10^{12}$ $M_\odot$ [64, 178, respectively]. It is important to note that even within confidence intervals, many of these results do not agree with one another.

As an alternate approach to these direct dynamical methods, in this work we constrain the Milky Way's dark matter halo mass through comparison of subhalo kinematics in a suite of high–resolution N–body simulations to corresponding observational measures of the Milky Way satellite population from *Gaia*. Herein, we utilize orbital parameters for the Milky Way satellites, derived primarily from proper motion measurements contained in the early third *Gaia* Data Release [EDR3, 87, 88]. In §3.2, we discuss our observed tracers of the Milky Way host potential along with the comparison suite of cosmological simulations. §3.3 details our primary analysis techniques, while our results are presented in §3.4. In §3.5, we examine various sources of potential systematic errors and points of further discussion, including the impact of satellites associated with the Large Magellanic Cloud, our adopted lower limit for peak subhalo velocity, orbital characteristics, and observational completeness. Additionally, in this section we make some predictions for how future observations might impact our results. Finally, we summarize in §3.6.

3.2 Data

3.2.1 *Gaia*

Gaia has spurred a dramatic improvement in our understanding of the orbital parameters for nearby stars, including those within the satellites of the Milky Way (MW) [88]. In the second and early third data releases [DR2 and EDR3, 86, 157, 87], *Gaia* provides precise parallaxes and/or proper motions for over one *billion* sources, in an absolute reference frame defined entirely by *Gaia* observations. From this vast data set, several groups calculated full phase–space information, including tangential velocities, for a majority of the MW satellites (e.g. using DR2: [103, 234, 83, 170, 198, 125] plus

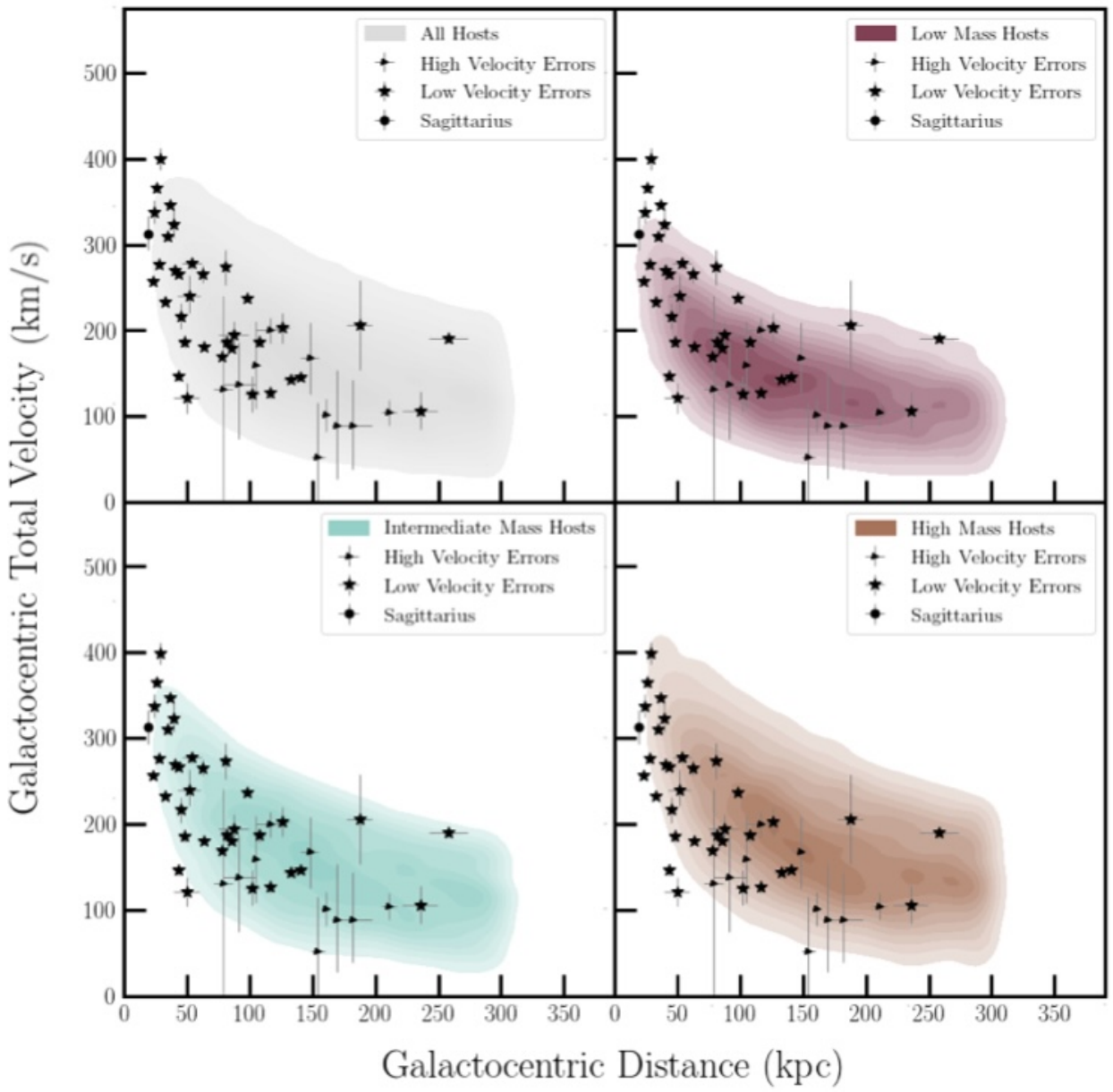

Figure 3.1: Comparison of phase–space distributions between Phat ELVIS subhalos (density contours) and satellites in [174] (MCV20a, black markers). In each plot, the stars denote satellites with low tangential velocity errors ($V_{\rm tan,err} \leq 0.30\ V_{\rm tan}$). The triangles denote all other satellites excluding Sagittarius, which is represented as the circle. Sagittarius is poorly reproduced by the simulations and thus omitted from this analysis. The total velocity information for Sagittarius comes from [83], which uses *Gaia* Data Release 2 proper motions. The total velocity errors are taken from MCV20a while the distance errors are taken from the literature (mainly [235] and references therein). The top left panel shows the phase–space density contours for subhalos across all 12 Phat ELVIS hosts. Meanwhile, in the three remaining panels, we display the corresponding contours with subhalos divided according to host mass — 0.7–1 $\times 10^{12}$ $M_\odot$ (low mass, burgundy shading), 1–1.2 $\times 10^{12}$ $M_\odot$ (intermediate mass, aqua shading), and 1.4–2 $\times 10^{12}$ $M_\odot$ (high mass, sienna shading). Each mass bin includes 4 hosts, with the adopted color scheme for the host mass sets carried throughout this paper.

[174, 152], which utilize EDR3). Herein, we utilize the Galactocentric tangential velocities from McConnachie & Venn, 2020 [174, hereafter referred to as MCV20a]. Heliocentric radial velocities are taken from McConnachie et al. 2012 [173] and converted to the Galactocentric reference frame using `astropy` [11, 10]. Heliocentric distances and associated errors are taken from [235][1], [127], [272], and [258]. These distances are also converted to the Galactocentric reference frame using `astropy`. These quantities, converted to the Galactocentric reference frame, along with other properties of the MW satellies used in this work can be found in Tables 3.1 and 3.3.

We limit our sample of Milky Way satellites to those systems within a Galactocentric distance of 300 kpc and exclude unconfirmed systems that are likely not galaxies (e.g. Indus I and DESJ0225+0304). In addition, we exclude the Sagittarius (Sgr) dwarf from our sample. Sgr is currently being disrupted via tidal interactions with the Milky Way [e.g. 108, 149, 141], such that it is poorly reproduced in our comparison simulation data set (see §3.2.2). Our primary sample includes 44 satellite galaxies. Figure 3.1 shows the distribution of these systems as a function of Galactocentric distance and total velocity. Finally, we identify a subsample of 34 systems with higher–precision tangential velocities, such that $|V_{\rm tan,err}/V_{\rm tan}| \leq 0.30$. While this subset of systems is biased towards smaller Galactocentric distance, it does span a broad range of velocities (see Fig. 3.1). The particular selection limit used to define this subsample was adopted to exclude those systems with exceptionally uncertain tangential velocities while maintaining a statistically significant sample size.

3.2.2 Phat ELVIS

As a comparison data set, we utilize the Phat ELVIS (phELVIS) suite of 12 high–resolution, dissipationless simulations of MW–like halos [128]. Building upon the ELVIS (Exploring the Local Volume In Simulations) suite of Local Group and MW–like simulations [90], phELVIS

[1]Data presented by [235] are compiled from [260, 53, 265, 145, 98, 257, 183, 259, 131, 159, 52, 214, 142, 184, 13, 143, 261, 15, 14, 181, 176, 227, 185, 210, 17, 21, 151, 99, 41, 61, 89, 54, 279].

incorporates the effects of tidal disruption due to an artificial disk potential [e.g. 91, 229]. This new suite includes a total of 24 MW–like simulations, encompassing 12 high–resolution cosmological dark matter–only (DMO) simulations of isolated MW–like halos and 12 re–runs of those DMO simulations with an embedded galaxy potential matching the observed MW disk and bulge (from here on referred to as the Disk runs). The 12 Disk runs begin as identical duplicates to the 12 DMO suites. At $z = 3$, a galaxy potential, including a stellar disk, gaseous disk, and Hernquist bulge component, is inserted into each of the Disk hosts. While the potentials temporally evolve, each Disk host ends up at $z = 0$ as an observationally–constrained MW [128].

Each simulation occurs within a global cosmological box of length 74.06 Mpc (50 h^{-1} Mpc) with a dark matter particle mass of 3×10^4 $M_\odot$ and a Plummer–equivalent force softening length of $\epsilon = 37$ parsecs. These parameters allow for the subhalo catalogs to be complete down to a maximum circular velocity of $V_{\rm max} > 4.5$ km s^{-1} (i.e. a total bound mass of $\gtrsim 5 \times 10^6$ $M_\odot$). The phELVIS halo catalogs are constructed of 152 snapshots, evenly spaced in scale factor with a time resolution of roughly 100 Myr. To increase the precision of the subhalo pericentric distances and infall times, we spline interpolate the subhalo positions and velocities to achieve a time resolution of $\sim$ 10 Myr. Phat ELVIS adopts the cosmology of [211] with the following parameters: $\Omega_{\rm m} = 0.3121$, $\Omega_\Lambda = 0.6879$, and $h = 0.6751$.

In order to more directly compare to the MW satellite population, we select subhalos from the phELVIS suite with $V_{\rm peak} > 6$ km s^{-1}. While suppression of galaxy formation due to reionization is often predicted to occur below a mass limit of $V_{\rm peak} \sim 20 - 25$ km s^{-1} [e.g. 95, 105, 194], the observed abundance of ultra–faint satellites of the MW are better matched via a lower mass limit [97]. Adopting a more inclusive mass selection yields a considerably larger subhalo population for comparison, better sampling the host potential and allowing control of systematics associated with observational completeness.

While the phELVIS subhalos catalogs at $z = 0$ provide thousands of subhalos for comparison, they are limited to a single snapshot of each subhalo orbit. To better sample the host potential, we expand

our subhalo population to include subhalos at two earlier snapshots. These two other snapshots were selected based on the average growth histories of the phELVIS hosts to minimize variation in the host mass. A majority of the hosts have minor ($\lesssim 2\%$) to no growth after $z = 0.05$, which corresponds to the original 8^{th} timestep prior to $z = 0$. The two snapshots chosen to examine here are evenly spread — specifically the 8^{th} and 4^{th} (corresponding to $z = 0.05, 0.02$, respectively). The vast majority ($\sim 90\%$) of the subhalo population is present at all 3 timesteps, with a small number of subhalos missing (or added) at earlier timesteps due to recent accretion, backsplashing, and/or tidal destruction.

Throughout this work, we focus on the 12 MW–like hosts in the Disk runs. The hosts with embedded disk potentials are chosen for their ability to better represent the observations relative to the dark matter–only (DMO) hosts. In the DMO runs, the greatest subhalo Galactocentric total velocities, which are all found at small Galactocentric distances, are systematically lower than those found in the Disk runs. This trend is seen in all three of the host halo mass ranges displayed in Fig. 3.1 and further strengthens the argument initially made in [128] — central–galaxy dynamics must be included to match observations of the satellite population. The Disk host halos range in virial mass[2] from $0.71 - 1.95 \times 10^{12}$ $M_\odot$. We split the hosts evenly into 3 groups based on mass — least massive, intermediate mass, and most massive. Specifically, the mass ranges of the 3 bins are: $0.71 - 0.96 \times 10^{12}$ $M_\odot$ (low mass), $1.04 - 1.20 \times 10^{12}$ $M_\odot$ (intermediate mass), and $1.40 - 1.95 \times 10^{12}$ $M_\odot$ (high mass). Excluding subhalos with $V_{\text{peak}} < 6$ kms^{-1}, there are an average of 1200 subhalos ($< R_{\text{vir}}$) associated with each of the 4 low–mass hosts, in comparison to an average of 1400 (2100) subhalos for each of the 4 intermediate–mass (high–mass) hosts. Within each of the 3 host mass bins, the halo–to–halo scatter in subhalo count is not great. The normalized, cumulative distribution of each bin is approximately the average of the 4 individual host distributions that comprise that particular bin. As shown in Figure 3.1, due to the tidal disruption of subhalos in the Disk runs, phELVIS includes exceedingly few analogs to the Sagittarius dwarf. As discussed in §3.2.1, for this reason Sgr is excluded from the sample of MW satellites studied.

[2]In the phELVIS simulations, virial mass, M_{vir}, follows the [34] definition.

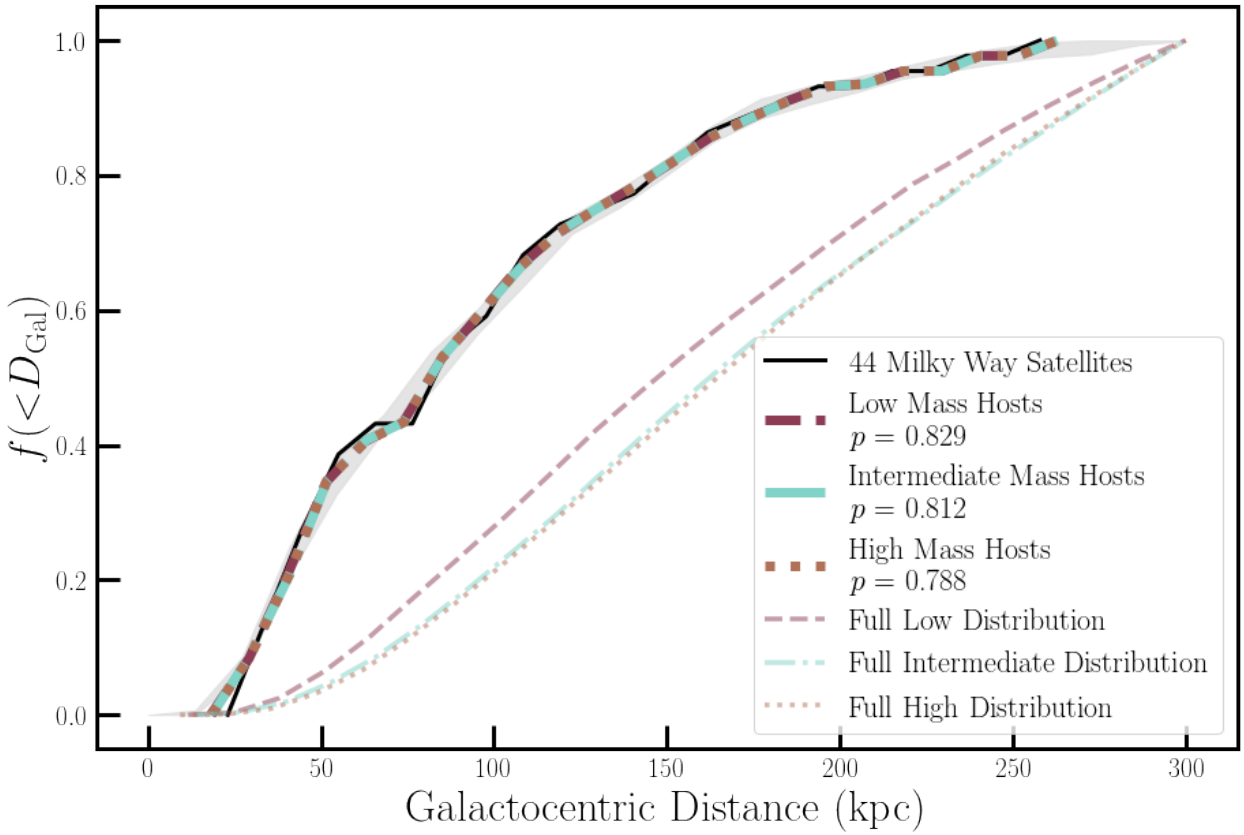

Figure 3.2: The cumulative distributions of MW–centric and host halo–centric physical distances are engineered to be nearly identical via our distance–matching scheme. The solid black line is the cumulative distribution of Galactocentric distances for our primary sample of 44 satellite galaxies. The dashed burgundy line, dash–dotted aqua line, and the dotted sienna line are the corresponding cumulative distributions for subhalos drawn from the three host halo sets, where Galactocentric distance is measured with respect to the corresponding host halo. The (thin) grey shaded region is the range of reported errors in the literature (see [235] and references therein). The Mann–Whitney U Test p–value statistic is calculated using these errors. The legend reports the harmonic mean of MWU p–values from 500 randomly–selected, distance–matched subhalo distributions. This tight comparison (as we cannot reject the null hypothesis that the distributions are drawn from the same parent population due to the two–sided p–values all being well above the statistical significance level of 0.05), reduces the potential biases associated with the incompleteness of the MW satellite population.

3.3 Analysis

To study how the dynamics of the MW satellites depend on host halo mass, we select subhalos from the phELVIS simulations from each of the the host mass divisions discussed in §3.2.2. We then compare the subhalo samples to the observational data set via Galactocentric velocities — namely, radial, tangential, and total. To mitigate selection effects driven by incompleteness in the sample of MW satellites, we match our sample of MW satellites to phELVIS halos via Galactocentric distance. For each of the three sets of host halos, we randomly select (with replacement) 10 subhalos for each satellite, selecting the subhalos from distance bins of width 10 kpc centered on the Galactocentric distance of the satellite, where there is an average of 600 subhhalos in each satellite's distance bin. These distance–matched subhalos are randomly selected from the parent catalog that combines the subhalo populations from all three timesteps. For our primary sample of 44 satellites, this produces three comparison samples of 440 halos each, associated with the low–mass, intermediate–mass, and high–mass hosts. As shown in Figure 3.2, this distance–based matching enforces a very close correlation between the Galactocentric distances of the MW satellite sample and our comparison subhalo samples. One caveat to this method of matching — it does not guarantee each distance–matched halo is located within $R_{\rm vir}$ of the host. For example, Leo I's Galactocentric distance is 272 kpc while only the 5 most–massive phELVIS host halos have virial radii greater than this distance. Thus, some of the subhalos, drawn from the lower–mass hosts and distanced–matched to Leo I, may reside beyond $R_{\rm vir}$. We choose not to match subhalos to observed systems on normalized distance (i.e. Galactocentric distance which has been normalized to the MW/host's virial radius) to avoid introducing biases associated with the boundedness of a system at or near the virial radius or possible tidal disruption for systems near the host halo's center.

To quantify the observation–to–simulation comparisons (i.e. to measure if the distanced–matched halos do not represent the MW satellites), we employ the Mann–Whitney U (MWU) test [163, 123]. This is a non–parametric statistical ranked summation test that examines two independent samples. This test does not require any knowledge of the underlying distribution in either of the independent

samples. To avoid possible underlying biases in the ranked summation [76], we increase our observational sample size by randomly sampling the observational quantities' errors to match the size of the distance matched halo population (i.e. 440 observational values are compared to 440 simulated values). For satellite characteristics that have asymmetric error distributions (e.g. for $V_{\rm tan}$ and $V_{\rm tot}$), the errors are drawn equally from the positive and negative sides. No galaxy in our observational set has plus–minus errors that are extremely different from one another. Fortunately, the MWU is attuned to only median changes, compared to say the Kolmogorov–Smirnov (KS) test which is sensitive to the shape of the underlying distributions as well as the medians. The null hypothesis for the MWU is that the two independent samples are, in fact, drawn from the same parent distribution. We report the MWU test results as the associated two–sided p–values. Our statistical significance level to reject the null hypothesis is set at $p \leq 0.05$.

In an additional step towards bias avoidance, we conduct the MWU test 500 times for each parameter. This is to reduce the possibility of sampling a randomly skewed distribution. 500 sets of $10N$ distance–matched subhalos and $10N$ measures of corresponding satellite properties (as drawn from the observed error distributions) are randomly drawn and a two–sided MWU p–value calculated for each. We then take the harmonic mean of these 500 p–values and use this as our statistical result.

To create a baseline to our distance–matched analysis, we compare the unmatched subhalo distributions in the same way as comparing the matched distributions. Here, we compare $10N$ subhalo properties randomly chosen from any subhalo in the host halo set (independent of distance) to a set of $10N$ values randomly sampled from the error distributions of the observational quantities. We do this twice — once where $N = 44$ for the full set of satellites and $N = 34$ for the set of systems with proportionally low tangential velocity errors. Finally, we create the random samples 500 times, comparing the unmatched set to the observational set each time and then take the harmonic mean of the resulting p–values. As detailed in Table **??**, the comparison of Galactocentric distances for both observational sets to each of the 3 unmatched host halo sets are rejected at greater than 5σ,

where 5σ maps to $p = 0.00001$ as determined by our choice of significance level ($p = 0.05$) and the fact that we calculate a two–sided p–value. The tangential and total velocity comparisons are also rejected at greater than 5σ for all three sets. The radial velocity p–values are a bit different in these comparisons. For the low–and intermediate–mass host halos sets, the p–values are rejected at greater than or near 3σ, with 3σ mapping to $p = 0.0027$. The comparison for the high–mass host halo set in radial velocity cannot be rejected ($p > 0.05$) — this is the only non–rejectable null hypothesis between the unmatched subhalo distributions and the observations.

3.4 Results

We refine halo mass constraints for the MW by comparing the MW satellites' Galactocentric velocities to distance–matched distributions of Phat ELVIS subhalos split into 3 groups based on host halo virial mass. The 3 host halo mass bins range from $< 10^{12}$ $M_\odot$ to $\sim 2 \times 10^{12}$ $M_\odot$, with $\sim 10^{12}$ $M_\odot$ being the intermediate bin. We focus on two sets of satellites drawn from the MCV20a sample — all MW satellites and satellites with proportionally small tangential velocity errors (see §3.2.1). These two subsets included 44 and 34 satellites, respectively.

The subhalo distribution from each of the 3 host halo sets is well matched in distance to each of the 2 main satellite sets, by design (see Fig. 3.2 and §3.3). Given these subhalo samples that are well matched on Galactocentric distance to the observed MW satellite population, the velocity distributions of each satellite set is then compared to the corresponding measure for the distance–matched subhalos from the 4 highest–mass host halos, the 4 intermediate–mass host halos, and the 4 lowest–mass host halos. This results in 3 harmonic mean p–values for the each of the velocity components. When $p \leq 0.05$, the MWU test's null hypothesis can be rejected, which equates to the galaxy sample being poorly represented by the distance–matched subhalos in a specific host halo mass set (based on that particular measure of velocity).

With tight distance–matched populations, we first examine the most well–constrained kinematic property — Galactocentric radial velocity ($V_{\rm rad}$). As illustrated in panel (a) of Figure 3.3, radial velocities for the main set of 44 satellites are in good agreement with the corresponding velocities for subhalos in the intermediate–mass host halo set, while the subhalos drawn from the low–mass and high–mass hosts are inconsistent with the observations at $\gtrsim 5\sigma$ ($p < 0.00001$).

Since the strength of *Gaia*'s data is the ability to calculate full 6–dimensional phase space, we take the analysis a step further by incorporating the not as richly studied Galactocentric total and tangential velocities. For the main set of 44 satellites, the preference for an intermediate–mass host halo is *not* evident when examining either of these two velocities — i.e. the associated p–values reject the null hypothesis that the two samples are drawn from the same parent distribution. As shown in panels (b) and (c) of Figure 3.3, the subhalos of the intermediate–mass hosts are inconsistent with the observational set. In panel (b) the tangential velocity comparison prefers the low–mass hosts, i.e. this is the only non–rejected p–value, while in panel (c) the total velocity comparison rules out all host mass ranges — i.e. all samples yield $p < 0.05$.

A caveat to the *Gaia*–derived velocities is that a significant group of the observed systems have proportionally large errors associated with their proper motions which translates to proportionally large errors associated with the system's tangential and total velocities. These larger uncertainties allow for the possibility of extreme velocities that are not well represented in the phELVIS simulations. Inclusion of these systems in the analysis potentially creates a bias primarily against higher–mass hosts. The systems in the MCV20a sample with proportionally high tangential velocity errors tend to have lower tangential and total velocities at further distances. These kinematically cool systems become more rare with increasing host halo mass — in higher–mass hosts, hotter systems are the norm. For example, Leo IV is one such system with proportionally large tangential velocity errors (i.e. $|V_{\rm tan,err}/V_{\rm tan}| \geq 0.30$). Of the 1108 halos within ±5 kpc of Leo IV's distance (154.59 ± 4.99 kpc) in the 4 highest–mass host halos, there are exactly 0 halos with a tangential velocity in the bottom range of Leo IV's 1σ tangential velocity error ($V_{\rm tan} < 14$ km s^{-1}).

To address this potential bias, we rerun our distance–matching analysis using the subsample of 34 satellites with low fractional uncertainty in $V_{\rm tan}$ — specifically $|V_{\rm tan,err}/V_{\rm tan}| \leq 0.30$. We then compare the resulting velocity distributions for this pared–down set. As illustrated in Fig. 3.4, the radial velocity comparison, panel (a), is essentially unaffected by the removal of systems with proportionally high tangential velocity errors. However, the comparison in tangential velocity space, panel (b), now prefers the intermediate–mass hosts. The preferred halo mass in the total velocity comparison also changes from Fig. 3.3 to now prefer the intermediate–mass hosts. The low–and high–mass hosts in all 3 velocity component comparisons are rejected ($p < 0.05$) at or near 3σ. All p–values discussed here can be found in Table 3.9.

To explore the limits of this preferred intermediate–mass range, $1.04 - 1.20 \times 10^{12}$ M$_\odot$, we rerun the analysis with thinner and wider intermediate–mass ranges. More specifically, we ran the analysis with a thinner intermediate mass range of $\sim 1.04 - 1.10 \times 10^{12}$ M$_\odot$ (3 host halos) and a wider intermediate mass range of $\sim 0.96 - 1.40 \times 10^{12}$ M$_\odot$ (6 intermediate–mass host halos instead of 4). We compare these varying host halo mass ranges to the observational set of systems with proportionally low tangential velocity errors. In the velocity comparisons for the thinner intermediate–mass host halo set, this new intermediate–mass host halo set of 3 halos is preferred across all 3 velocity components. The 3 p–values for this host halo set are all greater than the significance limit of 0.05, while the p–values for the low–and high–mass hosts in all 3 velocity components are rejected at or near 3σ. In the velocity comparisons for the wider host mass set, there is not one host halo set preferred across all 3 velocity components. Though the intermediate–mass sample is nearly preferred across the components — the radial and total velocity p–values are greater than the significance limit while the tangential velocity p–value is just below this limit ($p = 0.045$). *Overall, the results based on comparing the set of MW satellites with proportionally low tangential velocity errors to the phELVIS simulations strongly indicate that the Gaia–based distances and velocities are consistent with a MW dark matter halo mass of* $\sim 1 - 1.20 \times 10^{12}$ M$_\odot$.

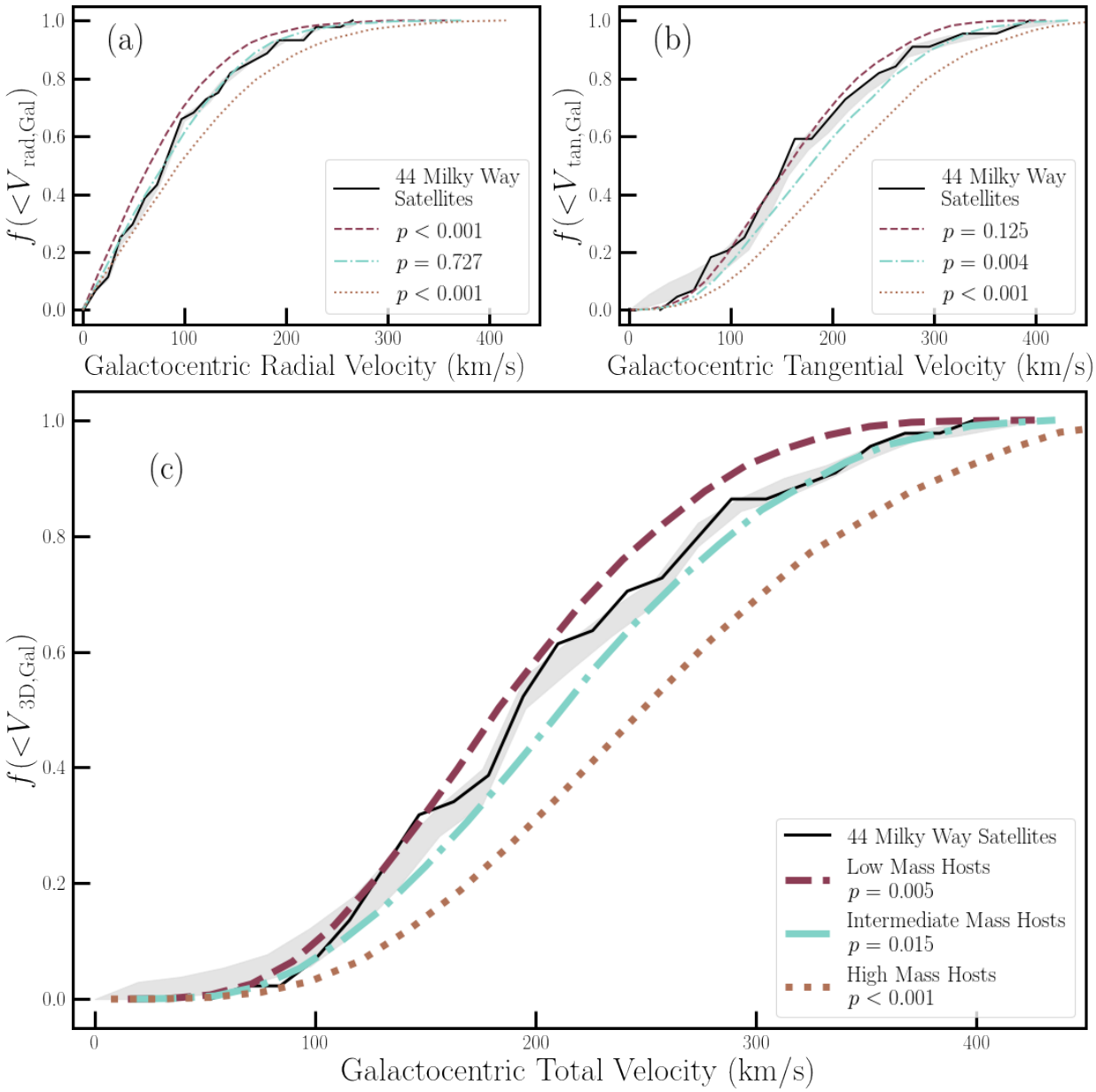

Figure 3.3: Cumulative distributions of Galactocentric velocities — namely in panel (a) $V_{\rm rad}$, in panel (b) $V_{\rm tan}$, and in panel (c) $V_{\rm tot}$ — for the MW satellites in comparison to that of the simulated subhalos. The solid black line is the distribution for the 44 satellite galaxies in the MCV20a sample. The dashed burgundy line, dash–dotted aqua line, and the dotted sienna line are the distributions for subhalos drawn from the three bins in host mass. The grey shaded regions are the cumulative distribution of the range of 500 randomly sampled values from each systems reported errors. In panel (a), the comparison in the well constrained parameter of Galactocentric radial velocity results in the preference towards only an intermediate mass MW dark matter halo. Panels (b) and (c) tell a different story. These subplots display how the inclusion of the further phase–space information from *Gaia* shifts the preference toward a less massive MW in Galactocentric tangential velocity, in that the low–mass hosts yield the only non–rejected p–value, while no host halo mass range is consistent with the observed Galactocentric total velocities for this sample.

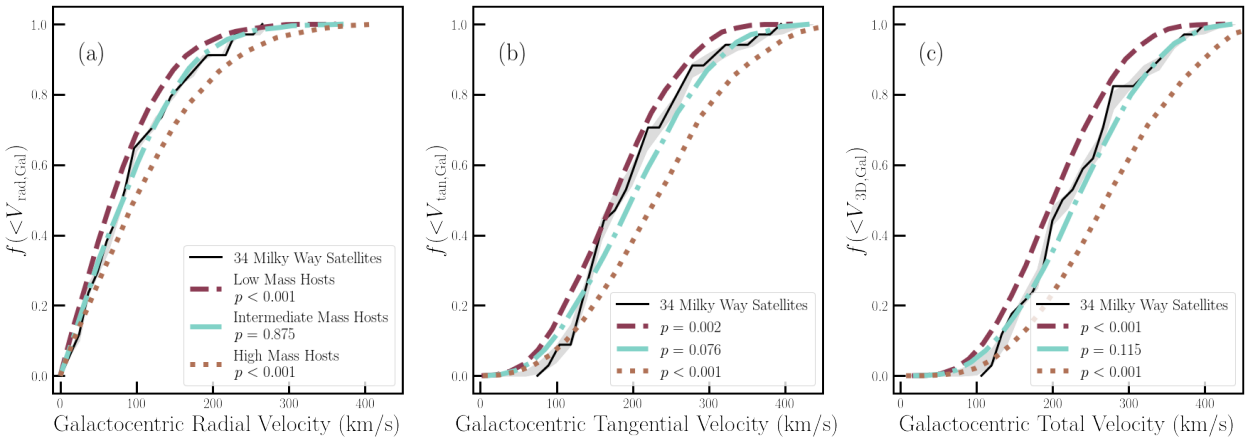

Figure 3.4: Cumulative distributions of all velocity components for the pared–down set of 34 satellites all with proportionally low tangential velocity errors. The color coding, line style and legend conventions are identical to Fig. 3.3. These three plots display how excluding satellites with their average plus–minus error $\geq 30\%$ of their tangential velocity settles the host mass preference on an intermediate mass MW. Specifically, compared to Fig. 3.3, the resulting p–values for the intermediate mass host halos in the Galactocentric tangential and total velocities are now above the statistical significance level of 0.05 while the p–values for the low–and high–mass host halos are rejected and therefore the intermediate mass hosts halos is the preferred host mass range.

3.5 Discussion

3.5.1 Large Magellanic Cloud (LMC) Satellites

Of the 12 MW–like systems in the phELVIS suite with an embedded disk potential, there is only 1 host with a Large Magellanic Cloud–like subhalo (i.e. with $M_{\rm vir} \geq 8\times10^{10}$ M$_\odot$). If this restriction is lowered to $M_{\rm vir} \geq 3\times10^{10}$ M$_\odot$, then there are 2 Large Magellanic Cloud–like subhalos throughout the 12 disk hosts. It can be argued that including MW satellites that were originally LMC satellites in our analysis may bias our results, as these systems may not be well–represented in the phELVIS simulation suite. Here, we explore the impact of removing LMC satellites from our observational sample of galaxies with low tangential velocity errors.

While there is some contention over which galaxies are satellites of the LMC, the derived proper motions from *Gaia* DR2 have allowed for more direct investigation into potential associations with the LMC. In addition to Horologium I, which has been found to be a likely LMC satellite in

multiple studies [223, 67, 200, 228], Carina II, Carina III, and Hydrus I have also been classified as long–term satellites of the LMC via their *Gaia* DR2 proper motions [125, 200], where long–term is defined by being bound to the LMC for at least 2 consecutive orbits. Furthermore, [200] found another 5 galaxies to be recently–captured LMC satellites (Reticulum II and Phoenix II) or have had prior interactions with the LMC (Sculptor, Segue 1, and Tucana III).

To explore how our results may be biased by the dynamical influence of the LMC, we fully rerun our distance–matching analysis on the set of MW satellites with low tangential velocity error fractions excluding the 9 LMC–associated satellites, which includes long–term satellites plus recent satellites and LMC interactors. When excluding these systems associated with the LMC, across all 3 velocity components, the null hypothesis is rejected when comparing to subhalos drawn from the low–and high–mass hosts (i.e. $p < 0.05$), with the distribution of observed velocities for the Milky Way satellites intermediate between these two subhalo samples (i.e. again favoring an intermediate–mass Milky Way). However, while the radial velocity distribution for subhalos drawn from the intermediate–mass sample is visually consistent with that of the Milky Way satellite population when excluding the LMC–associated satellites, we find that the tangential and total velocities are less consistent (as compared to the distributions in Fig. 3.4). As seen in Fig. 3.5 and Table 3.9, the intermediate–mass host samples yield non–rejected p–values, $p \geq 0.05$, when comparing to the observed radial, tangential and total velocities. Overall, when satellites associated with the LMC are removed from our analysis, the distance–matched subhalos continue to show a preference for an intermediate–mass host halo ($\sim 1 - 1.2 \times 10^{12}$ $M_\odot$).

So far in this work, all distance–matched subhalos are selected according to a peak maximum circular velocity limit of $V_{\rm peak} > 6$ km s^{-1}. As shown by [97], the abundance of Milky Way satellites can be reproduced with subahlos down to $V_{\rm peak} > 10$ km s^{-1} when excluding those systems associated with the LMC. While this more restrictive subhalo selection roughly quarters the subhalo populations, only Draco II does not have at least 10 subhalos in its distance bin across all host mass sets. As shown in Table 3.9, when limiting subhalos to $V_{\rm peak} > 10$ km s^{-1}, our

results are are clouded. The high–mass host samples are inconsistent with the observed Milky Way satellites across all 3 velocity measures. Meanwhile, the subhalos drawn from the low–and intermediate–mass hosts are consistent with the observed radial velocities, but unable to reproduce the tangential and total velocity distributions of the Milky Way satellites.

3.5.2 Pericentric Passage, Eccentricity & Satellite Infall

To explore the orbits of the observed MW satellites in various dark matter halo potentials, we calculate pericenters and orbital eccentricities for a low–, intermediate–, and high–mass MW potential using GALPY [24]. Assuming an NFW profile with a concentration of 15.3 along with the EDR3 proper motions and other satellite properties from the literature (i.e. RA, Dec, heliocentric distance, and line–of–sight velocity), we adopt 3 host potentials based on the average halo masses from our 3 host sets — i.e. average masses of 0.835, 1.120, 1.675×10^{12} $M_\odot$. The resulting inferred orbital properties (3 pericenters and 3 eccentricities) for the MW satellites can be found in Table 3.5 and 3.7.

Comparing the resulting 3 pericenteric passages derived using GALPY, there is a mild preference for smaller pericenters in increasing host potentials — e.g. for satellites $30 - 60$ kpc from the center of the Milky Way, the median pericenter in the largest host potential is $\sim$ 30 kpc, while the median in the smallest potential is $\gtrsim$ 35 kpc. This host mass–pericenter correlation is not as strong amongst the distance–matched phELVIS subhalos, where the median pericenters in this same distance bin ($30 - 60$ kpc) is roughly half the spread of that seen in the GALPY pericenters. While these predicted pericenters for all 44 satellites decrease with increasing host potential, the correlation between orbital eccentricity and host halo mass is more complicated. As illustrated in Fig. 3.6, for satellites currently in the outer MW halo ($70 < D_{\rm MW}/{\rm kpc} < 300$), there is not a strong correlation between host potential and orbital eccentricity. In the inner MW halo ($D_{\rm MW} < 70$ kpc), however, there is a clear negative correlation, such that eccentricity decreases with increasing host

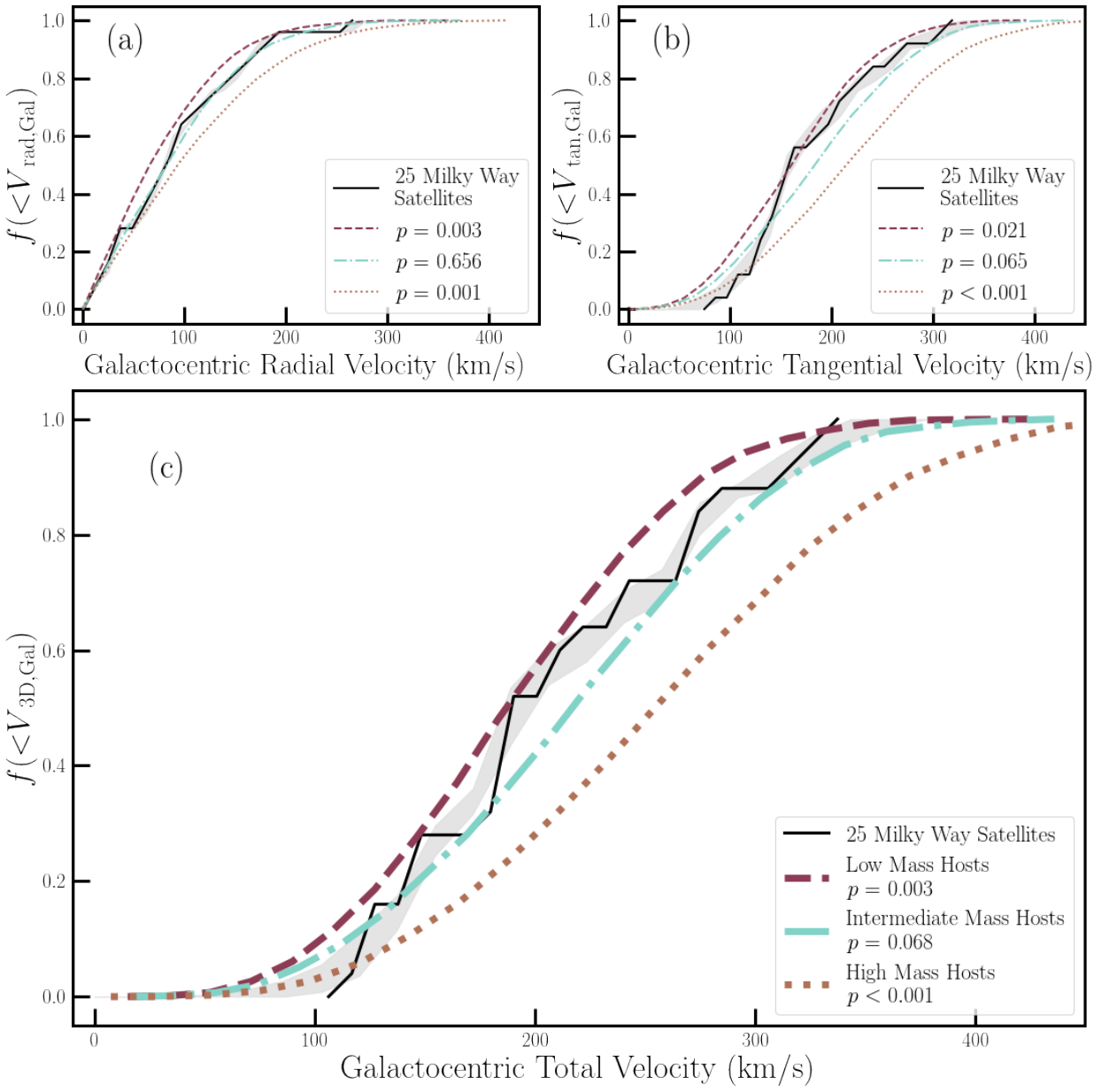

Figure 3.5: Cumulative distributions of individual Galactocentric velocity components for the set of (25) satellite galaxies excluding all 9 LMC–associated systems (and excluding satellites with proportionally high tangential velocity errors). The color coding, line style, and legend conventions are identical to Fig. 3.3. The exclusion of the 9 LMC–associated systems does not change the intermediate host mass preference. Across all 3 velocity component comparisons, the p–values for the low–and high–mass host halos are rejected ($p < 0.05$) while the intermediate–mass host halo p–values are above the significance limit.

potential for $\sim$ 75% of the satellites — i.e. orbits become more circular in greater potentials. The preferential circularization of orbits with increasing host mass is likely the result of satellite disruption associated with tidal forces. At a given host–centric distance within the inner halo, surviving satellites of more massive hosts tend to populate circular orbits, as tidal destruction has preferentially destroyed systems on more plunging orbits.

Beyond pericenter and eccentricity, another critical orbital parameter is the infall time onto the Milky Way (or host halo). Within the simulations, we are able to directly trace the infall of subhalos, such that infall time is defined as the lookback time when a subhalo *first* crossed the host halo's virial radius. For observed satellites of the MW, on the other hand, constraining the infall time is more challenging (given that we lack a DeLorean and a flux capacitor). Using *Gaia* proper motions from [83] to estimate the binding energy of each Milky Way satellite, [72] estimate the infall time according to a correlation between infall time and binding energy derived for subhalos in the phELVIS simulations [see also 215]. When computing the binding energy of the Milky Way satellites, [72] assume a host halo mass of 1.3×10^{12} $M_{\odot}$, which is directly between that of our intermediate–and high–mass host halo samples. As illustrated in Fig. 3.7, however, the distribution of infall times within phELVIS is largely independent of host mass.

For the 26 MW satellites with proportionally low tangential velocity errors and infall times estimated by [72], we draw distance–matched subhalo samples as described in §3.3. Figure 3.7 shows the distribution of infall times for these subsamples alongside that of the Milky Way satellites, as estimated by [72]. The inferred infall times for the MW satellite population are skewed to earlier cosmic times relative to the distance–matched samples of subhalos drawn from phELVIS. While the infall time for some of the MW satellites is quite well constrained, such as Leo I [27, 243], the disagreement between the cumulative distribution of infall times in the simulations and the results of [72] may be partially driven by an underestimation of the uncertainties in infall time for a subset of systems. On the other hand, it is possible that the Milky Way may be an outlier with regard to its accretion history, such that a larger fraction of its satellites were accreted at early cosmic

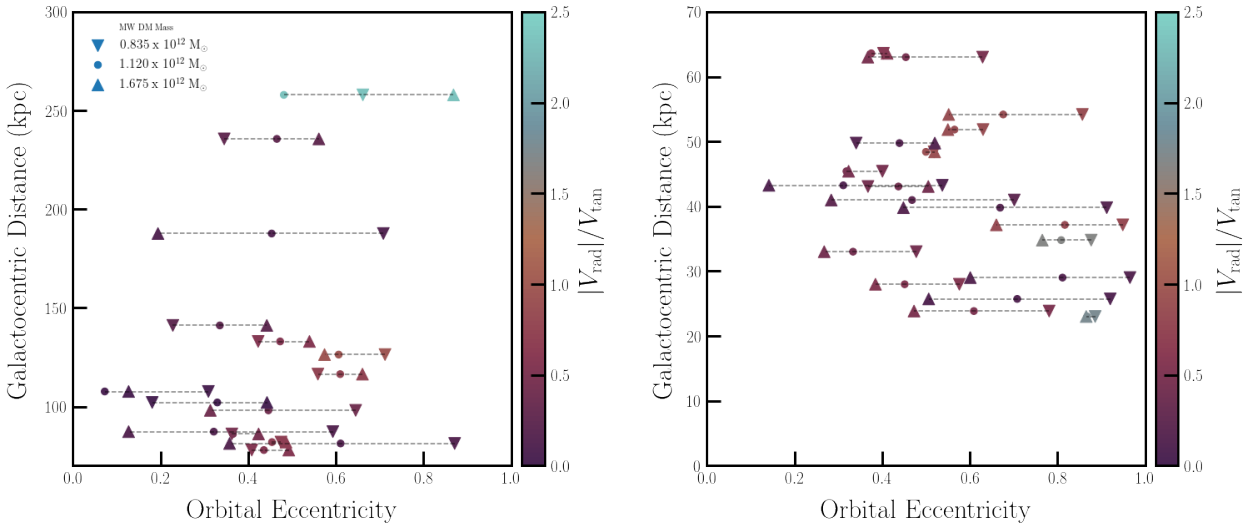

Figure 3.6: Galactocentric distance against orbital eccentricity for the MW satellites with proportionally low tangential velocity errors color coded by the ratio of Galactocentric radial velocity versus tangential velocity. The satellites are separated into two groups: *(left panel)* systems outside 70 kpc and *(right panel)* systems inside 70 kpc. These figures display trends in eccentricity — decreasing eccentricity with increasing MW dark matter halo mass for those systems inside 70 kpc *(right panel)* and the lack of a strong trend in eccentricity for those systems outside 70 kpc *(left panel)*. As seen by the color coding, $|V_{\rm rad}|/V_{\rm tan} > 1$ indicates more radial orbits while those < 1 point towards more circular orbits. Eccentricity may serve well as host mass diagnostics.

time, potentially via correlated accretion of substructures [66, 62]. While the likely recent infall of the LMC (and associated satellites) would counter this potential bias in accretion history to some degree [19, 126], the *possibly* anomalous satellite quenched fraction for the Milky Way might serve as further evidence of a bias towards early accretion — and excess quenching — relative to other nearby Milky Way–like systems [278, 74, 93].

3.5.3 Observational Completeness

With many new satellite galaxy discoveries within the past 2 decades [285, 279, 280, 287, 288, 16, 13, 61], the debate related to the observational completeness of the MW satellite population has been revived [254, 264, 266, 101, 91, 190, 116, 224, 42]. By matching our subhalo subsamples to the observed MW satellite population based on host–centric distance, our analysis effectively minimizes any systematic bias associated with incompleteness. To more fully explore the potential

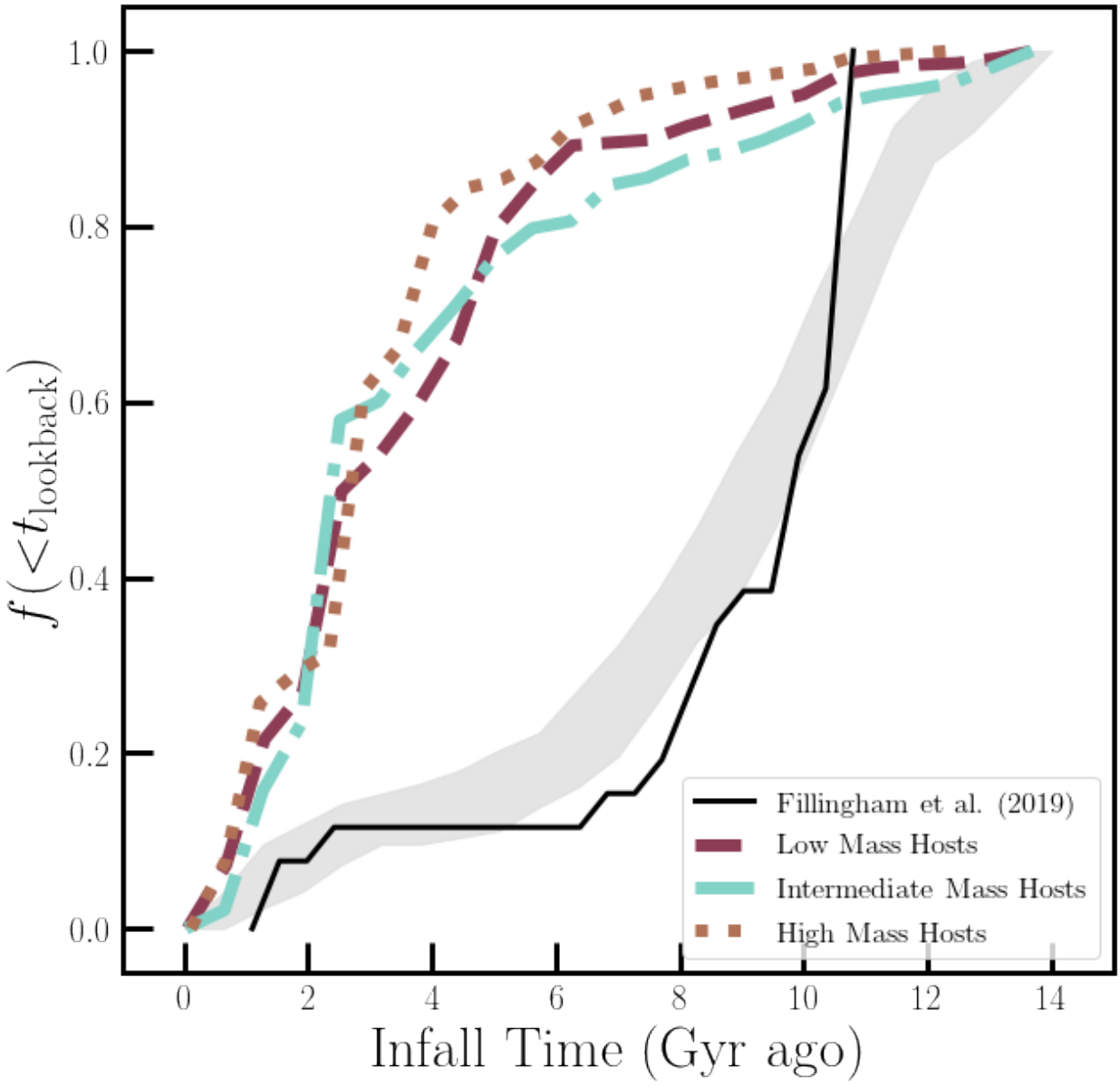

Figure 3.7: Cumulative distribution of satellite/subhalo infall times. The solid black line shows the cumulative distribution of first infall times for 26 MW satellites with low tangential velocity errors, as inferred by [72]. The grey shaded region is the cumulative distribution of the range of 500 randomly sampled values from each of the 26 systems' reported errors. The dashed burgundy line, dash–dotted aqua line, and the dotted sienna line are the corresponding distributions for distance–matched subhalos belonging to our adopted host–mass bins. As a whole, the distribution of infall times, as inferred from *Gaia* proper motions, does not match that found in the simulations, with the simulations favoring later (i.e. more recent) infall times.

impact of observational completeness on our results, however, we limit the Milky Way satellite population (and corresponding subhalo samples from phELVIS) to systems within 100 kpc. At these Galactocentric distances ($<$ 100 kpc), the MW satellite population is relatively complete, especially in the Southern Hemisphere thanks to surveys such as the Dark Energy Survey (DES) and other imaging campaigns using the Dark Energy Camera (DECam) on the Victor M. Blanco Telescope at the Cerro Tololo Inter–American Observatory [60].

In our observational data set of systems with proportionally low tangential velocity errors, there are 25 satellite galaxies within 100 kpc. For this restricted — yet largely complete — sample, the observed velocity distributions are again inconsistent with the kinematics of subhalos drawn from the low–and high–mass host samples (see Table **??**). Meanwhile, while the distributions of observed radial velocities for the nearby Milky Way satellites and for the distance–matched phELVIS subhalos in the intermediate–mass hosts are consistent, the tangential (and total) velocity distribution for the nearby MW satellites is inconsistent ($p < 0.05$) with that of the intermediate–mass subhalo distribution. This slight disagreement between the velocity distributions is likely due to a preference for circular orbits at small host–centric distance in phELVIS, such that the distribution of $V_{\rm tan}$ is biased towards higher velocities relative to that of the observed MW satellites. This perhaps indicates that the tidal disruption of subhalos within phELVIS may be slightly over–estimated or otherwise incomplete in is characterization of orbits within the inner part of the host halo.

3.5.4 Observational Predictions

As more MW satellites are discovered through deep and wide imaging surveys, such as the Legacy Survey of Space and Time (LSST) at the Vera Rubin Observatory [113] or the Nancy Grace Roman Space Telescope [9], or via future data releases from *Gaia*, the virial mass of the Milky Way might be further refined. Fig. 3.8 attempts to illustrate the potential future refinement based on

[2]All p–values discussed in this section can be found in Table **??**.

different observable quantities. The cumulative kernel density estimates plotted trace the unmatched distribution of all halos within 350 kpc of the respective host halo from hosts split into the three mass bins used throughout this work. The low–mass (burgundy dashed lines) and high–mass (sienna dotted lines) sets are compared to the intermediate–mass (black dash–dotted lines) host halo sets across 9 subhalo (or satellite) characteristics. MWU p–values were calculated for comparisons between the subhalo distributions drawn from the low–mass and high–mass hosts relative to those in the intermediate–mass hosts. Any characteristic with rejected p–values ($p < 0.05$) stand to be good metrics to test the preferred host mass range as new data becomes available.

Galactocentric total velocity, tangential velocity, physical Galactocentric distance, and infall have the most discernible differences between the host mass sets within phELVIS. Since infall must be inferred from simulations [72] or modeling the orbital history of the satellite [e.g. 200] and thus has greater measurement uncertainty, it is likely to be of less help in discriminating between different host mass regimes. Distance and total velocity have the largest differences between subhalo distributions. Subhalos in the more massive hosts are kinematically hotter and at further distances from the center of their host halo than those in the less massive hosts. As new satellites are discovered, it will be interesting to explore their phase space, and particularly their distance and total Galactocentric velocity, to further refine the halo mass of the Milky Way.

3.6 Summary

Using the Phat ELVIS suite of N–body Milky Way–like cosmological simulations with embedded disk potentials along with the full phase–space information for Milky Way satellites from *Gaia* EDR3, we constrain the dark matter halo mass of the Milky Way and find a preferred mass range of ~ 1–1.2×10^{12} $M_\odot$. A more complete summary of our main results are as follows:

1. As illustrated in Fig. 3.4, when limiting the observed sample of Milky Way satellites to those

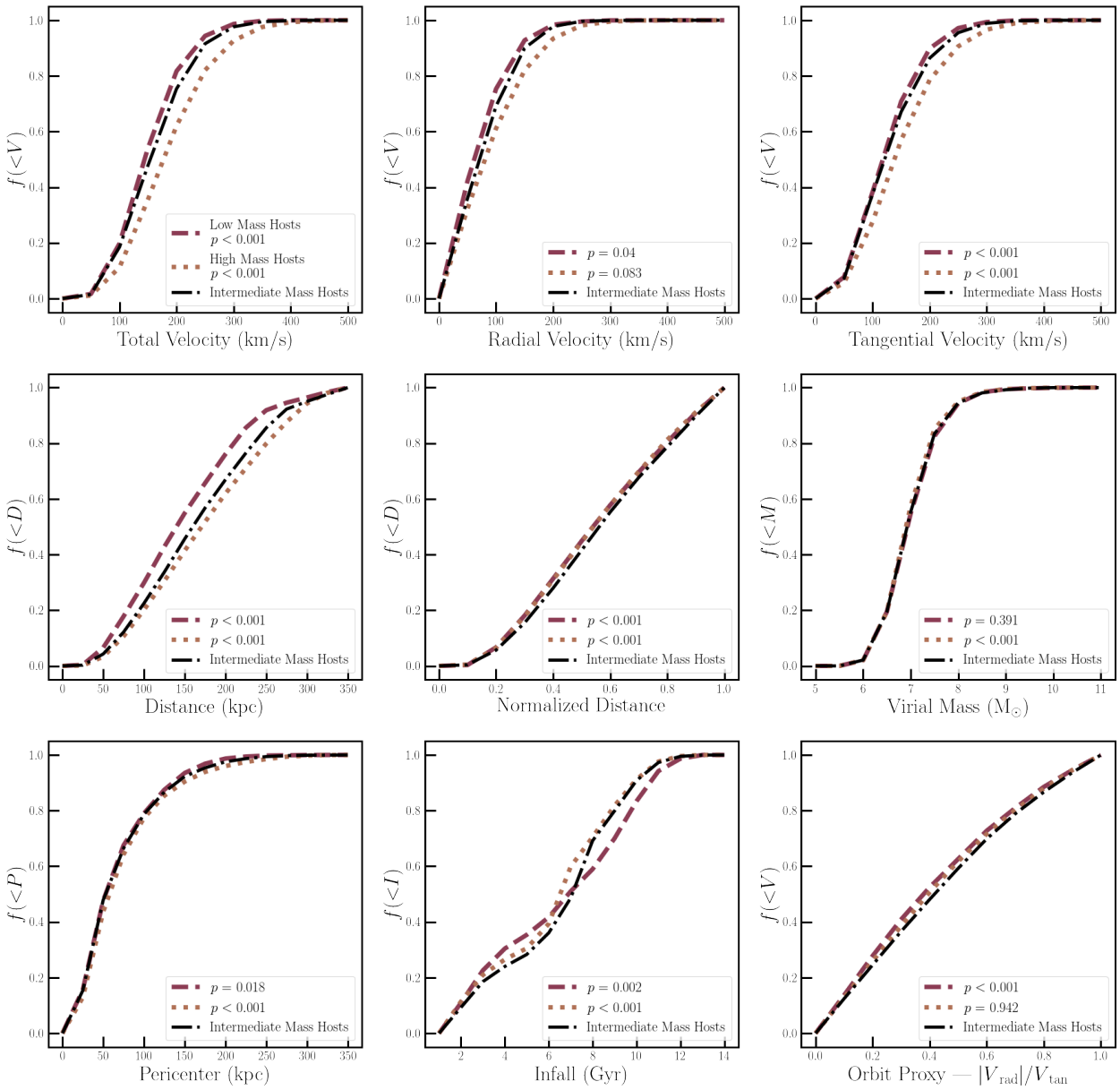

Figure 3.8: Cumulative distributions of all halos within 350 kpc of their respective host halo split into three host halo mass sets. The low mass (burgundy dashed lines) and high mass (sienna dotted lines) sets are compared to the intermediate mass (black dash–dotted lines) host halo sets across 9 subhalo properties. These plots illustrate which physical parameters of newly discovered satellites will assist us in further refining the dark matter mass content of the MW — namely two of the most straightforward to obtain properties — distance and total velocity.

systems with well–measured kinematics, we find that the observed distribution of satellite velocities ($V_{\rm rad}$, $V_{\rm tan}$, *and* $V_{\rm tot}$) are consistent with a host halo mass of $\sim 1 - 1.2 \times 10^{12}$ M$_\odot$.

2. Across all samples probed, the distribution of satellite velocities inferred from *Gaia* observations of the Milky Way satellites are inconsistent with that of subhalos populating host halos with masses $< 10^{12}$ M$_\odot$ or $> 1.2 \times 10^{12}$ M$_\odot$.

3. Excluding systems associated with the LMC does not significantly change our results, with the observed kinematics of the Milky Way satellites favoring a host halo mass of $\sim 1 - 1.2 \times 10^{12}$ M$_\odot$ when compared to distance–matched subhalo populations in phELVIS.

4. In the inner halo ($D_{\rm MW} < 100$ kpc), we find a correlation between host mass and the eccentricity of satellite orbits (as predicted by GALPY), such that at a given Galactocentric distance increasingly circular orbits are found in higher-mass hosts. This is likely a consequence of subhalo destruction preferentially removing satellites on more radial orbits in more massive hosts.

5. The distribution of infall times inferred from *Gaia* phase–space measures [72] are systematically skewed towards early cosmic times (i.e. early accretion) relative to that of distance–matched subhalos drawn from the phELVIS simulation suite.

6. The distribution of pericentric distances for subhalos in phELVIS show little dependence on host mass, in contrast to the expectations from GALPY that favor smaller pericentric distances for satellites in more massive host halos.

7. Looking towards the discovery of future Milky Way satellites, likely to be at the smallest galactic scales, by next–generation observational facilities, we show that the observed distribution of Galactocentric total velocity and Galactocentric distance stand to be good metrics to test the preferred host mass range for the Milky Way.

Galaxy	Confirmed?	$\mu_\alpha \cos\delta$ (mas / yr)	μ_δ (mas / yr)	$D_{\rm MW}$ (kpc)
Antlia II	Y	-0.09±0.01	0.12±0.01	133.0±6.0
Aquarius II	Y	-0.17±0.1	-0.43±0.08	105.3±3.3
Boötes I	Y	-0.39±0.01	-1.06±0.01	63.6±2.0
Boötes II	Y	$-2.33^{+0.09}_{-0.08}$	-0.41±0.06	39.8±1.0
Canes Venatici I	Y	-0.11±0.02	-0.12±0.02	210.8±6.0
Canes Venatici II	Y	-0.15±0.07	-0.27±0.06	160.6±4.0
Carina	Y	0.53±0.01	0.12±0.01	107.6±5.0
Carina II	Y	1.88±0.01	0.13±0.02	37.1±0.6
Carina III	Y	3.12±0.05	$1.54^{+0.06}_{-0.07}$	29.0±0.6
Columba I	P	0.19±0.06	-0.36±0.06	187.6±10.0
Coma Berenices	Y	0.41±0.02	-1.71±0.02	43.2±1.5
Crater II	Y	-0.07±0.02	-0.11±0.01	116.4±1.1
Draco	Y	0.042±0.005	-0.19±0.01	82.0±6.0
Draco II	P	1.08±0.07	0.91±0.08	23.9±3.8
Fornax	Y	0.382±0.001	-0.359±0.002	141.1±3.0
Grus I	P	0.07±0.05	$-0.29^{+0.06}_{-0.07}$	116.2±11.5
Grus II	P	0.38±0.03	-1.46±0.04	48.4±5.0
Hercules	Y	-0.03±0.04	-0.36±0.03	126.3±6.0
Horologium I	Y	0.82±0.03	-0.61±0.03	87.3±12.0
Horologium II	P	$0.76^{+0.2}_{-0.29}$	$-0.41^{+0.23}_{-0.21}$	79.1±7.5
Hydra II	P	-0.34±0.1	$-0.09^{+0.08}_{-0.09}$	148.1±7.5
Hydrus I	Y	3.79±0.01	-1.5±0.01	25.7±0.5
Leo I	Y	-0.05±0.01	-0.11±0.01	257.9±15.5
Leo II	Y	-0.14±0.02	-0.12±0.02	235.6±14.0
Leo IV	Y	-0.08±0.09	-0.21±0.08	154.6±5.0
Leo V	Y	-0.06±0.09	$-0.25^{+0.09}_{-0.08}$	169.8±4.0
Phoenix II	Y	0.48±0.04	-1.17±0.05	81.3±4.0
Pisces II	Y	0.11±0.11	$-0.24^{+0.12}_{-0.11}$	182.1±15.0
Reticulum II	Y	2.39±0.01	-1.36±0.02	33.0±1.4
Reticulum III	P	0.36±0.14	$0.05^{+0.19}_{-0.25}$	92.0±13.0
Sagittarius II	Y	-0.77±0.03	-0.89±0.02	63.0±2.3
Sculptor	Y	0.099±0.002	-0.16±0.002	86.1±5.0
Segue 1	Y	-2.21±0.06	-3.34±0.05	28.0±1.9
Segue 2	Y	1.47±0.04	-0.31±0.04	43.1±3.0
Sextans I	Y	-0.41±0.01	0.04±0.01	98.1±3.0

Table 3.1: Properties of the MW Satellite Galaxies (Part 1) used in this work. Column (1) Status of whether the system is a spectroscopically confirmed galaxy or not (i.e. Y = confirmed galaxy and P = not confirmed but probably a galaxy). Columns (2) & (3) Proper motions derived by [174] from *Gaia* EDR3 in mas yr^{-1}. Column (4) Galactocentric distance with errors in kpc.

Table 3.2: MW Satellite Phase Space Properties Part 1 *Continued*

Galaxy	Confirmed?	$\mu_\alpha \cos\delta$ (mas / yr)	μ_δ (mas / yr)	$D_{\rm MW}$ (kpc)
Triangulum II	P	0.56±0.05	0.07±0.06	34.8±1.6
Tucana II	Y	0.9±0.02	-1.26±0.02	54.2±7.9
Tucana III	P	-0.08±0.01	-1.62±0.02	23.0±1.9
Tucana IV	Y	0.54±0.06	-1.67±0.07	45.4±3.9
Tucana V	P	$-0.14^{+0.06}_{-0.05}$	$-1.15^{+0.08}_{-0.06}$	51.8±8.9
Ursa Major I	Y	-0.39±0.03	-0.63±0.03	102.1±5.8
Ursa Major II	Y	1.72±0.02	-1.89±0.03	41.0±1.9
Ursa Minor	Y	-0.124±0.004	0.078±0.04	77.9±4.0
Willman 1	Y	0.21±0.06	-1.08±0.09	49.7±9.9

Galaxy	$V_{\rm rad}$	$V_{\rm tan}$ (km / s)	$V_{\rm 3D}$ (km / s)	Notes (km / s)
Antlia II	70.4±0.5	125.0±6.1	143.5±5.3	1
Aquarius II	30.4±7.2	157.0±51.6	159.9±50.7	3
Boötes I	91.2±2.1	156.0±3.0	180.7±2.8	1
Boötes II	-54.3±3.9	$319.0^{+17.9}_{-16.0}$	$323.6^{+17.6}_{-15.8}$	1
Canes Venatici I	78.2±0.5	69.0±22.5	104.3±14.9	
Canes Venatici II	-96.7±0.2	31.0±62.9	101.5±19.2	
Carina	8.5±0.3	187.0±7.6	187.2±7.6	1
Carina II	219.5±1.9	268.0±3.8	346.4±3.2	1,2
Carina III	58.7±4.7	$395.0^{+12.4}_{-12.5}$	$399.3^{+12.3}_{-12.4}$	1,2
Columba I	-22.8±6.8	205.0±52.4	206.3±52.1	
Coma Berenices	31.9±0.7	264.0±4.2	265.9±4.2	1
Crater II	-76.0±-0.1	102.0±9.4	127.2±7.5	1

Table 3.3: Properties of the MW Satellite Galaxies (Part 2) used in this work. Column (1) Status of whether the system is a spectroscopically confirmed galaxy or not (i.e. Y = confirmed galaxy and P = not confirmed but probably a galaxy). Columns (2) –(4) Radial, tangential and total velocities, respectively, in the Galactocentric frame of reference, all in km s^{-1}. Galactocentric distance and radial velocity were converted from the heliocentric frame of reference using `astropy` and quantities from MCV20a, MCV20b and the heliocentric distances referenced in §3.2.1. Galactocentric tangential velocity was converted from the Galactocentric tangential velocity components provided in MCV20a. Total velocity was then calculated from its two components. Column (5) indicates the various subgroups a galaxy belongs to which are used throughout this work. 1 indicates belonging to the group of systems with proportionally low tangential velocity errors. 2 indicates the system is a long term satellite of the LMC as determined by [200]. 3 indicates the system is a short term satellite or recent interactor with the LMC as determined by [200].

Table 3.4: MW Satellite Phase Space Properties Part 2 *Continued*

Galaxy	V_{rad}	V_{tan} (km / s)	V_{3D} (km / s)	Notes (km / s)
Draco	-103.0±0.4	156.0±1.4	186.9±1.2	1
Draco II	-156.6±1.6	299.0±15.0	337.5±13.3	1
Fornax	-34.5±0.2	142.0±0.0	$146.1^{+5.3}_{-0.0}$	1
Grus I	-187.3±4.3	$71.0^{+38.0}_{-41.3}$	$200.3^{+14.1}_{-15.2}$	
Grus II	-124.8±1.7	139.0±10.2	186.8±7.7	1
Hercules	141.1±1.3	146.0±24.4	203.0±17.6	1
Horologium I	-28.4±4.3	193.0±15.9	195.1±15.8	1,2
Horologium II	29.1±25.0	$128.0^{+111.9}_{-157.7}$	$131.3^{+109.3}_{-153.8}$	
Hydra II	136.6±0.7	$97.0^{+71.8}_{-72.6}$	$167.5^{+41.6}_{-42.0}$	
Hydrus I	-40.1±1.4	363.0±5.0	365.2±4.9	1,2
Leo I	174.7±0.1	75.0±12.1	190.1±4.8	1
Leo II	26.5±0.3	103.0±22.6	106.3±21.9	1
Leo IV	8.6±0.2	52.0±63.8	52.7±62.9	
Leo V	55.8±1.6	$69.0^{+83.5}_{-78.6}$	$88.8^{+64.9}_{-61.1}$	
Phoenix II	-38.1±5.9	271.0±20.7	273.7±20.6	1,3
Pisces II	-75.7±8.7	$47.0^{+102.1}_{-93.7}$	$89.1^{+54.3}_{-49.9}$	
Reticulum II	-92.2±1.7	214.0±2.2	233.0±2.1	1,3
Reticulum III	113.4±17.9	$78.0^{+83.1}_{-109.1}$	$137.6^{+49.4}_{-63.6}$	
Sagittarius II	-115.7±1.8	239.0±10.4	265.5±9.4	1
Sculptor	76.3±0.3	163.0±0.0	180.0±0.1	1,3
Segue 1	136.9±0.0	240.0±6.5	276.3±5.7	1,3
Segue 2	59.9±5.0	134.0±7.2	146.8±6.9	1
Sextans I	88.1±0.1	220.0±4.0	237.0±3.7	1
Triangulum II	-265.6±3.2	159.0±8.9	309.5±5.3	1
Tucana II	-182.0±4.6	210.0±8.1	277.9±6.9	1
Tucana III	-223.4±2.6	126.0±2.0	256.5±2.5	1,3
Tucana IV	-90.6±5.3	197.0±16.0	216.9±14.7	1
Tucana V	-157.8±5.9	$181.0^{+30.9}_{-24.9}$	$240.1^{+23.6}_{-19.1}$	1
Ursa Major I	-0.8±0.7	126.0±20.8	126.0±20.8	1
Ursa Major II	-64.5±1.6	262.0±6.5	269.8±6.4	1
Ursa Minor	-83.4±1.4	148.0±0.0	169.9±0.7	1
Willman 1	16.7±1.9	120.0±17.5	121.2±17.3	1

Galaxy	$D_{\rm peri,l}$ (kpc)	$D_{\rm peri,i}$ (kpc)	$D_{\rm peri,h}$ (kpc)
Antlia II	69.8±13.1	54.9±10.8	43.4±8.3
Aquarius II	92.7±-45.2	72.5±-35.8	54.6±-25.5
Boötes I	43.9±3.1	37.4±3.2	30.8±2.9
Boötes II	39.1±1.0	39.0±1.0	38.8±1.1
Canes Venatici I	47.4±33.4	37.8±25.7	30.7±19.8
Canes Venatici II	9.8±32.0	8.3±25.5	7.2±20.4
Carina	107.3±5.1	106.5±5.7	83.6±25.3
Carina II	37.1±0.6	27.0±0.7	25.9±0.7
Carina III	28.9±0.6	28.5±0.6	28.4±0.6
Columba I	185.7±10.7	185.0±10.8	182.8±10.7
Coma Berenices	42.5±1.6	42.3±1.6	41.4±1.9
Crater II	39.9±8.4	31.9±6.5	25.8±5.0
Draco	49.0±5.9	41.2±5.3	33.8±4.3
Draco II	19.9±4.3	19.4±4.4	18.7±4.6
Fornax	98.7±12.6	73.4±10.1	55.9±7.2
Grus I	17.1±9.2	14.7±7.8	12.7±6.5
Grus II	26.0±9.4	22.4±9.0	18.9±7.8
Hercules	70.2±62.3	61.4±13.2	52.0±12.5
Horologium I	86.1±12.7	85.6±13.1	83.3±15.2
Horologium II	49.3±37.2	37.4±44.9	29.3±50.4
Hydra II	62.6±-7.5	52.8±-6.8	43.8±-5.7
Hydrus I	25.5±0.5	25.5±0.5	25.5±0.5
Leo I	257.7±15.5	257.7±15.5	35.6±6.4
Leo II	120.3±24.0	88.1±16.4	67.2±11.6
Leo IV	20.2±107.7	16.5±72.9	13.7±52.7
Leo V	32.5±89.2	26.1±70.1	21.3±52.8
Phoenix II	80.3±4.3	80.1±4.4	79.6±4.6
Pisces II	28.7±108.7	23.3±88.5	19.2±68.0
Reticulum II	28.7±2.3	27.3±2.7	24.8±3.3
Reticulum III	17.2±87.7	14.4±58.5	12.1±52.9
Sagittarius II	51.1±2.1	48.0±2.0	43.1±1.8
Sculptor	58.9±1.6	48.4±1.1	38.8±0.8
Segue 1	21.4±3.1	20.2±3.5	18.5±3.8
Segue 2	22.1±8.3	17.9±6.8	14.7±5.4
Sextans I	97.9±3.0	82.5±3.9	75.4±4.5

Table 3.5: Orbital Properties of the MW Satellite Galaxies used in this work. Columns (1) –(3) Pericentric passage distances, in kpc, for each system in a low, intermediate and high MW potential, with an NFW profile and concentration of 15.3, via GALPY. The corresponding MW dark matter halo masses used for the 3 potentials are $0.835, 1.120, 1.675 \times 10^{12}$ $M_\odot$, respectively. These are the average masses of the hosts in each of our fiducial phELVIS host sets.

Table 3.6: MW Satellite Orbital Properties *Continued*

Galaxy	$D_{\rm peri,l}$ (kpc)	$D_{\rm peri,i}$ (kpc)	$D_{\rm peri,h}$ (kpc)
Triangulum II	11.7±1.3	10.7±1.2	9.7±1.1
Tucana II	38.6±11.9	36.6±12.6	33.8±13.4
Tucana III	3.0±0.6	2.8±0.4	2.5±0.5
Tucana IV	36.1±6.3	32.5±7.1	27.6±7.0
Tucana V	27.9±9.4	24.7±8.7	21.4±7.7
Ursa Major I	70.6±3.7	51.4±2.6	39.3±1.9
Ursa Major II	39.3±2.2	38.9±2.4	38.1±2.7
Ursa Minor	44.8±8.1	36.4±7.0	29.5±5.6
Willman 1	24.6±21.4	19.4±15.2	15.7±11.2

Galaxy	$e_{\rm l}$	$e_{\rm i}$	$e_{\rm h}$	$t_{\rm infall}$ (Gyr)
Antlia II	0.4±-0.0	0.5±-0.0	0.5±-0.0	–
Aquarius II	0.2±0.3	0.2±0.3	0.3±0.3	$1.6^{+5.4}_{-3.5}$
Boötes I	0.4±0.0	0.4±-0.0	0.4±-0.0	$10.7^{+0.6}_{-1.9}$
Boötes II	0.9±-0.0	0.7±-0.0	0.4±-0.0	1.1±0.6
Canes Venatici I	0.7±-0.1	0.7±-0.1	0.8±-0.1	$9.4^{+0.9}_{-2.3}$
Canes Venatici II	0.9±-0.2	0.9±-0.2	0.9±-0.2	$9.0^{+1.0}_{-2.8}$
Carina	0.3±0.2	0.1±0.1	0.1±-0.1	$9.9^{+0.6}_{-2.7}$
Carina II	0.9±0.0	0.8±0.0	0.7±0.0	$7.9^{+2.5}_{-2.4}$
Carina III	1.0±0.0	0.8±0.1	0.6±0.1	$7.6^{+2.4}_{-2.7}$
Columba I	0.7±-0.0	0.5±-0.1	0.2±-0.1	–
Coma Berenices	0.5±0.1	0.3±0.1	0.1±0.0	$10.2^{+2.6}_{-3.3}$
Crater II	0.6±-0.1	0.6±-0.1	0.7±-0.0	$7.8^{+2.7}_{-3.0}$

Table 3.7: Orbital and Infall Properties of the MW Satellite Galaxies used in this work. Columns (1) –(3) Orbital eccentricities for each system in the three GALPY MW potentials, with smaller eccentricities corresponding to more circular orbits and larger eccentricities corresponding to more radial/plunging orbits. Column (4) Satellite infall times, in Gyr, as derived by [72].

Table 3.8: MW Satellite Orbital & Infall Properties *Continued*

Galaxy	$e_{\rm l}$	$e_{\rm i}$	$e_{\rm h}$	$t_{\rm infall}$ (Gyr)
Draco	0.5±0.0	0.5±-0.0	0.5±-0.0	$10.4^{+2.4}_{-3.1}$
Draco II	0.8±0.1	0.6±0.1	0.5±0.1	$10.2^{+1.8}_{-2.4}$
Fornax	0.2±-0.0	0.3±-0.0	0.4±-0.0	$10.7^{+0.8}_{-3.1}$
Grus I	0.9±-0.0	0.9±-0.0	0.9±-0.0	$1.1^{+1.0}_{-0.9}$
Grus II	0.5±0.0	0.5±-0.1	0.5±-0.1	–
Hercules	0.7±-0.1	0.6±0.0	0.6±-0.0	$6.6^{+2.3}_{-0.7}$
Horologium I	0.6±0.3	0.3±0.4	0.1±0.3	$8.8^{+1.8}_{-2.0}$
Horologium II	0.3±0.5	0.4±0.1	0.5±-0.2	–
Hydra II	0.7±0.0	0.7±0.0	0.7±0.0	$9.4^{+1.7}_{-1.8}$
Hydrus I	0.9±0.0	0.7±0.0	0.5±0.0	$10.7^{+1.3}_{-1.4}$
Leo I	0.7±0.0	0.5±0.0	0.9±-0.0	$10.5^{+1.5}_{-2.4}$
Leo II	0.3±-0.1	0.5±-0.0	0.6±-0.0	$2.3^{+0.6}_{-0.5}$
Leo IV	0.8±-0.7	0.8±-0.5	0.8±-0.4	$7.8^{+3.3}_{-2.0}$
Leo V	0.7±-0.4	0.7±-0.4	0.8±-0.3	10.4±1.4
Phoenix II	0.9±0.0	0.6±0.1	0.4±0.1	–
Pisces II	0.8±-0.4	0.8±-0.4	0.8±-0.4	–
Reticulum II	0.5±0.1	0.3±0.0	0.3±0.0	8.3±1.8
Reticulum III	0.8±-0.1	0.8±-0.2	0.8±-0.3	–
Sagittarius II	0.6±0.0	0.5±-0.0	0.4±-0.0	–
Sculptor	0.4±0.0	0.4±0.0	0.4±0.0	$10.6^{+1.6}_{-1.9}$
Segue 1	0.6±0.1	0.5±0.1	0.4±0.0	$9.9^{+1.7}_{-2.9}$
Segue 2	0.4±-0.1	0.4±-0.1	0.5±-0.1	$10.8^{+1.3}_{-1.4}$
Sextans I	0.6±0.1	0.4±0.0	0.3±0.0	$10.8^{+1.6}_{-1.9}$
Triangulum II	0.9±-0.0	0.8±-0.0	0.8±-0.0	$8.4^{+2.7}_{-0.9}$
Tucana II	0.9±0.1	0.7±0.2	0.6±0.1	$9.5^{+1.5}_{-2.1}$
Tucana III	0.9±-0.0	0.9±-0.0	0.9±-0.0	–
Tucana IV	0.4±0.1	0.3±-0.0	0.3±-0.0	–
Tucana V	0.6±0.0	0.6±-0.0	0.6±-0.0	–
Ursa Major I	0.2±0.0	0.3±0.0	0.4±0.0	$9.5^{+2.4}_{-2.8}$
Ursa Major II	0.7±0.1	0.5±0.1	0.3±0.1	$1.5^{+5.1}_{-1.6}$
Ursa Minor	0.4±-0.0	0.4±-0.0	0.5±-0.0	$10.7^{+1.4}_{-2.3}$
Willman 1	0.3±-0.2	0.4±-0.2	0.5±-0.1	$10.7^{+1.7}_{-2.0}$

	D_{MW}	V_{Rad}	V_{Tan}	V_{3D}
All Satellites (44) to Unmatched Subhalos				
Low Mass Hosts	< 0.001	< 0.001	< 0.001	< 0.001
Intermediate Mass Hosts	< 0.001	0.003	< 0.001	< 0.001
High Mass Hosts	< 0.001	0.367	< 0.001	< 0.001
Satellites with Proportionally Low Tangential Velocity Errors (LTVE) (34) to Unmatched Subhalos				
Low Mass Hosts	< 0.001	< 0.001	< 0.001	< 0.001
Intermediate Mass Hosts	< 0.001	0.001	< 0.001	< 0.001
High Mass Hosts	< 0.001	0.384	< 0.001	< 0.001
All Satellites (44)				
Low Mass Hosts	0.829	< 0.001	0.125	0.005
Intermediate Mass Hosts	0.812	0.727	0.004	0.015
High Mass Hosts	0.788	< 0.001	< 0.001	< 0.001
Satellites with Proportionally Low Tangential Velocity Errors (LTVE) (34)				
Low Mass Hosts	0.770	< 0.001	0.002	< 0.001
Intermediate Mass Hosts	0.744	0.875	0.076	0.115
High Mass Hosts	0.719	< 0.001	< 0.001	< 0.001
LTVE Satellites Excluding Satellites Associated with the LMC (25)				
Low Mass Hosts	0.834	0.003	0.021	0.003
Intermediate Mass Hosts	0.800	0.656	0.065	0.068
High Mass Hosts	0.814	0.001	< 0.001	< 0.001
LTVE Satellites with D_{MW} < 100 kpc (25)				
Low Mass Hosts	0.644	< 0.001	0.012	< 0.001
Intermediate Mass Hosts	0.641	0.061	0.005	0.044
High Mass Hosts	0.565	0.032	< 0.001	< 0.001
LTVE Satellites Excluding Satellites Associated with the LMC and using limit of V_{peak} > 10 km s^{-1} (25)				
Low Mass Hosts	0.769	0.060	0.015	0.003
Intermediate Mass Hosts	0.798	0.055	0.049	0.008
High Mass Hosts	0.730	< 0.001	< 0.001	< 0.001

Table 3.9: Mann–Whitney U Test p–values for the observation to distance–matched subhalo comparisons. The reported p–values are the harmonic means of 500 MWU Tests conducted on sets of $10N$ distance–matched subhalo properties and $10N$ MW satellite properties drawn from the properties' errors. These p–values are two–sided, i.e. $p_{max} = 1$. Our statistical significance level is set at $p = 0.05$. Values below this level reject the null hypothesis that the two compared distributions are drawn from the same parent population. Values above our chosen significance level signify that the null hypothesis cannot be rejected and are highlighted in yellow. Values are reported for our fiducial phELVIS host sets for all the various groups of satellites discussed throughout the paper.

Chapter 4

Star Stuff at the Smallest Scales: Detailed Chemical Abundances in Hydrus I

4.1 Introduction

While the entirety of the Local Group serves as a cosmic Rosetta Stone, ultra–faint dwarf galaxies (UFDs) do so at the smallest of galactic scales. UFDs serve as windows into the earliest stages of star and galaxy formation in the Universe [136, 79, 92, 271, 282, 117]. Relatively little is known about this elusive set of galaxies, though. The first UFD was discovered in the Sloan Digital Sky Survey in 2005 and since then more than 40 ultra–faint systems have been discovered and either spectroscopically confirmed as a galaxy or are at least probably galaxies, as opposed to globular clusters [279, 280, 235]. Thus far the study of UFDs has largely focused on discovery, determination of "galaxy–hood" and characterization of the galaxy's elemental abundances. Detailed chemical abundances, especially in these ancient systems, illuminate early Universe chemical evolution and nucleosynthesis events — the formation scenarios of the first stars and galaxies.

The preliminary work presented here details chemical abundances in 3 member stars in the Hydrus

I system, a satellite of the Large Magellanic Cloud (LMC) [125, 200]. Of the nearly 50 confirmed UFDs, Hydrus I (Hyi I) is only the 20th to have chemical abundance measurements of any member stars [235, 121]. This chapter reports on the observations and data reduction of 11 member stars of Hyi I and on some detailed chemical abundances of 3 of the 11 member stars.[1]

4.2 Observations & Data Reduction

11 member stars in Hyi I were observed over 3 nights on the Michigan/Magellan Fiber Spectrograph (M2FS) [171] and the Magellan Inamori Kyocera Echelle (MIKE) [18] spectrograph on the Magellan/Clay Telescope in Chile. The combined exposure time was 6.25 hours with 95μm slits and the seeing ranged from 1.5 – 0.6. Tables 4.1 and 4.2 detail some of the observational data used with more data presented for the 3 stars observed with the MIKE spectragraph, as those observations are fully reduced and analysis is mostly complete. The spectra taken with the MIKE instrument were reduced with CarPy [129], while the M2FS data was reduced using the just completed M2FS Reduction Pipeline[2].

To complete reduction on this data, updates to the pipeline were required — namely, the inclusion of a Coherent Point Drift Algorithm. Over the several nights of observations, the fiber placement on the instrument was slightly shifted resulting in mismatched arc frames which were then unable to be used in wavelength calibration. A Coherent Point Drift (CPD) algorithm is the perfect solution to correcting this mismatch! Commonly used in facial recognition software, this algorithm takes a skewed, or otherwise altered, set of source data points and calculates the path needed to shift the source points to match in bulk a set of reference points. We implemented a CPD algorithm built on Fast Fourier Transforms to achieve the quickest possible mismatch correction. This updated version of the reduction pipeline will be made publicly available in the coming publication.

[1] Full detailed chemical abundances of all 11 stars, along with the processes presented here will be discussed in a forthcoming publication.

[2] `www.github.com/alexji/m2fs_reduction`

Star	source_id	RA	Dec	G (mag)	BP (mag)
HyiI–1402	4632590247028988672	02:27:32.72	-79:14:43.0	15.39	16.02
HyiI–K165	4632211190394998528	02:27:37.37	-79:22:13.7	16.15	16.72
HyiI–K154	4632590590626285568	02:28:46.10	-79:12:40.8	16.28	16.83
HyiI–K150		02:29:26.66	-79:17:11.87	17.16	17.70
HyiI–K225		02:31:31.55	-79:20:48.23	17.64	18.10
HyiI–K052		02:30:33.47	-79:18:04.14	16.98	17.53
HyiI–K030		02:31:48.36	-79:18:51.19	17.94	18.42
HyiI–K102		02:27:27.13	-79:20:25.68	17.87	18.07
HyiI–K068		02:28:47.96	-79:26:36.33	16.88	17.41
HyiI–K077		02:28:21.48	-79:12:25.20	17.14	17.67
HyiI–K182		02:29:55.75	-79:18:18.23	17.57	18.07

Table 4.1: Observational data for 11 member stars in Hydrus I. Data missing from the 8 stars observed with the M2FS instrument on Magellan will be reported in the forthcoming publication. Note the source_ids are from *Gaia* Early Third Data Release.

Star	Instrument	g_0 (mag)	r_0 (mag)
HyiI–1402	MIKE	15.9115±0.02	15.1630±0.02
HyiI–K165	MIKE	16.5631±0.02	15.8640±0.02
HyiI–K154	MIKE	16.6729±0.02	15.8640±0.02
HyiI–K150	M2FS		
HyiI–K225	M2FS		
HyiI–K052	M2FS		
HyiI–K030	M2FS		
HyiI–K102	M2FS		
HyiI–K068	M2FS		
HyiI–K077	M2FS		
HyiI–K182	M2FS		

Table 4.2: Additional observational data for 11 member stars in Hydrus I. Data missing from the 8 stars observed with the M2FS instrument on Magellan will be reported in the forthcoming publication.

Star	$T_{\rm eff}$ (K)	log g (dex)	$v_{\rm t}$ (km s^{-1})	[M/H]
HyiI–1402	4727 ± 43	1.20 ± 0.16	2.31	−2.73
HyiI–K165	4787 ± 44	1.51 ± 0.16	1.75	−3.01
HyiI–K154	4880 ± 41	1.51 ± 0.16	2.00	−2.63

Table 4.3: Stellar parameters derived from a combination of photometric and spectroscopic data for the 3 member stars observed with the M2FS instrument.

4.3 Abundance Analysis and Details

Analyzing the chemical abundances was carried out using Spectroscopy Made Harder (`SMHR`, [43]). Upon full data reduction completion, radial velocity determination, order normalization and line measurement quality review, stellar parameters were determined through a photometric and spectroscopic data combination. Effective stellar temperature, $T_{\rm eff}$ and surface gravity, log g, were determined using data from *Gaia*'s Early Third Data Release [87]. Model metallicity, [M/H], and microturbulence, $v_{\rm t}$, were determined spectroscopically using `SMHR`. The final stellar parameters for the 3 analyzed stars are presented in Table 4.3.

A standard abundance analysis methodology was used which includes use of the 2017 version of `MOOG` [241, 242], a 1D LTE radiative transfer code with scattering, and `ATLAS` model atmospheres [44]. `SMHR` was then used to measure equivalent widths, interpolate `ATLAS`, run `MOOG` and fit syntheses. The abundances present in the following section are the results of equivalent width measurements only. Resulting abundances from spectral syntheses will be presented in the forthcoming publication.

4.3.1 Abundance Summary

Detailed abundance measurements for 10 elements are presented in Tables 4.4, 4.5 and 4.5 and displayed in Figure 4.1 compared to UFD star measurements in the literature, grey markers.

The UFD literature compilation is comprised of Boötes I, Boötes II, Carina I, Carina II, Coma Berenices, Grus I, Grus II, Hercules, Horologium I, Leo IV, Pisces II, Reticulum II, Segue 1, Segue 2, Triangulum II, Tucana II, Tucana III and Ursa Major II [81, 134, 186, 237, 78, 80, 118, 119, 120, 70, 192, 112, 94, 139, 138, 218, 219, 47, 122, 100, 165, 246]. We remind the reader that the following abundances have been determined through equivalent width measurements only.

α–elements: Mg, Si, Ca. Magnesium and calcium are measured from at least 6 and 8 lines, respectively. Alternatively, silicon is only measured from a single line, or in the case of HyiI–K165, from dual lines. the 4102 Å line is detected in all stars, while the weak 5948 Å line is detected in HyiI–K165 only.

Odd–Z elements: Na & K. Sodium is measured via the Na D doublet in each star. Potassium is not measured in HyiI–K165, is detected from 1 line only in HyiI–K154 and from dual lines in HyiI–1402, namely 7664 Å and 7698 Å.

Fe–peak elements: Ti, Cr, Ni, Zn. Abundances of 2 ionization states of Titanium are characterized in all 3 stars. Ti I is detected with at least 5 lines and Ti II with at least 19 lines. Chromium also has 2 examined ionization states — Cr I is measured with at least 4 lines in each star while Cr II is detected via a single line in both Hyi–K165 and Hyi–K154 and not detected in Hyi–1402. Nickel is detected in all stars via at least 3 spectral lines and Zinc is only measured in Hyi–K165 at the 4810 Å line.

Neutron Capture–element: Sr. Strontium is detected in all 3 stars via the 4077 Å and 4215 Å lines. Following suit with other UFDs, Hydrus I has low neutron capture abundance — the origin of which remains unknown [122].

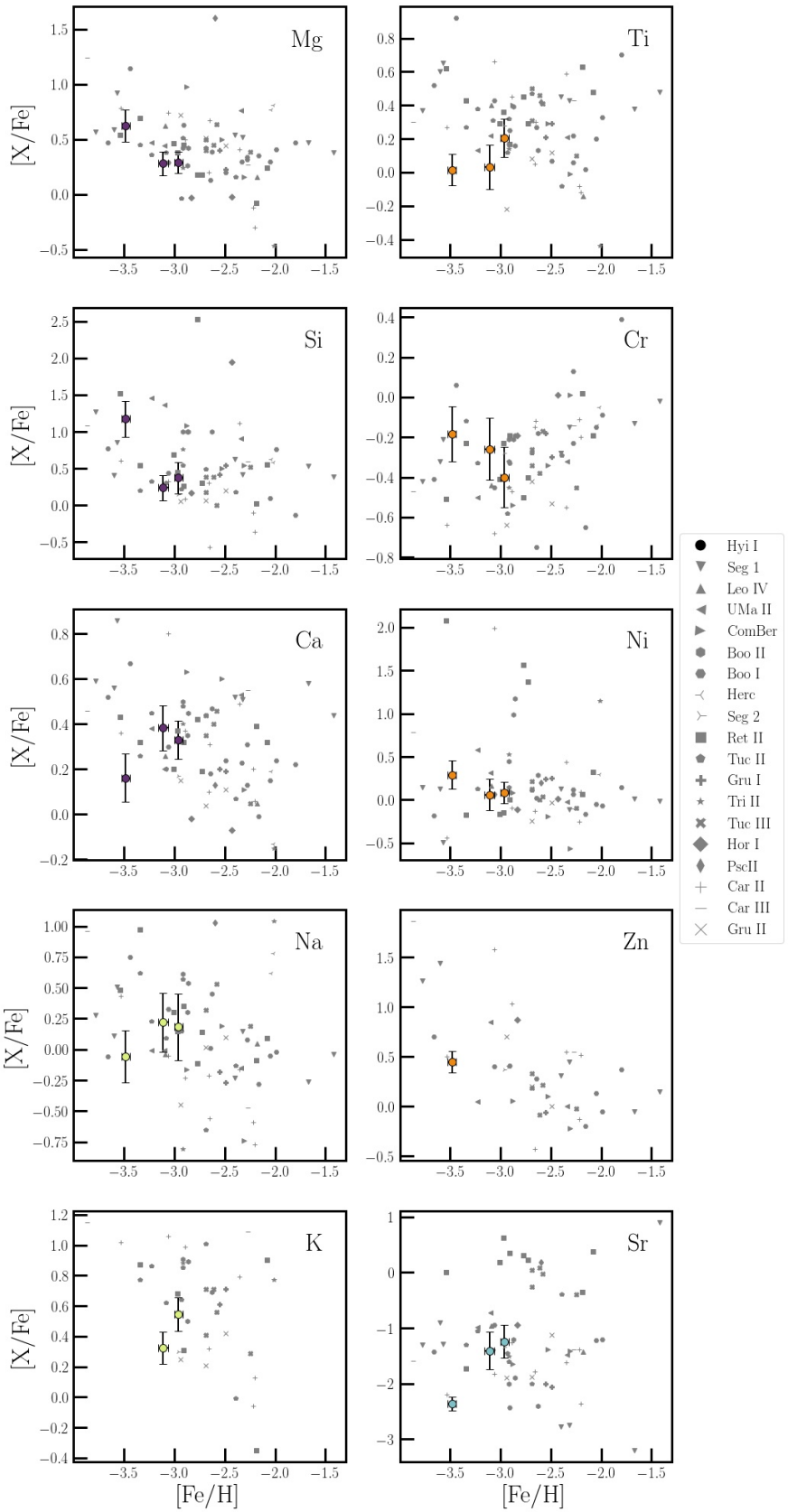

Figure 4.1: Hydrus I's Detailed Chemical Abundances

Table 4.4: Chemical Abundances for HyiI–1402

Elem.	N	logϵ	σ	[X/H]	$\sigma_{[X/H]}$	[X/Fe]	$\sigma_{[X/Fe]}$
Na	2	3.387	0.024	-2.778	0.272	0.183	0.269
Mg	6	4.941	0.133	-2.674	0.091	0.288	0.096
Si	1	4.921	0.0	-2.589	0.217	0.372	0.217
K	2	2.644	0.067	-2.416	0.112	0.545	0.111
Ca	9	3.695	0.148	-2.631	0.084	0.33	0.085
Ti	8	1.843	0.346	-3.091	0.186	-0.129	0.184
Ti II	29	2.141	0.166	-2.742	0.136	0.207	0.114
Cr	9	2.276	0.256	-3.362	0.153	-0.4	0.151
Fe I	98	4.542	0.181	-2.961	0.042	0.0	0.0
Fe II	17	4.527	0.177	-2.949	0.127	0.0	0.0
Ni	9	3.297	0.167	-2.88	0.124	0.082	0.124
Sr II	2	-1.183	0.223	-4.193	0.385	-1.244	0.299

Table 4.5: Chemical Abundances for HyiI–K165

Elem.	N	logϵ	σ	[X/H]	$\sigma_{[X/H]}$	[X/Fe]	$\sigma_{[X/Fe]}$
Na	2	2.769	0.07	-3.54	0.211	-0.056	0.209
Mg	7	4.748	0.285	-2.858	0.143	0.625	0.145
Si	2	5.155	0.325	-2.31	0.247	1.173	0.248
Ca	10	3.000	0.257	-3.322	0.105	0.161	0.107
Ti	6	1.994	0.458	-2.956	0.229	0.527	0.228
Ti II	20	1.47	0.204	-3.432	0.131	0.015	0.093
Cr	4	1.935	0.113	-3.669	0.139	-0.185	0.1378
Cr II	1	2.978	0.0	-2.662	0.112	0.785	0.117
Fe I	72	4.024	0.138	-3.483	0.041	0.0	0.0
Fe II	13	4.05	0.158	-3.447	0.098	0.0	0.0
Ni	3	3.008	0.161	-3.192	0.166	0.291	0.164
Zn	1	1.528	0.0	-3.032	0.107	0.451	0.108
Sr II	2	-2.933	0.006	-5.806	0.179	-2.359	0.121

Table 4.6: Chemical Abundances for HyiI–K154

Elem.	N	logϵ	σ	[X/H]	$\sigma_{[X/H]}$	[X/Fe]	$\sigma_{[X/Fe]}$
Na	2	3.4	0.027	-2.891	0.241	0.22	0.237
Mg	6	4.793	0.184	-2.829	0.103	0.282	0.108
Si	1	4.636	0.0	-2.874	0.177	0.237	0.176
K	1	2.243	0.0	-2.787	0.104	0.324	0.104
Ca	8	3.594	0.182	-2.727	0.098	0.384	0.1
Ti	5	2.127	0.329	-2.83	0.202	0.281	0.199
Ti II	19	1.776	0.228	-3.038	0.192	0.033	0.133
Cr	4	2.264	0.201	-3.371	0.157	-0.26	0.155
Cr II	1	3.387	0.0	-2.253	0.122	0.818	0.109
Fe I	58	4.414	0.142	-3.111	0.048	0.0	0.0
Fe II	12	4.408	0.188	-3.071	0.147	0.0	0.0
Ni	4	3.163	0.284	-3.051	0.184	0.06	0.183
Sr II	2	-1.587	0.335	-4.483	0.415	-1.411	0.336

4.4 Discussion: α–element evolution

With only 3 Hydrus I stars analyzed thus far, the α–Fe "knee" that is present in the abundance trends of many galaxies [252], which can provide some insight into overall star formation timescales for that galaxy, is not discernible in the 3 α–elements examined here (Mg, Ca, Si — the deep purple dots in Fig. 4.1). However in this preliminary data set, the 3 point trend in Ca is different that what is commonly seen. Here the star with the lowest calcium abundance is the most metal poor star, instead of being the least metal poor star. If this trend holds once the full data set of 11 stars is analyzed, possible anomalous star formation scenarios will be explored as α–elements are commonly produced in core–collapse supernovae which is indicated by higher abundances at lower metallicity.

The difference in trends across metallicity between Ca and Mg can indicate variations in the initial mass function (IMF) at these smallest galactic scales. With the emerging Ca trend being opposite of the common UFD trend, Figure 4.2 highlights the contrast in these α–element abundance variations across metallicity in individual UFDs. The periwinkle dots, outlined in black, is the [Mg/Fe] –[Ca/Fe] ratio across metallicity ([Fe/H]) for the 3 Hydrus I member stars with associated

errors and the grey markers are measurements for UFDs from the literature — identical to Fig. 4.1. While the Ca trend does not follow the common abundance decrease as metallicity increases, when the difference between [Mg/Fe] and [Ca/Fe] is examined, the trend follows suite with the other analyzed UFDs. Here [Mg/Ca] declines ~ 0.6 dex across $\gtrsim 0.5$ dex in [Fe/H]. Since high (low, < 0) [Mg/Ca] ratios can be interpreted as enrichment via massive (lower mass) stars with $M > 30\mathrm{M}_{\odot}$ ($M < 15\mathrm{M}_{\odot}$) [191, 49, 139, 256, 175], the extreme decline traces the possible high–mass end IMF variation within Hydrus I.

These α–element trends may also be a result of a UFDs evolutionary history. In some aspects UFDs do not display significant environmental dependence. Previous work has shown that the Milky Way's environment did not affect the UFDs star formation [217] and that they typically ceased forming stars by $z \sim 2$ (or a lookback time of ~ 10.3 Gyr) [33, 270]. Further work assessing environmental dependence has shown that for HyiI a conservative approximation of the tidal radius, to estimate the likely–hood of tidal mass stripping, results in $\sim 10\%$ of the systems stars being unbound [235]. When more realistic mass assumptions are used the likely–hood of stellar stripping drops completely (e.g. using recent results showing the MW's mass to be closer to 1.1×10^{12} $\mathrm{M}_{\odot}$ [216] than the 1.6×10^{12} $\mathrm{M}_{\odot}$ used in these calculations).

In addition to potential effects by the MW's environment, there is potential for HyiI to have been altered by the LMC. HyiI is, also, a satellite of the LMC — recent work even shows that HyiI was brought into the MW system via the Magellanic system. The exact likely–hood that the LMC has altered the structure or chemistry of it's UFD satellites is not yet known. Some theories that may affect the LMC UFD satellites specifically are the integrated galactic IMF theory [269, 175], which suggests that gas–poor galaxies cannot form the most massive stars, and Lyman–Werner feedback delayed Pop III star formation, which suggests that the UFD progenitors would then be more susceptible to external metal enrichment [162]. Future work exploring how these theories impact the LMC UFDs, such as HyiI, is critical.

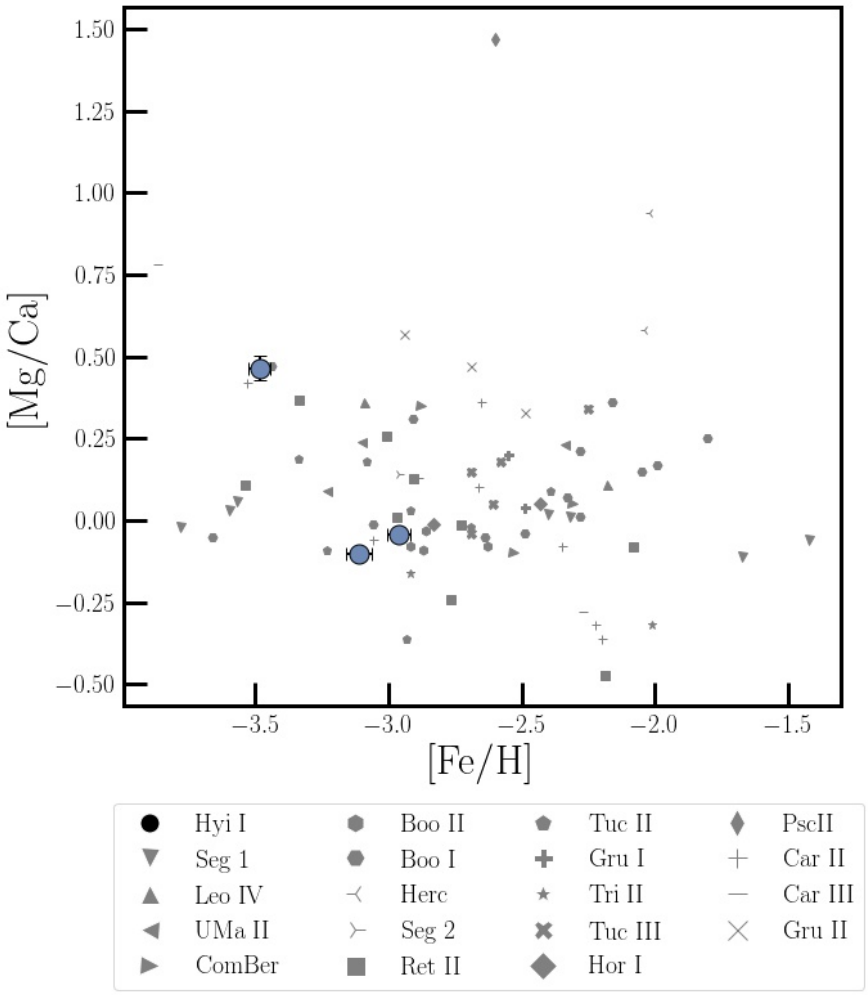

Figure 4.2: This figure highlights the contrast in α–element abundance variations across metallicity in individual galaxies. The grey markers are measurements for UFDs from the literature — identical to Fig. 4.1. The periwinkle dots, outlined in black, is the [Mg/Fe] – [Ca/Fe] ratio across metallicity ([Fe/H]) for the 3 Hydrus I member stars with associated errors. Interestingly, while the individual α–element trend in calcium does not follow what is seen in other UFDs such as Carina II [121], when the difference between these α–elements is examined, the trend follows suite with the other analyzed UFDs. This trend points to possible variations in the initial mass function at the smallest galactic scales.

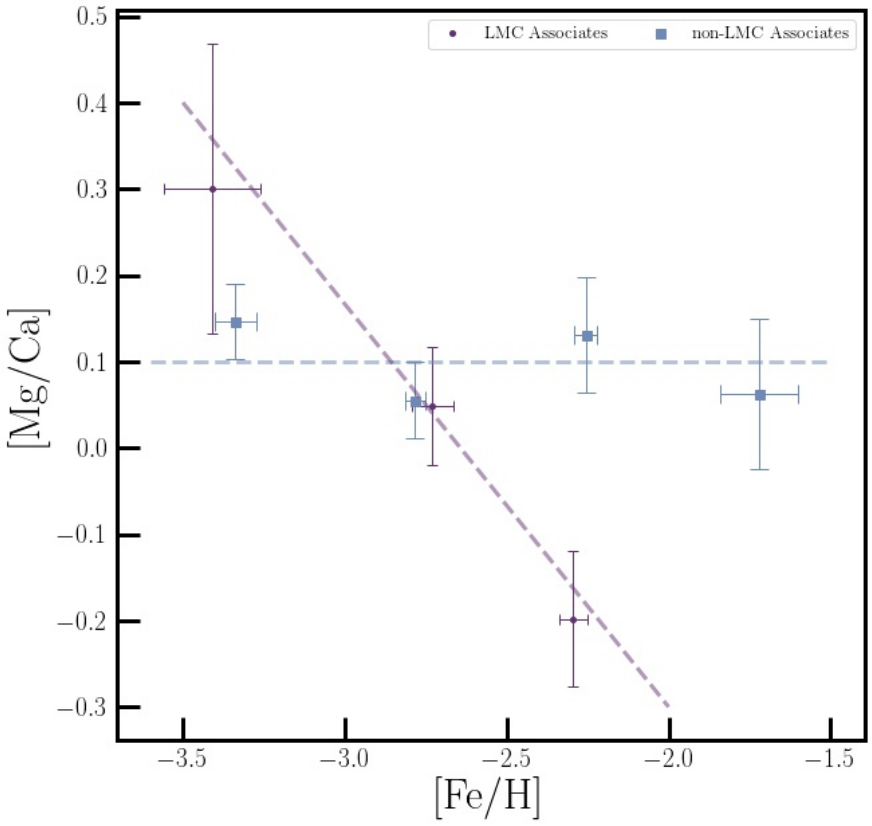

Figure 4.3: Stars from LMC UFD satellites are grouped and binned by metallicity then compared to grouped and metallicity–binned stars from MW UFD satellites. The purple circles, with associated errors, and dashed line show the negative trend with increasing metallicity for LMC satellites. The blue squares, with associated errors, and dashed line show the relatively flat trend across the metallicity range for UFDs which are not associated with the LMC. This serves as evidence that the LMC has impacted the evolution of it's UFD satellites.

4.5 Conclusion

This chapter presented preliminary detailed chemical abundances for 3 member stars in Hydrus I from data taken with the MIKE spectrograph on the Magellan Telescope. Hyi I, a satellite of both the MW and LMC, is only the 20th UFD to have detailed chemical abundances measured out of the over 40 known ultra–faint systems. A summary of these partial results are as follows:

- Detailed Abundances for 10 elements, visualized in Figure 4.1 and presented in Tables 4.4, 4.6 and 4.5, were determined using equivalent width measurements, the elements include α–elements, Mg, Si, and Ca, Odd–Z elements, Na and K, Fe–Peak elements, Ti, Cr, Ni and Zn, as well as Sr, a neutron capture element.
- The abundances within Hyi I follow suit with measurements in other UFDs which suggests similar formation and evolutionary histories within this set of ancient galaxies.
- As recently seen in other UFDs, amongst the 3 analzyed Hyi I stars there is a decreasing α–element ratio ([Mg/Ca]) trend across metallicity, highlighted in Figure 4.2. This trend suggests possible variations in the IMF at the smallest scales.
- This decreasing trend seems to be driven by the stars in MW UFD satellites which are also satellites of the LMC, as displayed in Figure 4.3, which highlights the possibility that the LMC's environment has impacted the evolution of our UFDs.
- Additionally, the M2FS data reduction pipeline has been updated during this work with a Coherent Point Drift Algorithm to correct occasional shifted arc frames during calibration.

It will be interesting to see if these trends hold when the 8 other observed Hyi I member stars are fully analyzed and spectral synthesis is completed for all 11 stars provided abundances for more elements — all of which will be presented in a forthcoming publication.

Chapter 5

Mentorship at the Smallest Scales: Peer Mentorship for Community and Confidence

5.1 Mentorship & Peer Mentorship Introduction

In the 2019 report of the National Academy of Science, Engineering, and Medicine (NASEM) entitled, "The Science of Effective Mentorship," mentorship is defined as "a professional, working alliance in which individuals work together over time to support the personal and professional growth, development, and success of the relational partners through the provision of career and psychosocial support" [188]. This definition highlights the critical role both mentor and mentee play in the effectiveness of the relationship. Research indicates that the frequency and quality of mentee–mentor interactions positively correlates with students' persistence in STEM degree programs. Mentorship has also been positively associated with students' identity, research self–efficacy and their sense of belonging. For students from historically underrepresented groups (HU), mentorship has been

positively correlated with enhanced recruitment into graduate school and research–related career pathways (see [207, 187, 189] for summary of the literature).

Importantly, the ability of mentors to meet the psychosocial needs of their mentees is associated with increases in how mentees perceive the quality of the mentoring relationship and satisfaction with that relationship [248, 262]. Additionally, skills in cultural awareness can help students from underrepresented groups navigate the often challenging experience they face in majority environments and reinforces their research self–efficacy [39]. In addition, quality mentorship increases HU students' sense of belonging, discipline identity development, and overall confidence to be a scientist [68]. Mentoring relationships can occur in many forms including the traditional dyad, single mentors working with multiple mentees, and groups of mentors working with a single mentee as a mentoring network. "Mentorship networks — the constellations of mentoring relationships and resources that a mentee taps for support — have gained increasing recognition both within and outside of STEMM." [188]. Thus, mentorship roles can be fulfilled by many individuals who engage with a given mentee including research advisors, instructors, program directors, program meeting leaders, committee members, peers, etc. [213].

Mentoring networks include many scales — with a student as a mentee, mentors can range from senior faculty (large scale connections), to administrators, counselor and professionals to other students/peers (small scale connections). Peer mentorship groups have been shown to promote collaboration, provide mentees with both psychosocial and career support and increase retention. In their 2014 study, Tenenbaum et al. demonstrated gains for both near–peer mentors and their mentees highlight the positive impacts on all engaged in this type of arrangement [249]. Peer or near–peer groups may also serve to enhance self–efficacy and diminish feelings of isolation. For example, the Fisk–Vanderbilt Master's–to–PhD Bridge Program has found that a tiered, peer–mentoring approach involving seniors linked to first year students, helps students feel emotionally supported [247].

Here we examine the role that peer mentorship programming plays in the success of Cal–Bridge

scholars. The remainder of the article is broken into three parts: first, we describe the impetus for the creation of Cal–Bridge's Peer Mentorship Program. Second, we describe the Cal–Bridge Program overall, UC Irvine's Physics and Astronomy Community Excellence Program — the precursory program this Peer Mentorship Program, and finally describe Cal–Bridge's Peer Mentorship Program. Next in coarse detail, we discuss the evaluation methods for the first year of the Peer Mentorship programming. The fourth section explores the programs effectiveness based on survey results and finally, we discuss lessons learned and future directions.

5.2 The Impetus

To investigate how the Cal–Bridge Scholarship Program overall was affecting the success, retention and advancement of its Scholars, an external evaluator (Scherr) conducted annual evaluations of the program, consisting primarily of interviews and surveys of scholars. Early in the program, we found that faculty mentoring was the element mentioned most frequently as very important to scholars' success. We also discovered some areas where the scholars identified gaps in the program, mainly around peer mentoring and providing a sense of community to the group.

It is well known that human beings have a need for affiliation and attachment that comes from belonging to a community. There is ample evidence that people survive and thrive when they feel socially connected [12, 63]. In the academic context, in their 2018 study, Estrada et al. describe the key role that social inclusion and a sense of belonging play in promoting persistence among HU students in academia. In particular, the development of discipline identity, a form of social identity, has been shown to be a strong predictor of persistence in STEM [46, 69, 96].

Quality mentorship increases HU students' sense of belonging, discipline identity development, and overall confidence to be a scientist [68]. Upon the success of a 1–year–old peer mentorship program co–created and lead by a Cal–Bridge Cohort 1 Alumna (Rodriguez Wimberly), Cal–Bridge's

Director (Rudolph) brought Rodriguez Wimberly onto the Cal–Bridge Leadership Team to create peer mentorship programming for Cal–Bridge Scholars. The goal of this new programming was to create the community and peer mentorship opportunities Scholars desired, results of the annual evaluations, and increase the Scholar's community, discipline identity, and confidence.

5.3 The Programs

5.3.1 Cal–Bridge Overview

Cal–Bridge is an NSF–funded bridge program that helps current STEM students in California State Universities (CSUs) and California Community Colleges (CCCs) stay on the path through their undergraduate studies, successfully apply to and succeed in graduate school, and enter the professional world well–positioned to enter the STEM workforce, possibly in a faculty position [220, 221]. The Cal–Bridge program (`www.calbridge.org`) is a partnership between all three tiers of the California higher education system: 9 University of California (UC), 23 CSU, and 116 community college campuses in California, with almost 300 faculty from the three systems participating.

Cal–Bridge Scholars are recruited from the CSU and community college campuses in the Cal–Bridge network, with the help of local faculty and/or staff liaisons at each campus. Community college students transfer to a participating CSU to join the bridge program. The current Cal–Bridge program originally focused on physics and astronomy, and more recently we have added computer science and computer engineering. Eventually, the program will expand to include other STEM fields. This work will focus on the physics and astronomy subprogram, which has existed since the program was founded in 2014.

The Cal–Bridge program uses research–validated selection methods to identify students from

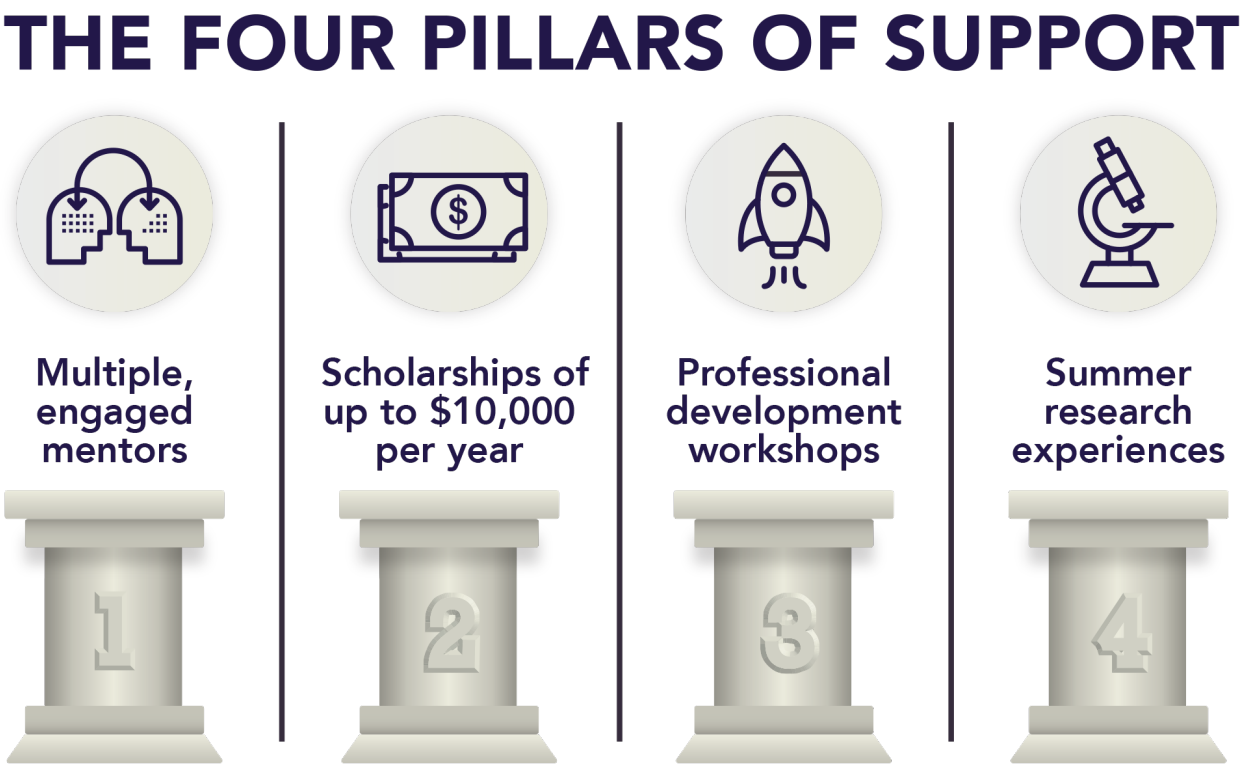

Figure 5.1: The Cal–Bridge 4 Pillars of Support

groups historically excluded from STEM (e.g., URMs, women, LGBTQ+, etc., collectively referred to as Historically Underrepresented or HU students) who display strong socioemotional competencies, along with academic potential, and provides them with the support necessary to successfully matriculate to a PhD program, targeted at the UC campuses in the Cal–Bridge network.

The philosophy of the Cal–Bridge program is based on the concept of high expectations coupled with the support required to meet those expectations. Once a student is selected into the Cal–Bridge program, they receive that support through four "pillars of support" (Figure 1): multi–level mentoring, professional development workshops, summer research experience opportunities, and financial aid, if the scholar qualifies. Each of these elements is designed to assist the scholar in achieving a high level of performance as an undergraduate as part of a process of helping them to prepare successful graduate school applications, and more importantly prepare them to be successful in graduate school.

5.3.2 PACE

The UC Irvine (UCI) Physics and Astronomy PACE (Physics & Astronomy Community Excellence) program (`www.uci-pace.github.io`) is a graduate student led mentoring organization — a peer–mentorship program for students by students. The program was created in response to department climate surveys which revealed that graduate students in the PhD program wanted improvement in the mentoring efforts by the department. A team, led by Rodriguez Wimberly (who went on to create the Cal–Bridge Peer Mentorship program) with fellow graduate student, Arianna Long, and advised by Professor Franklin Dollar, volunteered to create the program as a response to this need. Rodriguez Wimberly brought her experiences as a Cal–Bridge scholar, as well as experiences with the UCI Competitive Edge program, to bear on the design of the program, which later informed her creation of the Cal–Bridge Peer Mentorship program.

PACE programming consists of 3 main components, outlined in Table 5.1. These programs aim to normalize a holistic approach to success as a physics student and strengthen the graduate student community. This holistic approach to success combines topics on mental health and spreading awareness of non–cognitive resources with traditionally recognized steps toward academic success such as discussions on how to prepare for comprehensive exams and how to select a research advisor. The overall goal is to present all material in to emphasize equity and inclusion, major tenets of both PACE and Cal–Bridge. We now briefly describe these 3 programs.

Program component	Description
Fire up Fridays	Workshops for first–year graduate students on various topics
Exceleration	1–on–1 peer mentoring between first year and more senior graduate students
Stride!	Undergraduate–graduate mentoring focused on applying to graduate programs

Table 5.1: Major components of the UCI PACE program.

Fire Up Fridays

Fire Up Fridays (FUF) is a series of monthly workshops for the first year graduate students ($\sim$ 25 people) led by more senior graduate students ($\sim$ 10) and facilitated by the PACE Leadership team (2–5 people). These include structured and unstructured activities to foster community and resilience amongst the graduate population. The content for this program is influenced heavily by core curricula created by the National Center for Faculty Development and Diversity, University of California, Irvine's (UCI) Mentoring Excellence Program and PACE's leaders' and mentors' previous experiences as beginning graduate students [2, 3]. Topics covered in FUF sessions include time management, building a network of mentors, demystifying the physics comprehensive exam and personal wellness. During several sessions throughout an academic year, specific faculty are invited to discuss topics such as the comprehensive exam and funding within the department. Additionally, the UCI graduate academic counselor leads sessions on community, inclusivity, and wellness.

Exceleration

To provide more individualized peer mentoring to the first–year graduate students, the Exceleration program pairs up more senior graduates in the department with the incoming graduate cohort. The goal is to help guide the peer mentees through a healthy first year as a graduate student, with an emphasis on becoming a contributing member of the department and navigating life as a graduate student. Mentors and mentees are provided with brief (2–3 hours) training on mentorship, recommendations on meeting frequency and length (setting boundaries), conversation guidelines, and resources on being an effective mentee/mentor, based on the UCI Mentoring Excellence Program [3].

Stride!

Stride! combines the individualized (1–on–1 pairing) and group (workshops) peer mentorship styles, focusing on mentoring undergraduates in the department who are applying to graduate programs. Content for this program is heavily influenced by UCI's Summer Undergraduate Research Fellowship and Cal–Bridge workshops [6, 220]. Rising undergraduate seniors are matched with graduate students at the beginning of summer before senior year. Mentor–mentee pairs meet on a regular basis to navigate various aspects of the graduate school application process and the overall graduate school experience. Panels and workshops are held to provide the undergraduate mentees with multiple graduate student perspectives on topics including: Life as a Graduate Student, Picking a Graduate Program, The Graduate Program Application Process, and Application Essays and Research as a Graduate and as an Undergraduate.

5.3.3 Cal–Bridge Peer Mentorship Program Overview

In response to the Cal–Bridge scholar feedback request for more peer interactions within the program and based on the success of the first year of PACE, Cal–Bridge Director Rudolph asked Cal–Bridge Cohort 1 alumna Rodriguez Wimberly to create and direct the Cal–Bridge Peer Mentorship program using her experiences as a Cal–Bridge scholar and as co–founder and leader of the PACE program. Specifically, the 1–on–1 near–peer mentoring and small group activity elements of the PACE program were adapted to best serve the Cal–Bridge Scholar community. In the initial year of the Cal–Bridge Peer Mentorship Program, the PACE program components were implemented regionally (Northern and Southern California) to facilitate the possibility of in–person mentoring, though the coronavirus (COVID–19) pandemic interfered with in–person activities in the Spring 2020. In addition, a group of Cal–Bridge alumni attending PhD programs outside the UC system attempted to form a parallel program to promote peer–to–peer interactions; however, as we detail below, this group did not work in practice, and Cal–Bridge alumni were instead invited to join in

the on–line activities of the southern regional group. In practice, each regional group (Northern and Southern California) chose different approaches to peer mentorship in response to interest of the regional participants (see Table 5.2). In the second year, the components of the Peer Mentorship program were merged into a single, all online program of all scholars and alumni in response to the coronavirus (COVID–19) pandemic. We will report on this second year of the program in a future publication. While mentor training has yet to be implemented within these programs, Mentor–Mentee Contracts have been implemented. These lay ground rules for the following conversations and the ethical treatment of each party. Additionally, meetings with the peer mentors are held, prior to each workshop, to discuss behavior and the sensitivities needed regarding the particular workshop topic. As the program grows, funding will be sought to provide mentor training.

PACE Program Component	Cal–Bridge Peer Mentoring Adaptation	
	Area	Description
1–on–1 Peer Mentoring	Northern California	Near peer pairing based on geographic location and research interests
Group Peer Mentoring	Southern California	In person and via Slack — Q&A, Activities, Panels

Table 5.2: Major components of the Cal–Bridge Peer Mentorship program and the geographic region they were executed in.

Southern California Program

In Southern California, based on Rodriguez Wimberly's experience with PACE, the decision was made for the first year to focus on group activities rather than 1–on–1 near–peer mentoring for two reasons: 1) unlike the graduate student population at UC Irvine, Cal–Bridge scholars and alumni are spread out over the region, making 1–on–1 in–person meetings challenging, and 2) there was not an easy mechanism to provide the mentor training that PACE gave near–peer mentors. To facilitate possible spontaneous near–peer pairings, all peer mentors created a short biography highlighting their areas of expertise. These biographies were posted to a private south–scholars–only Slack

channel as part of an introduction to the peer mentoring program. Because Cal–Bridge scholars have significant exposure to mentoring relationships through their participation in the program, any senior Cal–Bridge scholar or alumni who were interested were accepted. However, as the program grows, there are plans to implement a more formal application process to become a peer mentor.

Spanning the full academic year (2019–2020), there were 6 virtual and two in–person workshops: the topics covered in the activities were "Building Your Mentor Map," "Graduate Applications Question and Answer," "Prospective Grad Visits Question and Answer," "Weekly Planning Activity," "Research Workflow Discussion," and "Accountability Meetings." This last workshop consisted of stating goals in the morning, encouraging one another, and then recapping progress at the end of the workday. Attendance at these activities ranged from a high for 4 mentors and 6 mentees to a low of 2 mentors and 1 mentee, with a general decrease as the year progressed. One possible reason for this drop, other than commitment fatigue, may have been the beginning of the coronavirus (COVID–19) pandemic. Regardless of attendance, lively conversations occurred in each session with multiple pieces of advice and concerns, fears, and experiences being shared.

The two in–person workshops were held during the lunch break of two of the mandatory Saturday Cal–Bridge workshops; thus, all the current scholars were in attendance. These two workshops began with a short introductory lecture on a topic ("Building a Mentoring Network" and "Balancing Academic and Familial/Personal Cultures") followed by multiple small group discussions with short regroup discussions, sharing, and activities. At the second workshop, the discussion quickly moved from the topic of balancing cultures to sharing the groups' anxieties and struggles related to the coronavirus pandemic. The state of emergency in California had been active for roughly 2.5 weeks at that point, and the statewide stay–at–home order began 2 days prior to the workshop. In fact, this coronavirus–centered discussion was scheduled to last half an hour but in fact extended past the intended workshop timeframe and lasted over 2 hours. Towards the end of this discussion, Cal–Bridge leadership joined and provided reassurance that their academic and professional aspirations need not be derailed by the pandemic and that the Cal–Bridge program

would continue to support them.

Northern California Program

The Cal–Bridge Northern California program focused their peer mentorship efforts on 1–on–1 pairing between scholars and a near–peer mentor. As the 2019–2020 Academic Year is only the second year of operation for Cal–Bridge North, the near–peer mentor pool was small, so non–Cal–Bridge PhD student volunteers were sought in Northern California UC departments — 15 students volunteered from the Berkeley, Davis and Santa Cruz campuses. These volunteer peer mentors ranged in academic level within their respective PhD programs (from 1st to 5th year) and with a range of mentoring experience — some mentors were actively working in peer mentoring programs within their own departments, others had prior experience during their undergraduate career while some had no prior experience. Each peer mentor volunteer was paired with a Cal–Bridge Scholar based on research interest and geographic location to facilitate physical meetings. The suggested interaction between mentors and mentees was at least 1 hour each month. Though in–person meetings were preferred, since institutions are geographically spread out in Northern California, the majority of the meetings took place digitally via Zoom or Skype. These suggestions were moderately successful as half the End of the Year survey respondents reported meeting with their peer mentor at least 3 times over the academic year with a quarter meeting monthly as recommended. The scope of the meetings was strictly separated from tutoring — they were used to give the mentees professional tips, share experiences, provide emotional support, and build their personal network in research.

Once the program started the mentors and mentees were free to organize the meetings with minimum intervention from the organizers. The experiences of both the volunteer peer mentors and the Scholars/mentees were gauged in the two Mid–Year Surveys, which focused strictly on the Northern California Scholars and the peer mentorship program wide End of the Year Survey.

In addition to the 1–on–1 near–peer mentoring, a group topical meeting was held. Topics included:

organizing research and classes, choosing a field of research (including how to approach professors and normalizing switching thesis advisors), and science communication to the general public. Even though Scholar attendance at this optional workshop was sparse, at 4 attendees, these participants rated their experience as having a neutral to very good impact. Of all the Mid–Year Survey respondents, the majority did indicate interest in future workshops similar to this. Finally, a Slack group was created for the Cal–Bridge North peer mentoring participants, but participation was low.

Alumni Program

As the Cal–Bridge program matures, more and more program alumni are choosing PhD programs outside of California. In the 2019–2020 academic year, there were 24 Cal–Bridge alumni attending non–UC graduate programs in various parts of the US. At the beginning of the academic year there was interest in creating a virtual network of peer mentoring from many of these former scholars. Initially some community building was attempted through peer mentoring discussions on Slack, but it was soon realized that the interested parties wished to serve as mentors to current Cal–Bridge scholars instead of each other. These wishes were not implemented in the 2019–2020 year, but four from this group did participate as mentors in Cal–Bridge South Slack activities; and this past 2020–2021 academic year, all former Cal–Bridge scholars were given the opportunity to participate as peer mentors to current scholars, thereby integrating the alumni into the main Peer Mentorship program. In the current 2020–2021 academic year, 16 alumni were matched with current scholars as near peer mentors. Six of these pairings are still active in Spring 2021.

5.4 Program Evaluation

In order to evaluate the Peer Mentorship program, a series of 4 scholar surveys were conducted — a survey at the beginning of academic year given to scholars in all geographic regions and at the

mid–year point two separate follow–up surveys were given to scholars attending CSUs in Northern California and at the end of the academic year a survey was given all scholars regardless of their region. We describe the surveys here.

5.4.1 Start of Academic Year Survey

All scholars and alumni were asked to complete a peer mentoring interest survey in August 2019 which was designed and administered by the peer mentoring program director (Rodriguez Wimberly). Here senior scholars and alumni could volunteer to act as a peer mentor in the academic year's activities and indicate their interest in being a mentee in the program. Of the 60 active scholar and 33 alumni in the 2019–2020 academic year, 41 in total responded to this initial interest survey with 78% showing interest in the programming —16 alumni were interested in serving as peer mentors and 5 of these alums were also interested in being a peer mentee while 12 active scholars were interested in being a peer mentee and 11 were interested in serving as peer mentors (7 of these 11 were interested in both). The responses to this survey were evaluated by the peer mentoring program director. A separate interest survey was created and administered for the active scholars in Northern California by that region's program leads (Gignac and Mazza). This survey simply requested information from participants on whether they would like to be paired with a peer mentor and academic demographic information (year in undergraduate program and field of interest). 11 scholars responded with 9 indicating interest in being paired with a peer mentor.

5.4.2 Mid–Academic Year Surveys

Two mid–academic year surveys were conducted for the participating Northern scholars in January and April 2020 which were designed and administered by that region's peer mentoring program leads (Gignac and Mazza). In both surveys, Scholars and peer mentors were asked to indicate the frequency of their 1–on–1 meetings, rate their experience in the program and overall usefulness,

as well as provide suggestions for improvement. For the January survey, 6 Scholars/peer mentees responded along with 9 peer mentors. This peer mentor group includes volunteer graduate students from outside the Cal–Bridge program. In the April survey, 4 peer mentees responded while only 3 peer mentors responded. For both surveys, responses were coded by the peer mentoring program director (Rodriguez Wimberly).

5.4.3 End of Academic Year Survey

In May 2020, all scholars and volunteer alumni mentors were requested to complete an end of the year survey regarding the peer mentoring program activities conducted. This survey was designed by the Southern California peer mentoring program lead (Rodriguez Wimberly) and the Northern California peer mentoring program leads (Gignac and Mazza). It was administered by the peer mentoring program director (Rodriguez Wimberly). All recipients were informed that responses to the survey are confidential: no member of the Cal–Bridge leadership team has access to information on who gave which responses, except the peer mentoring program director and leads (Rodriguez Wimberly, Gignac and Mazza). The alumni–mentors and scholar–mentees received separate end of the year surveys, though most questions on the alumni–mentor survey were simple rewordings from the scholar–mentee survey. The survey aimed to take a general census of the availability and awareness amongst Scholars and Alumni of various peer mentoring programs; evaluate the effectiveness of the specific program elements and activities; evaluate how the programming impacted their sense of community within the Cal–Bridge structure and gauge interest in continuing the program in following academic years. While only 17 active scholars indicated interest at the beginning of the academic year, 24 responded to this End of the Year survey with all but 1 of these 24 scholars having participated in at least one peer mentoring activity. Of the 16 alumni interested in serving as peer mentors at the beginning of the academic year, 6 responded to the end of the year survey. For both surveys, responses to open–ended questions were coded by the peer mentoring program director and Cal–Bridge's evaluator (Rodriguez Wimberly and Scherr,

respectively).

5.5 Peer Mentorship Program Effectiveness

In the Mid–Year Surveys given to Northern California Scholars, the 1–on–1 peer mentoring component was positively evaluated with a score from mentees from 3 to 5 (out of 5 maximum). Roughly 35% of the students indicated that the meetings had a positive impact on their studies or academic career, 35% had partial positive influence and the rest of the mentees still enjoyed the meetings. The most beneficial aspect of the meetings was learning about other people's experiences, normalizing fears and anxiety about the academic career and receiving assistance in clarifying the mentee's academic/career path. It was found from the survey that some pairs of mentor/mentees met several times (more than 5) in the quarter, while other pairs had trouble organizing meetings and could not meet. Interestingly, the volunteer (non–Cal–Bridge Scholars or Alumni) peer mentors desired an increased meeting frequency while the Scholar mentees were content with the frequency.

Overall participation in the first year of peer mentoring activities was far less than all other Cal–Bridge programming (e.g. the mandatory monthly professional development workshops), in part due to the optional versus required nature of these activities. The topics discussed during these peer mentoring sessions are similar to those covered in the required faculty–led Cal–Bridge workshops — e.g. graduate program application essay writing, goal planning and building your mentor network. The survey results revealed that providing information on academic resources, various structures available for personal organization, and general graduate program information were not valued as much as detailed highly current impactful topics — i.e., mentor maps are less valued than GRE Prep.

Is the desire to focus on highly current impactful topics, and consequentially immediate individual performance, the reason why this year's peer mentoring efforts had a seemingly null impact on

the scholars' sense of community within the program? One of the two main goals in creating this programming was to increase the sense of scholar community. Unfortunately, more End of the Year Survey respondents felt their participation in the program did not affect their relationships with current or former scholars (former scholars served as peer mentors) than those who felt it fully strengthened these relationships. Perhaps the nebulous definition of community is to blame here. It is surprising that the majority of respondents are interested in serving as a peer mentor in future years of the initiative yet there was the strong null response to the proposed strengthened community. This can certainly be mitigated through clearer communication of the program's goals at the beginning of the academic year, more precise definitions in survey questions and questions specifically seeking scholars' definition of certain activities –e.g., are leadership opportunities, such as serving as a peer mentor, thought of as community building or a professional development opportunity. A few other avenues that will be explored in the second year of peer mentoring programming to strengthen the scholar community is to offer opportunities to share personal and academic experiences, such as virtual social hours and conducting peer mentoring group sessions via Zoom, as opposed to through Slack, to increase face time amongst the scholars.

While the Mid–Year and End of the Year surveys highlight deficiencies in our initial year of programming, our efforts at minimum lived up to the value Scholars saw in peer mentoring prior to this programming. In fact, there is an exciting strong interest in future programming. The interest is so strong that respondents desire an increased frequency of sessions. Their wish will be granted! Additionally, we will monitor the programs progress more closely throughout the academic year via multiple short check in surveys, improved beginning and end of the year surveys, and tracking changes in the scholars' Mentor Maps from the start to the end of the academic year. In last year's peer mentoring activities, a Mentor Map session was conducted in person for scholars in Southern California but the primary goal of this activity was group discussion on what mentoring looks like in all forms and the role of peer mentors in their academic careers. An edited National Center For Faculty Diversity and Development Mentor Map was introduced to these scholars and an initial completion pass conducted but no collection or follow up occurred. In the second year

of the program, we are concretely implementing mentor mapping. A Cal–Bridge Mentor Map has been created which combines various aspects of other Mentor Maps, such as the NCFDD version. This new Mentor Map includes aspects of Goal Setting and more holistic success (i.e. sections for Mental and Physical Health in addition to traditionally academic categories). With this improved tool, scholars will be able to visualize their support networks and it's growth while directors track the program's success. Overall, minor changes will be implemented as a result of these survey results with the largest change being increased concise communication of the program's goals and structure.

5.6 Discussion & Future Work

In future years, we will explore topics or a combination of topics with the goal to achieve both immediate results and long term development. Another future point of interest is examining possible Cal–Bridge specific cultural phenomena. This scholarship program is unique in its approach to setting high expectations throughout a scholar's tenure in the program. Where many scholarship programs only offer opportunities, Cal–Bridge is meticulous in the maintenance of academic excellence throughout, especially in meeting certain class grade thresholds. The effect this 'pressure to perform' has on influencing the type of peer mentoring desired by the undergraduate scholars will be explored in future surveys and programming.

While similar opportunities are often available to Scholars at their home institutions, this peer mentorship program represents a community different from that found at any single institution — namely diverse Scholars with the shared plan of applying to PhD programs in their field — and is vital in sustaining a thriving community of diverse scientists within the Cal–Bridge program itself as research shows that peer mentorship also creates community and camaraderie (Lewis 2017). Additionally, this programming provides participants with opportunities to give back to their communities and learn in a more intimate environment than is often unavailable at universities

where student populations do not represent larger societal demographics.

The Cal–Bridge Program is working to expand the populations served to include PhD students and postdocs. Within this expanded program, we will create a Vertical Mentoring Structure where I will direct each level of peer mentorship. This expanded program will continue to broaden participation of HU students in STEM and provide leadership experiences for peer mentors through opportunities to lead workshops and 1–on–1 discussion. Throughout each of these proposed peer mentorship programs, participants will be surveyed regularly seeking feedback to improve the programs and the participants' experiences within STEM spaces. As has been done with previous Cal–Bridge Peer Mentorship evaluation surveys, the design, implementation and evaluation of results will be conducted in collaboration with experts in educational evaluations. For established programming, surveys will be conducted at the beginning, middle and end of each academic year as feedback to verify support of the students to the best of the program's ability. For new programming, an interest survey and focus group will be conducted to establish the needs and desires of the intended participants. After collected data has been anonymized and aggregated, or proper permission is received, it will be made available through future publications. These Peer Mentorship Programs, mentorship at the smallest scales, will continue to broaden the participation of students from historically underrepresented groups by creating a thriving community and leadership opportunities for these young, diverse scientists to strengthen their identities as researchers.

Chapter 6

Conclusion

The work presented here is a culmination of roughly 6 years of work which includes incredible growth as a scientist and invaluable work, guidance and support from a vast network of scientists. This chapter highlights the results of my gradute work.

6.1 The Suppression of Star Formation on the Smallest Scales

Using the ELVIS suite of Milky Way–and Local Group–like N–body simulations to constrain the infall times for dark matter subhalos likely to host the ultra–faint dwarf galaxy satellite population of the Milky Way, we explore the potential role of environment in suppressing star formation on small scales. Our principal results are as follows.

1. When incorporating the effects of subhalo tidal disruption due to the inclusion of the host's baryonic component, we find a shift in the typical infall time of ~ 0.7 Gyr for subhalos in the mass range of $M_{\rm halo} = 10^{7.9-9.75}$ $M_\odot$, such that subhalos are preferentially accreted at later cosmic time versus the same subhalos in a pure dark matter–only, N–body simulation.

2. For the 6 UFDs included in the Brown ([33]) sample, we find that there is a $\lesssim 0.1\%$ probability that the Milky Way environment was solely responsible for quenching their star formation at $z > 1$.

3. For larger samples of UFDs, the likelihood that environment plays a dominant role in quenching decreases dramatically, such that there is a $< 0.01\%$ probability that environmental mechanisms are responsible for quenching all 10 UFDs included in the Brown ([33]) and Weisz ([270]) samples.

4. Given the inability of environmental effects to reproduce the observed star–formation histories of observed UFDs, we conclude that reionization is the most likely mechanism by which star formation is suppressed on the smallest scales.

5. Finally, we predict that there is a population of $\gtrsim 250$ UFDs within $1 < R/R_{\rm vir} < 2$ of the Milky Way and M31, all with ancient stellar populations. Future imaging surveys, such as LSST, will be able to uncover much of this population.

Combined with previous results ([74] and [73]), our results produce a coherent physical picture describing the dominant quenching mechanism across the entire range of satellite (and host) masses (see Fig. 2.5). At the very smallest scales, we argue that the suppression of star formation is largely independent of environment and set by the minimum halo mass at which reionization curtails gas accretion.

6.2 Sizing from the Smallest Scales

Using the Phat ELVIS suite of N–body Milky Way–like cosmological simulations with embedded disk potentials along with the full phase–space information for Milky Way satellites from *Gaia* EDR3, we constrain the dark matter halo mass of the Milky Way and find a preferred mass range of ~ 1–1.2×10^{12} $M_\odot$. A more complete summary of our main results are as follows:

1. As illustrated in Fig. 3.4, when limiting the observed sample of Milky Way satellites to those systems with well–measured kinematics, we find that the observed distribution of satellite velocities ($V_{\rm rad}$, $V_{\rm tan}$, *and* $V_{\rm tot}$) are consistent with a host halo mass of $\sim 1 - 1.2 \times 10^{12}$ $M_\odot$.

2. Across all samples probed, the distribution of satellite velocities inferred from *Gaia* observations of the Milky Way satellites are inconsistent with that of subhalos populating host halos with masses $< 10^{12}$ $M_\odot$ or $> 1.2 \times 10^{12}$ $M_\odot$.

3. Excluding systems associated with the LMC does not significantly change our results, with the observed kinematics of the Milky Way satellites favoring a host halo mass of $\sim 1 - 1.2 \times 10^{12}$ $M_\odot$ when compared to distance–matched subhalo populations in phELVIS.

4. In the inner halo ($D_{\rm MW} < 100$ kpc), we find a correlation between host mass and the eccentricity of satellite orbits (as predicted by GALPY), such that at a given Galactocentric distance increasingly circular orbits are found in higher–mass hosts. This is likely a consequence of subhalo destruction preferentially removing satellites on more radial orbits in more massive hosts.

5. The distribution of infall times inferred from *Gaia* phase–space measures [72] are systematically skewed towards early cosmic times (i.e. early accretion) relative to that of distance–matched subhalos drawn from the phELVIS simulation suite.

6. The distribution of pericentric distances for subhalos in phELVIS show little dependence on host mass, in contrast to the expectations from GALPY that favor smaller pericentric distances for satellites in more massive host halos.

7. Looking towards the discovery of future Milky Way satellites, likely to be at the smallest galactic scales, by next–generation observational facilities, we show that the observed distribution of Galactocentric total velocity and Galactocentric distance stand to be good metrics to test the preferred host mass range for the Milky Way.

6.3 Star Stuff at the Smallest Scales

This chapter presented preliminary detailed chemical abundances for 3 member stars in Hydrus I from data taken with the MIKE spectrograph on the Magellan Telescope. Hyi I, a satellite of both the MW and LMC, is only the 20th UFD to have detailed chemical abundances measured out of the over 40 known ultra– faint systems, the very smallest on the scale of the galaxy mass. A summary of these partial results are as follows:

1. Detailed Abundances for 10 elements, visualized in Figure 4.1 and presented in Tables 4.4, 4.6 and 4.5, were determined using equivalent width measurements, the elements include α–elements, Mg, Si, and Ca, Odd–Z elements, Na and K, Fe–Peak elements, Ti, Cr, Ni and Zn, as well as Sr, a neutron capture element.

2. The abundances within Hyi I follow suit with measurements in other UFDs which suggests similar formation and evolutionary histories within this set of ancient galaxies.

3. As recently seen in other UFDs, amongst the 3 analzyed Hyi I stars there is a decreasing α–element ratio ([Mg/Ca]) trend across metallicity, highlighted in Figure 4.2. This trend suggests possible variations in the IMF at the smallest scales.

4. This decreasing trend seems to be driven by the stars in MW UFD satellites which are also satellites of the LMC, as displayed in Figure 4.3, which highlights the possibility that the LMC's environment has impacted the evolution of our UFDs.

5. Additionally, the M2FS data reduction pipeline has been updated during this work with a Coherent Point Drift Algorithm to correct occasional shifted arc frames during calibration.

It will be interesting to see if these trends hold when the 8 other observed Hyi I member stars are fully analyzed and spectral synthesis is completed for all 11 stars provided abundances for more elements — all of which will be presented in a forthcoming publication.

6.4 Mentorship at the Smallest Scales

The Cal–Bridge Scholarship Program is a California–wide bridge program preparing California State University physics, astronomy, and computer science undergraduate students primarily from historically underrepresented backgrounds to competitively apply for and succeed in STEM Ph.D. programs, specifically those at the University of California campuses. Within Cal–Bridge's 4–pillared support system — scholarship funds, professional development workshop, summer research experiences and multiple engaged mentors — a new peer mentorship program is becoming a vital part in both creating community amongst the Scholars, active, former and affiliate, and in increasing the academic confidence of participants. The Peer Mentorship Program is comprised of optional professional development workshops and the opportunity to participate in paired 1–on–1 peer mentorship meetings. Through evaluation surveys, participants reported that 1–on–1 meetings were most valued for the normalization of academic anxieties and for discussing each other's lived experiences. The most valued workshops focused on skills which would provide Scholars with immediate results such as test prep tips as opposed to a workshop learn how to build a weekly schedule. In future years, we will explore workshop topics or a combination of topics with the goal to achieve both immediate academic results and long term professional development. Another future point of interest is examining possible Cal–Bridge specific cultural phenomena, such as experienced 'pressure to perform' in an intensive scholarship program.

The Cal–Bridge Program is working to expand the populations served to include PhD students and postdocs. Within this expanded program, we will create a Vertical Mentoring Structure where I will direct each level of peer mentorship. This expanded program will continue to broaden participation of HU students in STEM and provide leadership experiences for peer mentors through opportunities to lead workshops and 1–on–1 discussion. Throughout each of these proposed peer mentorship programs, participants will be surveyed regularly seeking feedback to improve the programs and the participants' experiences within STEM spaces. As has been done with previous Cal–Bridge Peer Mentorship evaluation surveys, the design, implementation and evaluation of results will be

conducted in collaboration with experts in educational evaluations. After collected data has been anonymized and aggregated, or proper permission is received, it will be made available through future publications. These Peer Mentorship Programs, mentorship at the smallest scales, will continue to broaden the participation of students from historically underrepresented groups by creating a thriving community and leadership opportunities for these young, diverse scientists to strengthen their identities as researchers.

6.5 Future

As I gleefully transition into my new academic position, I will continue on as Director of the Cal–Bridge Peer Mentorship Program and focus growth of the programming over the coming 3 years to incorporate more leadership opportunities for alumni and strengthen the sense of community amongst current, former and affiliate Scholars. Upon expansion of the overall Cal–Bridge Scholarship Program, the Peer Mentorship programming will grow to include peer mentoring amongst graduate students and post doctoral researchers.

In my new role as a National Science Foundation Mathematical and Physical Science Ascend Postdoctoral Research Fellow at University of California, Riverside, I will expand my research scope to more robust studies of ultra–faint dwarf galaxy evolutionary histories. Proposed projects include conducting more detailed chemical abundance analyses on ultra–faints (visible from the Northern Hemisphere) and simulation–to–observation comparisons to constrain the evolutionary histories of the ultra–faint satellites. In further exploration, for the first time, I will investigate metal pollution throughout ultra–faints in hydrodynamic cosmological simulations. These 3 projects combined will create methodology for deeply studying galaxies at the smallest scales to illuminate the formation and evolution of the first stars and galaxies ever formed.

Bibliography

[1] A cosmic journey: A history of scientific cosmology.

[2] Faculty diversity.

[3] Mentoring excellence.

[4] Mercury online: Space news & opinion.

[5] Night sky.

[6] Surf: Graduate division: Uci.

[7] E. A. K. Adams and T. A. Oosterloo. Deep neutral hydrogen observations of Leo T with the Westerbork Synthesis Radio Telescope. *ArXiv e-prints*, Dec. 2017.

[8] S. H. Ahmed, A. M. Brooks, and C. R. Christensen. The role of baryons in creating statistically significant planes of satellites around Milky Way-mass galaxies. , 466(3):3119–3132, Apr. 2017.

[9] R. Akeson, L. Armus, E. Bachelet, V. Bailey, L. Bartusek, A. Bellini, D. Benford, D. Bennett, A. Bhattacharya, R. Bohlin, M. Boyer, V. Bozza, G. Bryden, S. Calchi Novati, K. Carpenter, S. Casertano, A. Choi, D. Content, P. Dayal, A. Dressler, O. Doré, S. M. Fall, X. Fan, X. Fang, A. Filippenko, S. Finkelstein, R. Foley, S. Furlanetto, J. Kalirai, B. S. Gaudi, K. Gilbert, J. Girard, K. Grady, J. Greene, P. Guhathakurta, C. Heinrich, S. Hemmati, D. Hendel, C. Henderson, T. Henning, C. Hirata, S. Ho, E. Huff, A. Hutter, R. Jansen, S. Jha, S. Johnson, D. Jones, J. Kasdin, P. Kelly, R. Kirshner, A. Koekemoer, J. Kruk, N. Lewis, B. Macintosh, P. Madau, S. Malhotra, K. Mandel, E. Massara, D. Masters, J. McEnery, K. McQuinn, P. Melchior, M. Melton, B. Mennesson, M. Peeples, M. Penny, S. Perlmutter, A. Pisani, A. Plazas, R. Poleski, M. Postman, C. Ranc, B. Rauscher, A. Rest, A. Roberge, B. Robertson, S. Rodney, J. Rhoads, J. Rhodes, J. Ryan, Russell, K. Sahu, D. Sand, D. Scolnic, A. Seth, Y. Shvartzvald, K. Siellez, A. Smith, D. Spergel, K. Stassun, R. Street, L.-G. Strolger, A. Szalay, J. Trauger, M. A. Troxel, M. Turnbull, R. van der Marel, A. von der Linden, Y. Wang, D. Weinberg, B. Williams, R. Windhorst, E. Wollack, H.-Y. Wu, J. Yee, and N. Zimmerman. The Wide Field Infrared Survey Telescope: 100 Hubbles for the 2020s. *arXiv e-prints*, page arXiv:1902.05569, Feb. 2019.

[10] Astropy Collaboration, A. M. Price-Whelan, B. M. Sipőcz, H. M. Günther, P. L. Lim, S. M. Crawford, S. Conseil, D. L. Shupe, M. W. Craig, N. Dencheva, A. Ginsburg, J. T. VanderPlas,

L. D. Bradley, D. Pérez-Suárez, M. de Val-Borro, T. L. Aldcroft, K. L. Cruz, T. P. Robitaille, E. J. Tollerud, C. Ardelean, T. Babej, Y. P. Bach, M. Bachetti, A. V. Bakanov, S. P. Bamford, G. Barentsen, P. Barmby, A. Baumbach, K. L. Berry, F. Biscani, M. Boquien, K. A. Bostroem, L. G. Bouma, G. B. Brammer, E. M. Bray, H. Breytenbach, H. Buddelmeijer, D. J. Burke, G. Calderone, J. L. Cano Rodríguez, M. Cara, J. V. M. Cardoso, S. Cheedella, Y. Copin, L. Corrales, D. Crichton, D. D'Avella, C. Deil, É. Depagne, J. P. Dietrich, A. Donath, M. Droettboom, N. Earl, T. Erben, S. Fabbro, L. A. Ferreira, T. Finethy, R. T. Fox, L. H. Garrison, S. L. J. Gibbons, D. A. Goldstein, R. Gommers, J. P. Greco, P. Greenfield, A. M. Groener, F. Grollier, A. Hagen, P. Hirst, D. Homeier, A. J. Horton, G. Hosseinzadeh, L. Hu, J. S. Hunkeler, Ž. Ivezić, A. Jain, T. Jenness, G. Kanarek, S. Kendrew, N. S. Kern, W. E. Kerzendorf, A. Khvalko, J. King, D. Kirkby, A. M. Kulkarni, A. Kumar, A. Lee, D. Lenz, S. P. Littlefair, Z. Ma, D. M. Macleod, M. Mastropietro, C. McCully, S. Montagnac, B. M. Morris, M. Mueller, S. J. Mumford, D. Muna, N. A. Murphy, S. Nelson, G. H. Nguyen, J. P. Ninan, M. Nöthe, S. Ogaz, S. Oh, J. K. Parejko, N. Parley, S. Pascual, R. Patil, A. A. Patil, A. L. Plunkett, J. X. Prochaska, T. Rastogi, V. Reddy Janga, J. Sabater, P. Sakurikar, M. Seifert, L. E. Sherbert, H. Sherwood-Taylor, A. Y. Shih, J. Sick, M. T. Silbiger, S. Singanamalla, L. P. Singer, P. H. Sladen, K. A. Sooley, S. Sornarajah, O. Streicher, P. Teuben, S. W. Thomas, G. R. Tremblay, J. E. H. Turner, V. Terrón, M. H. van Kerkwijk, A. de la Vega, L. L. Watkins, B. A. Weaver, J. B. Whitmore, J. Woillez, V. Zabalza, and Astropy Contributors. The Astropy Project: Building an Open-science Project and Status of the v2.0 Core Package. , 156(3):123, Sept. 2018.

[11] Astropy Collaboration, T. P. Robitaille, E. J. Tollerud, P. Greenfield, M. Droettboom, E. Bray, T. Aldcroft, M. Davis, A. Ginsburg, A. M. Price-Whelan, W. E. Kerzendorf, A. Conley, N. Crighton, K. Barbary, D. Muna, H. Ferguson, F. Grollier, M. M. Parikh, P. H. Nair, H. M. Unther, C. Deil, J. Woillez, S. Conseil, R. Kramer, J. E. H. Turner, L. Singer, R. Fox, B. A. Weaver, V. Zabalza, Z. I. Edwards, K. Azalee Bostroem, D. J. Burke, A. R. Casey, S. M. Crawford, N. Dencheva, J. Ely, T. Jenness, K. Labrie, P. L. Lim, F. Pierfederici, A. Pontzen, A. Ptak, B. Refsdal, M. Servillat, and O. Streicher. Astropy: A community Python package for astronomy. , 558:A33, Oct. 2013.

[12] R. F. Baumeister and M. R. Leary. The need to belong: desire for interpersonal attachments as a fundamental human motivation. *Psychological bulletin*, 117(3):497, 1995.

[13] K. Bechtol, A. Drlica-Wagner, E. Balbinot, A. Pieres, J. D. Simon, B. Yanny, B. Santiago, R. H. Wechsler, J. Frieman, A. R. Walker, P. Williams, E. Rozo, E. S. Rykoff, A. Queiroz, E. Luque, A. Benoit-Lévy, D. Tucker, I. Sevilla, R. A. Gruendl, L. N. da Costa, A. Fausti Neto, M. A. G. Maia, T. Abbott, S. Allam, R. Armstrong, A. H. Bauer, G. M. Bernstein, R. A. Bernstein, E. Bertin, D. Brooks, E. Buckley-Geer, D. L. Burke, A. Carnero Rosell, F. J. Castander, R. Covarrubias, C. B. D'Andrea, D. L. DePoy, S. Desai, H. T. Diehl, T. F. Eifler, J. Estrada, A. E. Evrard, E. Fernandez, D. A. Finley, B. Flaugher, E. Gaztanaga, D. Gerdes, L. Girardi, M. Gladders, D. Gruen, G. Gutierrez, J. Hao, K. Honscheid, B. Jain, D. James, S. Kent, R. Kron, K. Kuehn, N. Kuropatkin, O. Lahav, T. S. Li, H. Lin, M. Makler, M. March, J. Marshall, P. Martini, K. W. Merritt, C. Miller, R. Miquel, J. Mohr, E. Neilsen, R. Nichol, B. Nord, R. Ogando, J. Peoples, D. Petravick, A. A. Plazas, A. K. Romer, A. Roodman, M. Sako, E. Sanchez, V. Scarpine, M. Schubnell, R. C. Smith, M. Soares-Santos, F. Sobreira,

E. Suchyta, M. E. C. Swanson, G. Tarle, J. Thaler, D. Thomas, W. Wester, J. Zuntz, and DES Collaboration. Eight New Milky Way Companions Discovered in First-year Dark Energy Survey Data. , 807:50, July 2015.

[14] M. Bellazzini, N. Gennari, and F. R. Ferraro. The red giant branch tip and bump of the Leo II dwarf spheroidal galaxy. , 360(1):185–193, June 2005.

[15] M. Bellazzini, N. Gennari, F. R. Ferraro, and A. Sollima. The distance to the Leo I dwarf spheroidal galaxy from the red giant branch tip. *Mon. Not. R. Astron. Soc*, 354:708–712, 2004.

[16] V. Belokurov, M. G. Walker, N. W. Evans, G. Gilmore, M. J. Irwin, D. Just, S. Koposov, M. Mateo, E. Olszewski, L. Watkins, and L. Wyrzykowski. Big Fish, Little Fish: Two New Ultra-faint Satellites of the Milky Way. , 712:L103–L106, Mar. 2010.

[17] V. Belokurov, D. B. Zucker, N. W. Evans, J. T. Kleyna, S. Koposov, S. T. Hodgkin, M. J. Irwin, G. Gilmore, M. I. Wilkinson, M. Fellhauer, D. M. Bramich, P. C. Hewett, S. Vidrih, J. T. A. De Jong, J. A. Smith, H.-W. Rix, E. F. Bell, R. F. G. Wyse, H. J. Newberg, P. A. Mayeur, B. Yanny, C. M. Rockosi, O. Y. Gnedin, D. P. Schneider, T. C. Beers, J. C. Barentine, H. Brewington, J. Brinkmann, M. Harvanek, S. J. Kleinman, J. Krzesinski, D. Long, A. Nitta, and S. A. Snedden. Cats and Dogs, Hair and a Hero: A Quintet of New Milky Way Companions. , 654:897–906, Jan. 2007.

[18] R. Bernstein, S. A. Shectman, S. M. Gunnels, S. Mochnacki, and A. E. Athey. MIKE: A Double Echelle Spectrograph for the Magellan Telescopes at Las Campanas Observatory. In M. Iye and A. F. M. Moorwood, editors, *Instrument Design and Performance for Optical/Infrared Ground-based Telescopes*, volume 4841 of *Society of Photo-Optical Instrumentation Engineers (SPIE) Conference Series*, pages 1694–1704, Mar. 2003.

[19] G. Besla, N. Kallivayalil, L. Hernquist, B. Robertson, T. J. Cox, R. P. van der Marel, and C. Alcock. Are the Magellanic Clouds on Their First Passage about the Milky Way? , 668(2):949–967, Oct. 2007.

[20] M. Bettinelli, S. L. Hidalgo, S. Cassisi, A. Aparicio, and G. Piotto. The star formation history of the Sextans dwarf spheroidal galaxy: a true fossil of the pre-reionization era. , 476(1):71–79, May 2018.

[21] E. Boettcher, B. Willman, R. Fadely, J. Strader, M. Baker, E. Hopkins, T. T. Ananna, E. C. Cunningham, T. Douglas, J. Gilbert, A. Preston, and A. P. Sturner. A SEARCH FOR RR LYRAE STARS IN SEGUE 2 AND SEGUE 3. *The Astronomical Journal*, 146:94–103, 2013.

[22] S. Bose, A. J. Deason, V. Belokurov, and C. S. Frenk. The little things matter: relating the abundance of ultrafaint satellites to the hosts' assembly history. , 495(1):743–757, June 2020.

[23] A. Boselli, L. Cortese, M. Boquien, S. Boissier, B. Catinella, G. Gavazzi, C. Lagos, and A. Saintonge. Cold gas properties of the Herschel Reference Survey. III. Molecular gas stripping in cluster galaxies. , 564:A67, Apr. 2014.

[24] J. Bovy. galpy: A python Library for Galactic Dynamics. , 216(2):29, Feb. 2015.

[25] M. Boylan-Kolchin, J. S. Bullock, and M. Kaplinghat. Too big to fail? The puzzling darkness of massive Milky Way subhaloes. , 415(1):L40–L44, July 2011.

[26] M. Boylan-Kolchin, J. S. Bullock, and M. Kaplinghat. The Milky Way's bright satellites as an apparent failure of ΛCDM. , 422(2):1203–1218, May 2012.

[27] M. Boylan-Kolchin, J. S. Bullock, S. T. Sohn, G. Besla, and R. P. van der Marel. The Space Motion of Leo I: The Mass of the Milky Way's Dark Matter Halo. , 768(2):140, May 2013.

[28] M. Boylan-Kolchin, V. Springel, S. D. M. White, and A. Jenkins. There's no place like home? Statistics of Milky Way-mass dark matter haloes. , 406(2):896–912, Aug. 2010.

[29] M. Boylan-Kolchin, D. R. Weisz, J. S. Bullock, and M. C. Cooper. The Local Group: the ultimate deep field. , 462:L51–L55, Oct. 2016.

[30] A. M. Brooks, M. Kuhlen, A. Zolotov, and D. Hooper. A Baryonic Solution to the Missing Satellites Problem. , 765(1):22, Mar. 2013.

[31] A. M. Brooks and A. Zolotov. Why Baryons Matter: The Kinematics of Dwarf Spheroidal Satellites. , 786(2):87, May 2014.

[32] T. M. Brown, J. Tumlinson, M. Geha, E. N. Kirby, D. A. VandenBerg, R. R. Muñoz, J. S. Kalirai, J. D. Simon, R. J. Avila, P. Guhathakurta, A. Renzini, and H. C. Ferguson. The Primeval Populations of the Ultra-faint Dwarf Galaxies. , 753:L21, July 2012.

[33] T. M. Brown, J. Tumlinson, M. Geha, J. D. Simon, L. C. Vargas, D. A. VandenBerg, E. N. Kirby, J. S. Kalirai, R. J. Avila, M. Gennaro, H. C. Ferguson, R. R. Muñoz, P. Guhathakurta, and A. Renzini. The Quenching of the Ultra-faint Dwarf Galaxies in the Reionization Era. , 796:91, Dec. 2014.

[34] G. L. Bryan and M. L. Norman. Statistical Properties of X-Ray Clusters: Analytic and Numerical Comparisons. , 495(1):80–99, Mar. 1998.

[35] T. Buck, A. A. Dutton, and A. V. Macciò. Simulated ΛCDM analogues of the thin plane of satellites around the Andromeda galaxy are not kinematically coherent structures. *Monthly Notices of the Royal Astronomical Society*, 460(4):4348–4365, aug 2016.

[36] J. S. Bullock and M. Boylan-Kolchin. Small-Scale Challenges to the ΛcDM Paradigm, aug 2017.

[37] J. S. Bullock, A. V. Kravtsov, and D. H. Weinberg. Reionization and the Abundance of Galactic Satellites. , 539(2):517–521, Aug. 2000.

[38] M. T. Busha, R. H. Wechsler, P. S. Behroozi, B. F. Gerke, A. A. Klypin, and J. R. Primack. Statistics of Satellite Galaxies around Milky-Way-like Hosts. , 743(2):117, Dec. 2011.

[39] A. M. Byars-Winston, J. Branchaw, C. Pfund, P. Leverett, and J. Newton. Culturally diverse undergraduate researchers' academic outcomes and perceptions of their research mentoring relationships. *International journal of science education*, 37(15):2533–2554, 2015.

[40] N. Caldwell, M. G. Walker, M. Mateo, E. W. Olszewski, S. Koposov, V. Belokurov, G. Torrealba, A. Geringer-Sameth, and C. I. Johnson. Crater 2: An Extremely Cold Dark Matter Halo. , 839(1):20, Apr. 2017.

[41] J. L. Carlin, D. J. Sand, R. R. Muñoz, K. Spekkens, B. Willman, D. Crnojević, D. A. Forbes, J. Hargis, E. Kirby, A. H. G. Peter, A. J. Romanowsky, and J. Strader. Deep Subaru Hyper Suprime-Cam Observations of Milky Way Satellites Columba I and Triangulum II *. *The Astronomical Journal*, 154:267, 2017.

[42] S. G. Carlsten, J. E. Greene, A. H. G. Peter, J. P. Greco, and R. L. Beaton. Radial Distributions of Dwarf Satellite Systems in the Local Volume. , 902(2):124, Oct. 2020.

[43] A. R. Casey, S. C. Keller, G. Da Costa, A. Frebel, and E. Maunder. Hunting the Parent of the Orphan Stream. II. The First High-resolution Spectroscopic Study. , 784(1):19, Mar. 2014.

[44] F. Castelli and R. L. Kurucz. Is missing Fe I opacity in stellar atmospheres a significant problem? , 419:725–733, May 2004.

[45] M. Cautun, A. Benítez-Llambay, A. J. Deason, C. S. Frenk, A. Fattahi, F. A. Gómez, R. J. J. Grand, K. A. Oman, J. F. Navarro, and C. M. Simpson. The milky way total mass profile as inferred from Gaia DR2. , 494(3):4291–4313, Apr. 2020.

[46] M. M. Chemers, E. L. Zurbriggen, M. Syed, B. K. Goza, and S. Bearman. The role of efficacy and identity in science career commitment among underrepresented minority students. *Journal of Social Issues*, 67(3):469–491, 2011.

[47] A. Chiti, A. Frebel, A. P. Ji, H. Jerjen, D. Kim, and J. E. Norris. Chemical Abundances of New Member Stars in the Tucana II Dwarf Galaxy. , 857(1):74, Apr. 2018.

[48] G. Clementini, M. Cignoni, R. Contreras Ramos, L. Federici, V. Ripepi, M. Marconi, M. Tosi, and I. Musella. Variability and Star Formation in Leo T, the Lowest Luminosity Star-forming Galaxy Known Today. , 756:108, Sept. 2012.

[49] J. G. Cohen, A. McWilliam, N. Christlieb, S. Shectman, I. Thompson, J. Melendez, L. Wisotzki, and D. Reimers. A New Type of Extremely Metal-poor Star. , 659(2):L161–L164, Apr. 2007.

[50] M. L. M. Collins, N. F. Martin, R. M. Rich, R. A. Ibata, S. C. Chapman, A. W. Mcconnachie, A. M. Ferguson, M. J. Irwin, and G. F. Lewis. COMPARING THE OBSERVABLE PROPERTIES OF DWARF GALAXIES ON AND OFF THE ANDROMEDA PLANE. *The Astrophysical Journal Letters*, 799(6pp):13, 2015.

[51] A. R. Conn, G. F. Lewis, R. A. Ibata, Q. A. Parker, D. B. Zucker, A. W. McConnachie, N. F. Martin, D. Valls-Gabaud, N. Tanvir, M. J. Irwin, A. M. N. Ferguson, and S. C. Chapman. The Three-Dimensional Structure of the M31 Satellite System; Strong Evidence for an Inhomogeneous Distribution of Satellites. *Astrophysical Journal*, 766(2):120, jan 2013.

[52] D. Crnojević, D. J. Sand, D. Zaritsky, K. Spekkens, B. Willman, and J. R. Hargis. Deep Imaging of Eridanus II and Its Lone Star Cluster. , 824:L14, June 2016.

[53] M. Dall'Ora, G. Clementini, K. Kinemuchi, V. Ripepi, M. Marconi, L. Di Fabrizio, C. Greco, C. T. Rodgers, C. Kuehn, and H. A. Smith. Variable Stars in the Newly Discovered Milky Way Satellite in Bootes. *The Astrophysical Journal*, 653(2):L109–L112, dec 2006.

[54] M. Dall'ora, K. Kinemuchi, V. Ripepi, C. T. Rodgers, G. Clementini, L. D. Fabrizio, H. A. Smith, M. Marconi, I. Musella, C. Greco, C. A. Kuehn, M. Arcio Catelan, B. J. Pritzl, and T. C. Beers. STELLAR ARCHAEOLOGY IN THE GALACTIC HALO WITH THE ULTRA-FAINT DWARFS. VI. URSA MAJOR II *. *The Astrophysical Journal*, 752:42, 2012.

[55] L. J. M. Davies, A. S. G. Robotham, S. P. Driver, M. Alpaslan, I. K. Baldry, J. Bland-Hawthorn, S. Brough, M. J. I. Brown, M. E. Cluver, B. W. Holwerda, A. M. Hopkins, M. A. Lara-López, S. Mahajan, A. J. Moffett, M. S. Owers, and S. Phillipps. Galaxy And Mass Assembly (GAMA): growing up in a bad neighbourhood - how do low-mass galaxies become passive? , 455:4013–4029, Feb. 2016.

[56] J. T. A. de Jong, J. Harris, M. G. Coleman, N. F. Martin, E. F. Bell, H.-W. Rix, J. M. Hill, E. D. Skillman, D. J. Sand, E. W. Olszewski, D. Zaritsky, D. Thompson, E. Giallongo, R. Ragazzoni, A. DiPaola, J. Farinato, V. Testa, and J. Bechtold. The Structural Properties and Star Formation History of Leo T from Deep LBT Photometry. , 680:1112–1119, June 2008.

[57] G. De Lucia, S. Weinmann, B. M. Poggianti, A. Aragón-Salamanca, and D. Zaritsky. The environmental history of group and cluster galaxies in a Λ cold dark matter universe. , 423:1277–1292, June 2012.

[58] A. J. Deason, D. Erkal, V. Belokurov, A. Fattahi, F. A. Gómez, R. J. J. Grand , R. Pakmor, X.-X. Xue, C. Liu, C. Yang, L. Zhang, and G. Zhao. The mass of the Milky Way out to 100 kpc using halo stars. *arXiv e-prints*, page arXiv:2010.13801, Oct. 2020.

[59] E. D'Onghia, V. Springel, L. Hernquist, and D. Keres. Substructure Depletion in the Milky Way Halo by the Disk. , 709:1138–1147, Feb. 2010.

[60] A. Drlica-Wagner, K. Bechtol, S. Mau, M. McNanna, E. O. Nadler, A. B. Pace, T. S. Li, A. Pieres, E. Rozo, J. D. Simon, A. R. Walker, R. H. Wechsler, T. M. C. Abbott, S. Allam, J. Annis, E. Bertin, D. Brooks, D. L. Burke, A. C. Rosell, M. Carrasco Kind, J. Carretero, M. Costanzi, L. N. da Costa, J. De Vicente, S. Desai, H. T. Diehl, P. Doel, T. F. Eifler, S. Everett, B. Flaugher, J. Frieman, J. García-Bellido, E. Gaztanaga, D. Gruen, R. A. Gruendl, J. Gschwend, G. Gutierrez, K. Honscheid, D. J. James, E. Krause, K. Kuehn, N. Kuropatkin, O. Lahav, M. A. G. Maia, J. L. Marshall, P. Melchior, F. Menanteau, R. Miquel, A. Palmese, A. A. Plazas, E. Sanchez, V. Scarpine, M. Schubnell, S. Serrano, I. Sevilla-Noarbe, M. Smith, E. Suchyta, G. Tarle, and DES Collaboration. Milky Way Satellite Census. I. The Observational Selection Function for Milky Way Satellites in DES Y3 and Pan-STARRS DR1. , 893(1):47, Apr. 2020.

[61] A. Drlica-Wagner, K. Bechtol, E. S. Rykoff, E. Luque, A. Queiroz, Y.-Y. Mao, R. H. Wechsler, J. D. Simon, B. Santiago, B. Yanny, E. Balbinot, S. Dodelson, A. Fausti Neto, D. J. James, T. S. Li, M. A. G. Maia, J. L. Marshall, A. Pieres, K. Stringer, A. R. Walker, T. M. C. Abbott, F. B. Abdalla, S. Allam, A. Benoit-Lévy, G. M. Bernstein, E. Bertin, D. Brooks, E. Buckley-Geer, D. L. Burke, A. Carnero Rosell, M. Carrasco Kind, J. Carretero, M. Crocce, L. N. da Costa, S. Desai, H. T. Diehl, J. P. Dietrich, P. Doel, T. F. Eifler, A. E. Evrard, D. A. Finley, B. Flaugher, P. Fosalba, J. Frieman, E. Gaztanaga, D. W. Gerdes, D. Gruen, R. A. Gruendl, G. Gutierrez, K. Honscheid, K. Kuehn, N. Kuropatkin, O. Lahav, P. Martini, R. Miquel, B. Nord, R. Ogando, A. A. Plazas, K. Reil, A. Roodman, M. Sako, E. Sanchez, V. Scarpine, M. Schubnell, I. Sevilla-Noarbe, R. C. Smith, M. Soares-Santos, F. Sobreira, E. Suchyta, M. E. C. Swanson, G. Tarle, D. Tucker, V. Vikram, W. Wester, Y. Zhang, J. Zuntz, and DES Collaboration. Eight Ultra-faint Galaxy Candidates Discovered in Year Two of the Dark Energy Survey. , 813:109, Nov. 2015.

[62] R. D'Souza and E. F. Bell. The infall of dwarf satellite galaxies are influenced by their host's massive accretions. , 504(4):5270–5286, July 2021.

[63] R. Dunbar, R. I. M. Dunbar, and L. Barrett. *Oxford handbook of evolutionary psychology*. Oxford University Press, USA, 2007.

[64] G. Eadie and M. Jurić. The Cumulative Mass Profile of the Milky Way as Determined by Globular Cluster Kinematics from Gaia DR2. , 875(2):159, Apr. 2019.

[65] G. Efstathiou. Suppressing the formation of dwarf galaxies via photoionization. , 256:43P–47P, May 1992.

[66] L. M. Elias, L. V. Sales, P. Creasey, M. C. Cooper, J. S. Bullock, R. M. Rich, and L. Hernquist. Stellar halos in Illustris: probing the histories of Milky Way-mass galaxies. , 479(3):4004–4016, Sept. 2018.

[67] D. Erkal and V. A. Belokurov. Limit on the LMC mass from a census of its satellites. *arXiv e-prints*, page arXiv:1907.09484, July 2019.

[68] M. Estrada, P. R. Hernandez, and P. W. Schultz. A longitudinal study of how quality mentorship and research experience integrate underrepresented minorities into stem careers. *CBE—Life Sciences Education*, 17(1):ar9, 2018.

[69] M. Estrada, A. Woodcock, P. R. Hernandez, and P. Schultz. Toward a model of social influence that explains minority student integration into the scientific community. *Journal of educational psychology*, 103(1):206, 2011.

[70] S. Feltzing, K. Eriksson, J. Kleyna, and M. I. Wilkinson. Evidence of enrichment by individual SN from elemental abundance ratios in the very metal-poor dSph galaxy Boötes I. , 508(1):L1–L4, Dec. 2009.

[71] S. P. Fillingham, M. C. Cooper, M. Boylan-Kolchin, J. S. Bullock, S. Garrison-Kimmel, and C. Wheeler. Environmental quenching of low-mass field galaxies. , 477(4):4491–4498, July 2018.

[72] S. P. Fillingham, M. C. Cooper, T. Kelley, M. K. Rodriguez Wimberly, M. Boylan-Kolchin, J. S. Bullock, S. Garrison-Kimmel, M. S. Pawlowski, and C. Wheeler. Characterizing the Infall Times and Quenching Timescales of Milky Way Satellites with *Gaia* Proper Motions. *arXiv e-prints*, page arXiv:1906.04180, June 2019.

[73] S. P. Fillingham, M. C. Cooper, A. B. Pace, M. Boylan-Kolchin, J. S. Bullock, S. Garrison-Kimmel, and C. Wheeler. Under pressure: quenching star formation in low-mass satellite galaxies via stripping. , 463:1916–1928, Dec. 2016.

[74] S. P. Fillingham, M. C. Cooper, C. Wheeler, S. Garrison-Kimmel, M. Boylan-Kolchin, and J. S. Bullock. Taking care of business in a flash: constraining the time-scale for low-mass satellite quenching with ELVIS. , 454:2039–2049, Dec. 2015.

[75] A. Fitts, M. Boylan-Kolchin, O. D. Elbert, J. S. Bullock, P. F. Hopkins, J. Oñorbe, A. Wetzel, C. Wheeler, C.-A. Faucher-Giguère, D. Kereš, E. D. Skillman, and D. R. Weisz. fire in the field: simulating the threshold of galaxy formation. , 471:3547–3562, Nov. 2017.

[76] Y. Fong and Y. Huang. Modified wilcoxonâmannâwhitney test and power against strong null. *The American Statistician*, 73(1):43–49, 2019. PMID: 30899120.

[77] A. S. Font, I. G. McCarthy, and V. Belokurov. Can cosmological simulations capture the diverse satellite populations of observed Milky Way analogues? *arXiv e-prints*, page arXiv:2011.12974, Nov. 2020.

[78] P. François, L. Monaco, P. Bonifacio, C. Moni Bidin, D. Geisler, and L. Sbordone. Abundance ratios of red giants in low-mass ultra-faint dwarf spheroidal galaxies. , 588:A7, Apr. 2016.

[79] A. Frebel and V. Bromm. Chemical Signatures of the First Galaxies: Criteria for One-shot Enrichment. , 759(2):115, Nov. 2012.

[80] A. Frebel, J. D. Simon, M. Geha, and B. Willman. High-Resolution Spectroscopy of Extremely Metal-Poor Stars in the Least Evolved Galaxies: Ursa Major II and Coma Berenices. , 708(1):560–583, Jan. 2010.

[81] A. Frebel, J. D. Simon, and E. N. Kirby. Segue 1: An Unevolved Fossil Galaxy from the Early Universe. , 786:74, May 2014.

[82] K. Freeman and J. Bland-Hawthorn. The New Galaxy: Signatures of Its Formation. , 40:487–537, Jan. 2002.

[83] T. K. Fritz, G. Battaglia, M. S. Pawlowski, N. Kallivayalil, R. van der Marel, S. T. Sohn, C. Brook, and G. Besla. Gaia DR2 proper motions of dwarf galaxies within 420 kpc. Orbits, Milky Way mass, tidal influences, planar alignments, and group infall. , 619:A103, Nov. 2018.

[84] T. K. Fritz, A. Di Cintio, G. Battaglia, C. Brook, and S. Taibi. The mass of our Galaxy from satellite proper motions in the Gaia era. *arXiv e-prints*, page arXiv:2001.02651, Jan 2020.

[85] T. K. Fritz, M. Lokken, N. Kallivayalil, A. Wetzel, S. T. Linden, P. Zivick, and E. J. Tollerud. The Orbit and Origin of the Ultra-faint Dwarf Galaxy Segue˜1. *ArXiv e-prints*, Nov. 2017.

[86] Gaia Collaboration, A. G. A. Brown, A. Vallenari, T. Prusti, J. H. J. de Bruijne, C. Babusiaux, C. A. L. Bailer-Jones, M. Biermann, D. W. Evans, L. Eyer, F. Jansen, C. Jordi, S. A. Klioner, U. Lammers, L. Lindegren, X. Luri, F. Mignard, C. Panem, D. Pourbaix, S. Randich, P. Sartoretti, H. I. Siddiqui, C. Soubiran, F. van Leeuwen, N. A. Walton, F. Arenou, U. Bastian, M. Cropper, R. Drimmel, D. Katz, M. G. Lattanzi, J. Bakker, C. Cacciari, J. Castañeda, L. Chaoul, N. Cheek, F. De Angeli, C. Fabricius, R. Guerra, B. Holl, E. Masana, R. Messineo, N. Mowlavi, K. Nienartowicz, P. Panuzzo, J. Portell, M. Riello, G. M. Seabroke, P. Tanga, F. Thévenin, G. Gracia-Abril, G. Comoretto, M. Garcia-Reinaldos, D. Teyssier, M. Altmann, R. Andrae, M. Audard, I. Bellas-Velidis, K. Benson, J. Berthier, R. Blomme, P. Burgess, G. Busso, B. Carry, A. Cellino, G. Clementini, M. Clotet, O. Creevey, M. Davidson, J. De Ridder, L. Delchambre, A. Dell'Oro, C. Ducourant, J. Fernández-Hernández, M. Fouesneau, Y. Frémat, L. Galluccio, M. García-Torres, J. González-Núñez, J. J. González-Vidal, E. Gosset, L. P. Guy, J. L. Halbwachs, N. C. Hambly, D. L. Harrison, J. Hernández, D. Hestroffer, S. T. Hodgkin, A. Hutton, G. Jasniewicz, A. Jean-Antoine-Piccolo, S. Jordan, A. J. Korn, A. Krone-Martins, A. C. Lanzafame, T. Lebzelter, W. Löffler, M. Manteiga, P. M. Marrese, J. M. Martín-Fleitas, A. Moitinho, A. Mora, K. Muinonen, J. Osinde, E. Pancino, T. Pauwels, J. M. Petit, A. Recio-Blanco, P. J. Richards, L. Rimoldini, A. C. Robin, L. M. Sarro, C. Siopis, M. Smith, A. Sozzetti, M. Süveges, J. Torra, W. van Reeven, U. Abbas, A. Abreu Aramburu, S. Accart, C. Aerts, G. Altavilla, M. A. Álvarez, R. Alvarez, J. Alves, R. I. Anderson, A. H. Andrei, E. Anglada Varela, E. Antiche, T. Antoja, B. Arcay, T. L. Astraatmadja, N. Bach, S. G. Baker, L. Balaguer-Núñez, P. Balm, C. Barache, C. Barata, D. Barbato, F. Barblan, P. S. Barklem, D. Barrado, M. Barros, M. A. Barstow, S. Bartholomé Muñoz, J. L. Bassilana, U. Becciani, M. Bellazzini, A. Berihuete, S. Bertone, L. Bianchi, O. Bienaymé, S. Blanco-Cuaresma, T. Boch, C. Boeche, A. Bombrun, R. Borrachero, D. Bossini, S. Bouquillon, G. Bourda, A. Bragaglia, L. Bramante, M. A. Breddels, A. Bressan, N. Brouillet, T. Brüsemeister, E. Brugaletta, B. Bucciarelli, A. Burlacu, D. Busonero, A. G. Butkevich, R. Buzzi, E. Caffau, R. Cancelliere, G. Cannizzaro, T. Cantat-Gaudin, R. Carballo, T. Carlucci, J. M. Carrasco, L. Casamiquela, M. Castellani, A. Castro-Ginard, P. Charlot, L. Chemin, A. Chiavassa, G. Cocozza, G. Costigan, S. Cowell, F. Crifo, M. Crosta, C. Crowley, J. Cuypers, C. Dafonte, Y. Damerdji, A. Dapergolas, P. David, M. David, P. de Laverny, F. De Luise, R. De March, D. de Martino, R. de Souza, A. de Torres, J. Debosscher, E. del Pozo, M. Delbo, A. Delgado, H. E. Delgado, P. Di Matteo, S. Diakite, C. Diener, E. Distefano, C. Dolding, P. Drazinos, J. Durán, B. Edvardsson, H. Enke, K. Eriksson, P. Esquej, G. Eynard Bontemps, C. Fabre, M. Fabrizio, S. Faigler, A. J. Falcão, M. Farràs Casas, L. Federici, G. Fedorets, P. Fernique, F. Figueras, F. Filippi, K. Findeisen, A. Fonti, E. Fraile, M. Fraser, B. Frézouls, M. Gai, S. Galleti, D. Garabato, F. García-Sedano, A. Garofalo, N. Garralda, A. Gavel, P. Gavras, J. Gerssen, R. Geyer, P. Giacobbe, G. Gilmore, S. Girona, G. Giuffrida, F. Glass, M. Gomes, M. Granvik, A. Gueguen, A. Guerrier, J. Guiraud, R. Gutiérrez-Sánchez, R. Haigron, D. Hatzidimitriou, M. Hauser, M. Haywood, U. Heiter, A. Helmi, J. Heu, T. Hilger, D. Hobbs, W. Hofmann, G. Holland, H. E. Huckle, A. Hypki, V. Icardi, K. Janßen, G. Jevardat de Fombelle, P. G. Jonker, Á. L. Juhász, F. Julbe, A. Karampelas, A. Kewley, J. Klar, A. Kochoska, R. Kohley, K. Kolenberg, M. Kontizas, E. Kontizas,

S. E. Koposov, G. Kordopatis, Z. Kostrzewa-Rutkowska, P. Koubsky, S. Lambert, A. F. Lanza, Y. Lasne, J. B. Lavigne, Y. Le Fustec, C. Le Poncin-Lafitte, Y. Lebreton, S. Leccia, N. Leclerc, I. Lecoeur-Taibi, H. Lenhardt, F. Leroux, S. Liao, E. Licata, H. E. P. Lindstrøm, T. A. Lister, E. Livanou, A. Lobel, M. López, S. Managau, R. G. Mann, G. Mantelet, O. Marchal, J. M. Marchant, M. Marconi, S. Marinoni, G. Marschalkó, D. J. Marshall, M. Martino, G. Marton, N. Mary, D. Massari, G. Matijevič, T. Mazeh, P. J. McMillan, S. Messina, D. Michalik, N. R. Millar, D. Molina, R. Molinaro, L. Molnár, P. Montegriffo, R. Mor, R. Morbidelli, T. Morel, D. Morris, A. F. Mulone, T. Muraveva, I. Musella, G. Nelemans, L. Nicastro, L. Noval, W. O'Mullane, C. Ordénovic, D. Ordóñez-Blanco, P. Osborne, C. Pagani, I. Pagano, F. Pailler, H. Palacin, L. Palaversa, A. Panahi, M. Pawlak, A. M. Piersimoni, F. X. Pineau, E. Plachy, G. Plum, E. Poggio, E. Poujoulet, A. Prša, L. Pulone, E. Racero, S. Ragaini, N. Rambaux, M. Ramos-Lerate, S. Regibo, C. Reylé, F. Riclet, V. Ripepi, A. Riva, A. Rivard, G. Rixon, T. Roegiers, M. Roelens, M. Romero-Gómez, N. Rowell, F. Royer, L. Ruiz-Dern, G. Sadowski, T. Sagristà Sellés, J. Sahlmann, J. Salgado, E. Salguero, N. Sanna, T. Santana-Ros, M. Sarasso, H. Savietto, M. Schultheis, E. Sciacca, M. Segol, J. C. Segovia, D. Ségransan, I. C. Shih, L. Siltala, A. F. Silva, R. L. Smart, K. W. Smith, E. Solano, F. Solitro, R. Sordo, S. Soria Nieto, J. Souchay, A. Spagna, F. Spoto, U. Stampa, I. A. Steele, H. Steidelmüller, C. A. Stephenson, H. Stoev, F. F. Suess, J. Surdej, L. Szabados, E. Szegedi-Elek, D. Tapiador, F. Taris, G. Tauran, M. B. Taylor, R. Teixeira, D. Terrett, P. Teyssand ier, W. Thuillot, A. Titarenko, F. Torra Clotet, C. Turon, A. Ulla, E. Utrilla, S. Uzzi, M. Vaillant, G. Valentini, V. Valette, A. van Elteren, E. Van Hemelryck, M. van Leeuwen, M. Vaschetto, A. Vecchiato, J. Veljanoski, Y. Viala, D. Vicente, S. Vogt, C. von Essen, H. Voss, V. Votruba, S. Voutsinas, G. Walmsley, M. Weiler, O. Wertz, T. Wevers, Ł. Wyrzykowski, A. Yoldas, M. Žerjal, H. Ziaeepour, J. Zorec, S. Zschocke, S. Zucker, C. Zurbach, and T. Zwitter. Gaia Data Release 2. Summary of the contents and survey properties. , 616:A1, Aug. 2018.

[87] Gaia Collaboration, A. G. A. Brown, A. Vallenari, T. Prusti, J. H. J. de Bruijne, C. Babusiaux, and M. Biermann. Gaia Early Data Release 3: Summary of the contents and survey properties. *arXiv e-prints*, page arXiv:2012.01533, Dec. 2020.

[88] Gaia Collaboration, T. Prusti, J. H. J. de Bruijne, A. G. A. Brown, A. Vallenari, C. Babusiaux, C. A. L. Bailer-Jones, U. Bastian, M. Biermann, D. W. Evans, L. Eyer, F. Jansen, C. Jordi, S. A. Klioner, U. Lammers, L. Lindegren, X. Luri, F. Mignard, D. J. Milligan, C. Panem, V. Poinsignon, D. Pourbaix, S. Randich, G. Sarri, P. Sartoretti, H. I. Siddiqui, C. Soubiran, V. Valette, F. van Leeuwen, N. A. Walton, C. Aerts, F. Arenou, M. Cropper, R. Drimmel, E. Høg, D. Katz, M. G. Lattanzi, W. O'Mullane, E. K. Grebel, A. D. Holland, C. Huc, X. Passot, L. Bramante, C. Cacciari, J. Castañeda, L. Chaoul, N. Cheek, F. De Angeli, C. Fabricius, R. Guerra, J. Hernández, A. Jean-Antoine-Piccolo, E. Masana, R. Messineo, N. Mowlavi, K. Nienartowicz, D. Ordóñez-Blanco, P. Panuzzo, J. Portell, P. J. Richards, M. Riello, G. M. Seabroke, P. Tanga, F. Thévenin, J. Torra, S. G. Els, G. Gracia-Abril, G. Comoretto, M. Garcia-Reinaldos, T. Lock, E. Mercier, M. Altmann, R. Andrae, T. L. Astraatmadja, I. Bellas-Velidis, K. Benson, J. Berthier, R. Blomme, G. Busso, B. Carry, A. Cellino, G. Clementini, S. Cowell, O. Creevey, J. Cuypers, M. Davidson, J. De Ridder, A. de Torres, L. Delchambre, A. Dell'Oro, C. Ducourant, Y. Frémat, M. García-Torres,

E. Gosset, J. L. Halbwachs, N. C. Hambly, D. L. Harrison, M. Hauser, D. Hestroffer, S. T. Hodgkin, H. E. Huckle, A. Hutton, G. Jasniewicz, S. Jordan, M. Kontizas, A. J. Korn, A. C. Lanzafame, M. Manteiga, A. Moitinho, K. Muinonen, J. Osinde, E. Pancino, T. Pauwels, J. M. Petit, A. Recio-Blanco, A. C. Robin, L. M. Sarro, C. Siopis, M. Smith, K. W. Smith, A. Sozzetti, W. Thuillot, W. van Reeven, Y. Viala, U. Abbas, A. Abreu Aramburu, S. Accart, J. J. Aguado, P. M. Allan, W. Allasia, G. Altavilla, M. A. Álvarez, J. Alves, R. I. Anderson, A. H. Andrei, E. Anglada Varela, E. Antiche, T. Antoja, S. Antón, B. Arcay, A. Atzei, L. Ayache, N. Bach, S. G. Baker, L. Balaguer-Núñez, C. Barache, C. Barata, A. Barbier, F. Barblan, M. Baroni, D. Barrado y Navascués, M. Barros, M. A. Barstow, U. Becciani, M. Bellazzini, G. Bellei, A. Bello García, V. Belokurov, P. Bendjoya, A. Berihuete, L. Bianchi, O. Bienaymé, F. Billebaud, N. Blagorodnova, S. Blanco-Cuaresma, T. Boch, A. Bombrun, R. Borrachero, S. Bouquillon, G. Bourda, H. Bouy, A. Bragaglia, M. A. Breddels, N. Brouillet, T. Brüsemeister, B. Bucciarelli, F. Budnik, P. Burgess, R. Burgon, A. Burlacu, D. Busonero, R. Buzzi, E. Caffau, J. Cambras, H. Campbell, R. Cancelliere, T. Cantat-Gaudin, T. Carlucci, J. M. Carrasco, M. Castellani, P. Charlot, J. Charnas, P. Charvet, F. Chassat, A. Chiavassa, M. Clotet, G. Cocozza, R. S. Collins, P. Collins, G. Costigan, F. Crifo, N. J. G. Cross, M. Crosta, C. Crowley, C. Dafonte, Y. Damerdji, A. Dapergolas, P. David, M. David, P. De Cat, F. de Felice, P. de Laverny, F. De Luise, R. De March, D. de Martino, R. de Souza, J. Debosscher, E. del Pozo, M. Delbo, A. Delgado, H. E. Delgado, F. di Marco, P. Di Matteo, S. Diakite, E. Distefano, C. Dolding, S. Dos Anjos, P. Drazinos, J. Durán, Y. Dzigan, E. Ecale, B. Edvardsson, H. Enke, M. Erdmann, D. Escolar, M. Espina, N. W. Evans, G. Eynard Bontemps, C. Fabre, M. Fabrizio, S. Faigler, A. J. Falcão, M. Farràs Casas, F. Faye, L. Federici, G. Fedorets, J. Fernández-Hernández, P. Fernique, A. Fienga, F. Figueras, F. Filippi, K. Findeisen, A. Fonti, M. Fouesneau, E. Fraile, M. Fraser, J. Fuchs, R. Furnell, M. Gai, S. Galleti, L. Galluccio, D. Garabato, F. García-Sedano, P. Garé, A. Garofalo, N. Garralda, P. Gavras, J. Gerssen, R. Geyer, G. Gilmore, S. Girona, G. Giuffrida, M. Gomes, A. González-Marcos, J. González-Núñez, J. J. González-Vidal, M. Granvik, A. Guerrier, P. Guillout, J. Guiraud, A. Gúrpide, R. Gutiérrez-Sánchez, L. P. Guy, R. Haigron, D. Hatzidimitriou, M. Haywood, U. Heiter, A. Helmi, D. Hobbs, W. Hofmann, B. Holl, G. Holland , J. A. S. Hunt, A. Hypki, V. Icardi, M. Irwin, G. Jevardat de Fombelle, P. Jofré, P. G. Jonker, A. Jorissen, F. Julbe, A. Karampelas, A. Kochoska, R. Kohley, K. Kolenberg, E. Kontizas, S. E. Koposov, G. Kordopatis, P. Koubsky, A. Kowalczyk, A. Krone-Martins, M. Kudryashova, I. Kull, R. K. Bachchan, F. Lacoste-Seris, A. F. Lanza, J. B. Lavigne, C. Le Poncin-Lafitte, Y. Lebreton, T. Lebzelter, S. Leccia, N. Leclerc, I. Lecoeur-Taibi, V. Lemaitre, H. Lenhardt, F. Leroux, S. Liao, E. Licata, H. E. P. Lindstrøm, T. A. Lister, E. Livanou, A. Lobel, W. Löffler, M. López, A. Lopez-Lozano, D. Lorenz, T. Loureiro, I. MacDonald, T. Magalhães Fernandes, S. Managau, R. G. Mann, G. Mantelet, O. Marchal, J. M. Marchant, M. Marconi, J. Marie, S. Marinoni, P. M. Marrese, G. Marschalkó, D. J. Marshall, J. M. Martín-Fleitas, M. Martino, N. Mary, G. Matijevič, T. Mazeh, P. J. McMillan, S. Messina, A. Mestre, D. Michalik, N. R. Millar, B. M. H. Miranda, D. Molina, R. Molinaro, M. Molinaro, L. Molnár, M. Moniez, P. Montegriffo, D. Monteiro, R. Mor, A. Mora, R. Morbidelli, T. Morel, S. Morgenthaler, T. Morley, D. Morris, A. F. Mulone, T. Muraveva, I. Musella, J. Narbonne, G. Nelemans, L. Nicastro, L. Noval, C. Ordénovic, J. Ordieres-Meré, P. Osborne, C. Pagani, I. Pagano, F. Pailler, H. Palacin, L. Palaversa, P. Parsons, T. Paulsen, M. Pecoraro, R. Pedrosa, H. Pentikäinen, J. Pereira, B. Pichon, A. M. Piersimoni, F. X. Pineau,

E. Plachy, G. Plum, E. Poujoulet, A. Prša, L. Pulone, S. Ragaini, S. Rago, N. Rambaux, M. Ramos-Lerate, P. Ranalli, G. Rauw, A. Read, S. Regibo, F. Renk, C. Reylé, R. A. Ribeiro, L. Rimoldini, V. Ripepi, A. Riva, G. Rixon, M. Roelens, M. Romero-Gómez, N. Rowell, F. Royer, A. Rudolph, L. Ruiz-Dern, G. Sadowski, T. Sagristà Sellés, J. Sahlmann, J. Salgado, E. Salguero, M. Sarasso, H. Savietto, A. Schnorhk, M. Schultheis, E. Sciacca, M. Segol, J. C. Segovia, D. Segransan, E. Serpell, I. C. Shih, R. Smareglia, R. L. Smart, C. Smith, E. Solano, F. Solitro, R. Sordo, S. Soria Nieto, J. Souchay, A. Spagna, F. Spoto, U. Stampa, I. A. Steele, H. Steidelmüller, C. A. Stephenson, H. Stoev, F. F. Suess, M. Süveges, J. Surdej, L. Szabados, E. Szegedi-Elek, D. Tapiador, F. Taris, G. Tauran, M. B. Taylor, R. Teixeira, D. Terrett, B. Tingley, S. C. Trager, C. Turon, A. Ulla, E. Utrilla, G. Valentini, A. van Elteren, E. Van Hemelryck, M. van Leeuwen, M. Varadi, A. Vecchiato, J. Veljanoski, T. Via, D. Vicente, S. Vogt, H. Voss, V. Votruba, S. Voutsinas, G. Walmsley, M. Weiler, K. Weingrill, D. Werner, T. Wevers, G. Whitehead, Ł. Wyrzykowski, A. Yoldas, M. Žerjal, S. Zucker, C. Zurbach, T. Zwitter, A. Alecu, M. Allen, C. Allende Prieto, A. Amorim, G. Anglada-Escudé, V. Arsenijevic, S. Azaz, P. Balm, M. Beck, H. H. Bernstein, L. Bigot, A. Bijaoui, C. Blasco, M. Bonfigli, G. Bono, S. Boudreault, A. Bressan, S. Brown, P. M. Brunet, P. Bunclark, R. Buonanno, A. G. Butkevich, C. Carret, C. Carrion, L. Chemin, F. Chéreau, L. Corcione, E. Darmigny, K. S. de Boer, P. de Teodoro, P. T. de Zeeuw, C. Delle Luche, C. D. Domingues, P. Dubath, F. Fodor, B. Frézouls, A. Fries, D. Fustes, D. Fyfe, E. Gallardo, J. Gallegos, D. Gardiol, M. Gebran, A. Gomboc, A. Gómez, E. Grux, A. Gueguen, A. Heyrovsky, J. Hoar, G. Iannicola, Y. Isasi Parache, A. M. Janotto, E. Joliet, A. Jonckheere, R. Keil, D. W. Kim, P. Klagyivik, J. Klar, J. Knude, O. Kochukhov, I. Kolka, J. Kos, A. Kutka, V. Lainey, D. LeBouquin, C. Liu, D. Loreggia, V. V. Makarov, M. G. Marseille, C. Martayan, O. Martinez-Rubi, B. Massart, F. Meynadier, S. Mignot, U. Munari, A. T. Nguyen, T. Nordlander, P. Ocvirk, K. S. O'Flaherty, A. Olias Sanz, P. Ortiz, J. Osorio, D. Oszkiewicz, A. Ouzounis, M. Palmer, P. Park, E. Pasquato, C. Peltzer, J. Peralta, F. Péturaud, T. Pieniluoma, E. Pigozzi, J. Poels, G. Prat, T. Prod'homme, F. Raison, J. M. Rebordao, D. Risquez, B. Rocca-Volmerange, S. Rosen, M. I. Ruiz-Fuertes, F. Russo, S. Sembay, I. Serraller Vizcaino, A. Short, A. Siebert, H. Silva, D. Sinachopoulos, E. Slezak, M. Soffel, D. Sosnowska, V. Straižys, M. ter Linden, D. Terrell, S. Theil, C. Tiede, L. Troisi, P. Tsalmantza, D. Tur, M. Vaccari, F. Vachier, P. Valles, W. Van Hamme, L. Veltz, J. Virtanen, J. M. Wallut, R. Wichmann, M. I. Wilkinson, H. Ziaeepour, and S. Zschocke. The Gaia mission. , 595:A1, Nov. 2016.

[89] A. Garofalo, F. Cusano, G. Clementini, V. Ripepi, M. Dall'ora, M. I. Moretti, G. Coppola, I. Musella, and M. Marconi. VARIABLE STARS IN THE ULTRA-FAINT DWARF SPHEROIDAL GALAXY URSA MAJOR I *. *The Astrophysical Journal*, 767:62, 2013.

[90] S. Garrison-Kimmel, M. Boylan-Kolchin, J. S. Bullock, and K. Lee. ELVIS: Exploring the Local Volume in Simulations. , 438:2578–2596, Mar. 2014.

[91] S. Garrison-Kimmel, A. Wetzel, J. S. Bullock, P. F. Hopkins, M. Boylan-Kolchin, C.-A. Faucher-Giguère, D. Kereš, E. Quataert, R. E. Sanderson, A. S. Graus, and T. Kelley. Not so lumpy after all: modelling the depletion of dark matter subhaloes by Milky Way-like galaxies. , 471:1709–1727, Oct. 2017.

[92] M. Geha, T. M. Brown, J. Tumlinson, J. S. Kalirai, J. D. Simon, E. N. Kirby, D. A. VandenBerg, R. R. Muñoz, R. J. Avila, P. Guhathakurta, and H. C. Ferguson. The Stellar Initial Mass Function of Ultra-faint Dwarf Galaxies: Evidence for IMF Variations with Galactic Environment. , 771:29, July 2013.

[93] M. Geha, R. H. Wechsler, Y.-Y. Mao, E. J. Tollerud, B. Weiner, R. Bernstein, B. Hoyle, S. Marchi, P. J. Marshall, R. Muñoz, and Y. Lu. The SAGA Survey. I. Satellite Galaxy Populations around Eight Milky Way Analogs. , 847(1):4, Sept. 2017.

[94] G. Gilmore, J. E. Norris, L. Monaco, D. Yong, R. F. G. Wyse, and D. Geisler. Elemental Abundances and their Implications for the Chemical Enrichment of the Boötes I Ultrafaint Galaxy. , 763(1):61, Jan. 2013.

[95] N. Y. Gnedin. Effect of Reionization on Structure Formation in the Universe. , 542(2):535–541, Oct. 2000.

[96] M. J. Graham, J. Frederick, A. Byars-Winston, A.-B. Hunter, and J. Handelsman. Increasing persistence of college students in stem. *Science*, 341(6153):1455–1456, 2013.

[97] A. S. Graus, J. S. Bullock, T. Kelley, M. Boylan-Kolchin, S. Garrison-Kimmel, and Y. Qi. How low does it go? Too few Galactic satellites with standard reionization quenching. , 488(4):4585–4595, Oct. 2019.

[98] C. Greco, M. Dall'Ora, G. Clementini, V. Ripepi, L. Di Fabrizio, K. Kinemuchi, M. Marconi, I. Musella, H. A. Smith, C. T. Rodgers, C. Kuehn, T. C. Beers, M. Catelan, and B. J. Pritzl. On the newly discovered Canes Venatici II dSph galaxy. *The Astrophysical Journal*, 675(2):L73–L76, dec 2007.

[99] A. Hamanowicz, P. Pietrukowicz, A. Udalski, P. Mróz, I. Soszyński, M. K. Szymański, J. Skowron, R. Poleski, Ł. Wyrzykowski, S. Kozłowski, M. Pawlak, and K. Ulaczyk. OGLE Study of the Sagittarius Dwarf Spheroidal Galaxy and its M54 Globular Cluster. , 66(2):197–217, June 2016.

[100] T. T. Hansen, J. D. Simon, J. L. Marshall, T. S. Li, D. Carollo, D. L. DePoy, D. Q. Nagasawa, R. A. Bernstein, A. Drlica-Wagner, F. B. Abdalla, S. Allam, J. Annis, K. Bechtol, A. Benoit-Lévy, D. Brooks, E. Buckley-Geer, A. Carnero Rosell, M. Carrasco Kind, J. Carretero, C. E. Cunha, L. N. da Costa, S. Desai, T. F. Eifler, A. Fausti Neto, B. Flaugher, J. Frieman, J. García-Bellido, E. Gaztanaga, D. W. Gerdes, D. Gruen, R. A. Gruendl, J. Gschwend, G. Gutierrez, D. J. James, E. Krause, K. Kuehn, N. Kuropatkin, O. Lahav, R. Miquel, A. A. Plazas, A. K. Romer, E. Sanchez, B. Santiago, V. Scarpine, R. C. Smith, M. Soares-Santos, F. Sobreira, E. Suchyta, M. E. C. Swanson, G. Tarle, A. R. Walker, and DES Collaboration. An r-process Enhanced Star in the Dwarf Galaxy Tucana III. , 838(1):44, Mar. 2017.

[101] J. R. Hargis, B. Willman, and A. H. G. Peter. Too Many, Too Few, or Just Right? The Predicted Number and Distribution of Milky Way Dwarf Galaxies. , 795(1):L13, Nov. 2014.

[102] C. R. Harris, K. J. Millman, S. J. van der Walt, R. Gommers, P. Virtanen, D. Cournapeau, E. Wieser, J. Taylor, S. Berg, N. J. Smith, R. Kern, M. Picus, S. Hoyer, M. H. van Kerkwijk,

M. Brett, A. Haldane, J. F. del Río, M. Wiebe, P. Peterson, P. Gérard-Marchant, K. Sheppard, T. Reddy, W. Weckesser, H. Abbasi, C. Gohlke, and T. E. Oliphant. Array programming with NumPy. *Nature*, 585(7825):357–362, Sept. 2020.

[103] A. Helmi, F. Van Leeuwen, P. J. McMillan, D. Massari, T. Antoja, A. C. Robin, L. Lindegren, U. Bastian, F. Arenou, C. Babusiaux, M. Biermann, M. A. Breddels, D. Hobbs, C. Jordi, E. Pancino, C. Reylé, J. Veljanoski, A. G. Brown, A. Vallenari, T. Prusti, J. H. De Bruijne, C. A. Bailer-Jones, D. W. Evans, L. Eyer, F. Jansen, S. A. Klioner, U. Lammers, X. Luri, F. Mignard, C. Panem, D. Pourbaix, S. Randich, P. Sartoretti, H. I. Siddiqui, C. Soubiran, N. A. Walton, M. Cropper, R. Drimmel, D. Katz, M. G. Lattanzi, J. Bakker, C. Cacciari, J. Castañeda, L. Chaoul, N. Cheek, F. De Angeli, C. Fabricius, R. Guerra, B. Holl, E. Masana, R. Messineo, N. Mowlavi, K. Nienartowicz, P. Panuzzo, J. Portell, M. Riello, G. M. Seabroke, P. Tanga, F. Thévenin, G. Gracia-Abril, G. Comoretto, D. Teyssier, M. Garcia-Reinaldos, M. Altmann, R. Andrae, M. Audard, I. Bellas-Velidis, K. Benson, J. Berthier, R. Blomme, P. Burgess, G. Busso, B. Carry, A. Cellino, G. Clementini, M. Clotet, O. Creevey, M. Davidson, J. De Ridder, L. Delchambre, A. Dell'Oro, C. Ducourant, J. Fernández-Hernández, M. Fouesneau, Y. Frémat, L. Galluccio, M. García-Torres, J. González-Núñez, J. J. González-Vidal, E. Gosset, L. P. Guy, J. L. Halbwachs, N. C. Hambly, D. L. Harrison, J. Hernández, D. Hestroffer, S. T. Hodgkin, A. Hutton, G. Jasniewicz, A. Jean-Antoine-Piccolo, S. Jordan, A. J. Korn, A. Krone-Martins, A. C. Lanzafame, T. Lebzelter, W. Löffler, M. Manteiga, P. M. Marrese, J. M. Martín-Fleitas, A. Moitinho, A. Mora, K. Muinonen, J. Osinde, T. Pauwels, J. M. Petit, A. Recio-Blanco, P. J. Richards, L. Rimoldini, L. M. Sarro, C. Siopis, M. Smith, A. Sozzetti, M. Söveges, J. Torra, W. Van Reeven, A. Abreu Aramburu, U. Abbas, S. Accart, C. Aerts, G. Altavilla, M. A. Álvarez, R. Alvarez, J. Alves, R. I. Anderson, A. H. Andrei, E. Anglada Varela, E. Antiche, B. Arcay, T. L. Astraatmadja, N. Bach, S. G. Baker, L. Balaguer-Núñez, P. Balm, C. Barache, C. Barata, D. Barbato, F. Barblan, P. S. Barklem, D. Barrado, M. Barros, M. A. Barstow, S. Bartholomé Muñoz, J. L. Bassilana, U. Becciani, M. Bellazzini, A. Berihuete, S. Bertone, L. Bianchi, O. Bienaymé, S. Blanco-Cuaresma, T. Boch, C. Boeche, A. Bombrun, R. Borrachero, D. Bossini, S. Bouquillon, G. Bourda, A. Bragaglia, L. Bramante, A. Bressan, N. Brouillet, T. Brösemeister, E. Brugaletta, B. Bucciarelli, A. Burlacu, D. Busonero, A. G. Butkevich, R. Buzzi, E. Caffau, R. Cancelliere, G. Cannizzaro, T. Cantat-Gaudin, R. Carballo, T. Carlucci, J. M. Carrasco, L. Casamiquela, M. Castellani, A. Castro-Ginard, P. Charlot, A. Chiavassa, L. Chemin, G. Cocozza, G. Costigan, S. Cowell, F. Crifo, M. Crosta, C. Crowley, J. Cuypersy, C. Dafonte, Y. Damerdji, A. Dapergolas, P. David, M. David, P. De Laverny, F. De Luise, R. De March, D. De Martino, R. De Souza, A. De Torres, J. Debosscher, E. Del Pozo, M. Delbo, A. Delgado, H. E. Delgado, P. Di Matteo, S. Diakite, C. Diener, E. Distefano, C. Dolding, P. Drazinos, J. Durán, B. Edvardsson, H. Enke, K. Eriksson, P. Esquej, G. Eynard Bontemps, C. Fabre, M. Fabrizio, S. Faigler, A. J. Falcão, M. Farràs Casas, L. Federici, G. Fedorets, P. Fernique, F. Figueras, F. Filippi, K. Findeisen, A. Fonti, E. Fraile, M. Fraser, B. Frézouls, M. Gai, S. Galleti, D. Garabato, F. García-Sedano, A. Garofalo, N. Garralda, A. Gavel, P. Gavras, J. Gerssen, R. Geyer, P. Giacobbe, G. Gilmore, G. Giuffrida, S. Girona, F. Glass, M. Gomes, M. Granvik, A. Gueguen, A. Guerrier, J. Guiraud, R. Gutiérrez-Sánchez, W. Hofmann, G. Holland, H. E. Huckle, A. Hypki, V. Icardi, K. Janßen, G. Jevardat De Fombelle, P. G. Jonker, A. L. Juhász, F. Julbe, A. Karampelas, A. Kewley, J. Klar, A. Kochoska, R. Kohley,

K. Kolenberg, M. Kontizas, E. Kontizas, S. E. Koposov, G. Kordopatis, Z. Kostrzewa-Rutkowska, P. Koubsky, S. Lambert, A. F. Lanza, Y. Lasne, J. B. Lavigne, Y. Le Fustec, C. Le Poncin-Lafitte, Y. Lebreton, S. Leccia, N. Leclerc, I. Lecoeur-Taibi, H. Lenhardt, F. Leroux, S. Liao, E. Licata, H. E. Lindstrøm, T. A. Lister, E. Livanou, A. Lobel, M. López, S. Managau, R. G. Mann, G. Mantelet, O. Marchal, J. M. Marchant, M. Marconi, S. Marinoni, G. Marschalkó, D. J. Marshall, M. Martino, G. Marton, N. Mary, G. Matijevic, T. Mazeh, S. Messina, D. Michalik, N. R. Millar, D. Molina, R. Molinaro, L. Molnár, P. Montegriffo, R. Mor, R. Morbidelli, T. Morel, D. Morris, A. F. Mulone, T. Muraveva, I. Musella, G. Nelemans, L. Nicastro, L. Noval, W. O'Mullane, C. Ordénovic, D. Ordóñez-Blanco, P. Osborne, C. Pagani, I. Pagano, F. Pailler, H. Palacin, L. Palaversa, A. Panahi, M. Pawlak, A. M. Piersimoni, F. X. Pineau, E. Plachy, G. Plum, E. Poggio, E. Poujoulet, A. Prša, L. Pulone, E. Racero, S. Ragaini, N. Rambaux, M. Ramos-Lerate, S. Regibo, F. Riclet, V. Ripepi, A. Riva, A. Rivard, G. Rixon, T. Roegiers, M. Roelens, M. Romero-Gómez, N. Rowell, F. Royer, L. Ruiz-Dern, G. Sadowski, T. Sagristà Sellés, J. Sahlmann, J. Salgado, E. Salguero, N. Sanna, T. Santana-Ros, M. Sarasso, H. Savietto, M. Schultheis, E. Sciacca, M. Segol, D. Ségransan, J. C. Segovia, I. C. Shih, L. Siltala, A. F. Silva, R. L. Smart, K. W. Smith, E. Solano, F. Solitro, R. Sordo, S. Soria Nieto, J. Souchay, A. Spagna, F. Spoto, U. Stampa, I. A. Steele, H. Steidelmöller, C. A. Stephenson, H. Stoev, F. F. Suess, J. Surdej, L. Szabados, E. Szegedi-Elek, D. Tapiador, F. Taris, G. Tauran, M. B. Taylor, R. Teixeira, D. Terrett, P. Teyssandier, W. Thuillot, A. Titarenko, F. Torra Clotet, C. Turon, A. Ulla, E. Utrilla, S. Uzzi, M. Vaillant, G. Valentini, V. Valette, A. Van Elteren, E. Van Hemelryck, M. Van Leeuwen, M. Vaschetto, A. Vecchiato, Y. Viala, D. Vicente, S. Vogt, C. Von Essen, H. Voss, V. Votruba, S. Voutsinas, G. Walmsley, M. Weiler, O. Wertz, T. Wevems, L. Wyrzykowski, A. Yoldas, M. Žerjal, H. Ziaeepour, J. Zorec, S. Zschocke, S. Zucker, C. Zurbach, and T. Zwitter. Gaia Data Release 2: Kinematics of globular clusters and dwarf galaxies around the Milky Way. *Astronomy and Astrophysics*, 616:A12, aug 2018.

[104] M. Hirschmann, G. De Lucia, D. Wilman, S. Weinmann, A. Iovino, O. Cucciati, S. Zibetti, and Á. Villalobos. The influence of the environmental history on quenching star formation in a Λ cold dark matter universe. , 444(3):2938–2959, Nov. 2014.

[105] M. Hoeft, G. Yepes, S. Gottlöber, and V. Springel. Dwarf galaxies in voids: suppressing star formation with photoheating. , 371(1):401–414, Sept. 2006.

[106] E. P. Hubble. Extragalactic nebulae. , 64:321–369, Dec. 1926.

[107] J. D. Hunter. Matplotlib: A 2D Graphics Environment. *Computing in Science and Engineering*, 9(3):90–95, May 2007.

[108] R. A. Ibata, G. Gilmore, and M. J. Irwin. A dwarf satellite galaxy in Sagittarius. , 370(6486):194–196, July 1994.

[109] R. A. Ibata, N. G. Ibata, G. F. Lewis, N. F. Martin, A. Conn, P. Elahi, V. Arias, and N. Fernando. A thousand shadows of Andromeda: rotating planes of satellites in the Millennium-II cosmological simulation. *Astrophysical Journal Letters*, 784(1):L6, mar 2014.

[110] R. A. Ibata, G. F. Lewis, A. R. Conn, M. J. Irwin, A. W. McConnachie, S. C. Chapman, M. L. Collins, M. Fardal, A. M. N. Ferguson, N. G. Ibata, A. D. Mackey, N. F. Martin, J. Navarro, R. M. Rich, D. Valls-Gabaud, and L. M. Widrow. A Vast Thin Plane of Co-rotating Dwarf Galaxies Orbiting the Andromeda Galaxy. *Nature*, 493(7430):62–65, jan 2013.

[111] M. J. Irwin, V. Belokurov, N. W. Evans, E. V. Ryan-Weber, J. T. A. de Jong, S. Koposov, D. B. Zucker, S. T. Hodgkin, G. Gilmore, P. Prema, L. Hebb, A. Begum, M. Fellhauer, P. C. Hewett, R. C. Kennicutt, Jr., M. I. Wilkinson, D. M. Bramich, S. Vidrih, H.-W. Rix, T. C. Beers, J. C. Barentine, H. Brewington, M. Harvanek, J. Krzesinski, D. Long, A. Nitta, and S. A. Snedden. Discovery of an Unusual Dwarf Galaxy in the Outskirts of the Milky Way. , 656:L13–L16, Feb. 2007.

[112] M. N. Ishigaki, W. Aoki, N. Arimoto, and S. Okamoto. Chemical compositions of six metal-poor stars in the ultra-faint dwarf spheroidal galaxy Boötes I. , 562:A146, Feb. 2014.

[113] Ž. Ivezić, S. M. Kahn, J. A. Tyson, B. Abel, E. Acosta, R. Allsman, D. Alonso, Y. AlSayyad, S. F. Anderson, J. Andrew, and et al. LSST: From Science Drivers to Reference Design and Anticipated Data Products. , 873:111, Mar. 2019.

[114] M. Jeon, G. Besla, and V. Bromm. Connecting the first galaxies with ultra faint dwarfs in the Local Group: chemical signatures of Population III stars. *ArXiv e-prints*, Feb. 2017.

[115] P. Jethwa, D. Erkal, and V. Belokurov. A Magellanic origin of the DES dwarfs. , 461:2212–2233, Sept. 2016.

[116] P. Jethwa, D. Erkal, and V. Belokurov. The upper bound on the lowest mass halo. , 473(2):2060–2083, Jan. 2018.

[117] A. P. Ji, A. Frebel, and V. Bromm. Preserving chemical signatures of primordial star formation in the first low-mass stars. , 454(1):659–674, Nov. 2015.

[118] A. P. Ji, A. Frebel, R. Ezzeddine, and A. R. Casey. Chemical Diversity in the Ultra-faint Dwarf Galaxy Tucana II. , 832(1):L3, Nov. 2016.

[119] A. P. Ji, A. Frebel, J. D. Simon, and A. Chiti. Complete Element Abundances of Nine Stars in the r-process Galaxy Reticulum II. , 830(2):93, Oct. 2016.

[120] A. P. Ji, A. Frebel, J. D. Simon, and M. Geha. High-resolution Spectroscopy of Extremely Metal-poor Stars in the Least-evolved Galaxies: Bootes II. , 817(1):41, Jan. 2016.

[121] A. P. Ji, T. S. Li, J. D. Simon, J. Marshall, A. K. Vivas, A. B. Pace, K. Bechtol, A. Drlica-Wagner, S. E. Koposov, T. T. Hansen, S. Allam, R. A. Gruendl, M. D. Johnson, M. McNanna, N. E. D. Noël, D. L. Tucker, and A. R. Walker. Detailed Abundances in the Ultra-faint Magellanic Satellites Carina II and III. , 889(1):27, Jan. 2020.

[122] A. P. Ji, J. D. Simon, A. Frebel, K. A. Venn, and T. T. Hansen. Chemical Abundances in the Ultra-faint Dwarf Galaxies Grus I and Triangulum II: Neutron-capture Elements as a Defining Feature of the Faintest Dwarfs. , 870(2):83, Jan. 2019.

[123] E. Jones, T. Oliphant, P. Peterson, et al. SciPy: Open source scientific tools for Python, 2001. [Online; accessed 2015-08-25].

[124] P. R. Kafle, S. Sharma, G. F. Lewis, and J. Bland-Hawthorn. On the Shoulders of Giants: Properties of the Stellar Halo and the Milky Way Mass Distribution. , 794(1):59, Oct. 2014.

[125] N. Kallivayalil, L. V. Sales, P. Zivick, T. K. Fritz, A. Del Pino, S. T. Sohn, G. Besla, R. P. van der Marel, J. F. Navarro, and E. Sacchi. The Missing Satellites of the Magellanic Clouds? Gaia Proper Motions of the Recently Discovered Ultra-faint Galaxies. , 867(1):19, Nov. 2018.

[126] N. Kallivayalil, R. P. van der Marel, G. Besla, J. Anderson, and C. Alcock. Third-epoch Magellanic Cloud Proper Motions. I. Hubble Space Telescope/WFC3 Data and Orbit Implications. , 764(2):161, Feb. 2013.

[127] I. D. Karachentsev and O. G. Kashibadze. Masses of the local group and of the M81 group estimated from distortions in the local velocity field. *Astrophysics*, 49(1):3–18, Jan. 2006.

[128] T. Kelley, J. S. Bullock, S. Garrison-Kimmel, M. Boylan-Kolchin, M. S. Pawlowski, and A. S. Graus. Phat ELVIS: The inevitable effect of the Milky Way's disc on its dark matter subhaloes. , 487(3):4409–4423, Aug. 2019.

[129] D. D. Kelson. Optimal Techniques in Two-dimensional Spectroscopy: Background Subtraction for the 21st Century. , 115(808):688–699, June 2003.

[130] J. D. P. Kenney and J. S. Young. The effects of environment on the molecular and atomic gas properties of large Virgo cluster spirals. , 344:171–199, Sept. 1989.

[131] K. Kinemuchi, H. C. Harris, H. A. Smith, N. A. Silbermann, L. A. Snyder, A. P. Lacluyzé, and C. L. Clark. The variable stars of the Draco dwarf spheroidal galaxy: Revisited. *Astronomical Journal*, 136(5):1921–1939, nov 2008.

[132] E. N. Kirby, M. Boylan-Kolchin, J. G. Cohen, M. Geha, J. S. Bullock, and M. Kaplinghat. Segue 2: The Least Massive Galaxy. , 770:16, June 2013.

[133] E. N. Kirby, J. G. Cohen, J. D. Simon, and P. Guhathakurta. Triangulum II: Possibly a Very Dense Ultra-faint Dwarf Galaxy. , 814:L7, Nov. 2015.

[134] E. N. Kirby, J. G. Cohen, J. D. Simon, P. Guhathakurta, A. O. Thygesen, and G. E. Duggan. Triangulum II. Not Especially Dense After All. , 838:83, Apr. 2017.

[135] E. N. Kirby, J. D. Simon, and J. G. Cohen. Spectroscopic Confirmation of the Dwarf Galaxies Hydra II and Pisces II and the Globular Cluster Laevens 1. , 810:56, Sept. 2015.

[136] E. N. Kirby, J. D. Simon, M. Geha, P. Guhathakurta, and A. Frebel. Uncovering Extremely Metal-Poor Stars in the Milky Way's Ultrafaint Dwarf Spheroidal Satellite Galaxies. , 685(1):L43, Sept. 2008.

[137] A. Klypin, A. V. Kravtsov, O. Valenzuela, and F. Prada. Where Are the Missing Galactic Satellites? , 522(1):82–92, Sept. 1999.

[138] A. Koch, S. Feltzing, D. Adén, and F. Matteucci. Neutron-capture element deficiency of the Hercules dwarf spheroidal galaxy. , 554:A5, June 2013.

[139] A. Koch, A. McWilliam, E. K. Grebel, D. B. Zucker, and V. Belokurov. The Highly Unusual Chemical Composition of the Hercules Dwarf Spheroidal Galaxy. , 688(1):L13, Nov. 2008.

[140] E. Komatsu, K. M. Smith, J. Dunkley, C. L. Bennett, B. Gold, G. Hinshaw, N. Jarosik, D. Larson, M. R. Nolta, L. Page, D. N. Spergel, M. Halpern, R. S. Hill, A. Kogut, M. Limon, S. S. Meyer, N. Odegard, G. S. Tucker, J. L. Weiland, E. Wollack, and E. L. Wright. Seven-year Wilkinson Microwave Anisotropy Probe (WMAP) Observations: Cosmological Interpretation. , 192:18, Feb. 2011.

[141] S. E. Koposov, V. Belokurov, N. W. Evans, G. Gilmore, M. Gieles, M. J. Irwin, G. F. Lewis, M. Niederste-Ostholt, J. Peñarrubia, M. C. Smith, D. Bizyaev, E. Malanushenko, V. Malanushenko, D. P. Schneider, and R. F. G. Wyse. The Sagittarius Streams in the Southern Galactic Hemisphere. , 750(1):80, May 2012.

[142] S. E. Koposov, V. Belokurov, G. Torrealba, and N. W. Evans. Beasts of the Southern Wild: Discovery of Nine Ultra Faint Satellites in the Vicinity of the Magellanic Clouds. , 805:130, June 2015.

[143] S. E. Koposov, M. G. Walker, V. Belokurov, A. R. Casey, A. Geringer-Sameth, D. Mackey, G. Da Costa, D. Erkal, P. Jethwa, M. Mateo, E. W. Olszewski, and J. I. Bailey. Snake in the Clouds: A new nearby dwarf galaxy in the Magellanic bridge. *Monthly Notices of the Royal Astronomical Society*, 479(4):5343–5361, oct 2018.

[144] P. Kroupa, C. Theis, and C. M. Boily. The great disk of Milky-Way satellites and cosmological sub-structures. *Astronomy and Astrophysics*, 431(2):517–521, feb 2005.

[145] C. Kuehn, K. Kinemuchi, V. Ripepi, G. Clementini, M. Dall'Ora, L. Di Fabrizio, C. T. Rodgers, C. Greco, M. Marconi, I. Musella, H. A. Smith, M. Catelan, T. C. Beers, and B. J. Pritzl. Variable Stars in the Newly Discovered Milky Way Dwarf Spheroidal Satellite Canes Venatici I. *The Astrophysical Journal*, 674(2):L81–L84, sep 2007.

[146] B. P. M. Laevens, N. F. Martin, R. A. Ibata, H.-W. Rix, E. J. Bernard, E. F. Bell, B. Sesar, A. M. N. Ferguson, E. F. Schlafly, C. T. Slater, W. S. Burgett, K. C. Chambers, H. Flewelling, K. A. Hodapp, N. Kaiser, R.-P. Kudritzki, R. H. Lupton, E. A. Magnier, N. Metcalfe, J. S. Morgan, P. A. Price, J. L. Tonry, R. J. Wainscoat, and C. Waters. A New Faint Milky Way Satellite Discovered in the Pan-STARRS1 3π Survey. , 802:L18, Apr. 2015.

[147] D. Larson, J. Dunkley, G. Hinshaw, E. Komatsu, M. R. Nolta, C. L. Bennett, B. Gold, M. Halpern, R. S. Hill, N. Jarosik, A. Kogut, M. Limon, S. S. Meyer, N. Odegard, L. Page, K. M. Smith, D. N. Spergel, G. S. Tucker, J. L. Weiland, E. Wollack, and E. L. Wright. Seven-year Wilkinson Microwave Anisotropy Probe (WMAP) Observations: Power Spectra and WMAP-derived Parameters. , 192:16, Feb. 2011.

[148] R. B. Larson, B. M. Tinsley, and C. N. Caldwell. The evolution of disk galaxies and the origin of S0 galaxies. , 237:692–707, May 1980.

[149] D. R. Law, S. R. Majewski, and K. V. Johnston. Evidence for a Triaxial Milky Way Dark Matter Halo from the Sagittarius Stellar Tidal Stream. , 703(1):L67–L71, Sept. 2009.

[150] E. Ledinauskas and K. Zubovas. Reignited star formation in dwarf galaxies that were quenched during reionization. , 615:A64, July 2018.

[151] H. Lee, E. K. Grebel, and P. W. Hodge. Astrophysics Nebular abundances of nearby southern dwarf galaxies. *A&A*, 401:141–159, 2003.

[152] H. Li, F. Hammer, C. Babusiaux, M. S. Pawlowski, Y. Yang, F. Arenou, C. Du, and J. Wang. Gaia EDR3 proper motions of Milky Way dwarfs I: 3D Motions and Orbits. *arXiv e-prints*, page arXiv:2104.03974, Apr. 2021.

[153] T. S. Li, J. D. Simon, A. Drlica-Wagner, K. Bechtol, M. Y. Wang, J. García-Bellido, J. Frieman, J. L. Marshall, D. J. James, L. Strigari, A. B. Pace, E. Balbinot, Y. Zhang, T. M. C. Abbott, S. Allam, A. Benoit-Lévy, G. M. Bernstein, E. Bertin, D. Brooks, D. L. Burke, A. Carnero Rosell, M. Carrasco Kind, J. Carretero, C. E. Cunha, C. B. D'Andrea, L. N. da Costa, D. L. DePoy, S. Desai, H. T. Diehl, T. F. Eifler, B. Flaugher, D. A. Goldstein, D. Gruen, R. A. Gruendl, J. Gschwend, G. Gutierrez, E. Krause, K. Kuehn, H. Lin, M. A. G. Maia, M. March, F. Menanteau, R. Miquel, A. A. Plazas, A. K. Romer, E. Sanchez, B. Santiago, M. Schubnell, I. Sevilla-Noarbe, R. C. Smith, F. Sobreira, E. Suchyta, G. Tarle, D. Thomas, D. L. Tucker, A. R. Walker, R. H. Wechsler, W. Wester, B. Yanny, and (DES Collaboration. Farthest Neighbor: The Distant Milky Way Satellite Eridanus II. , 838:8, Mar. 2017.

[154] T. S. Li, J. D. Simon, A. B. Pace, G. Torrealba, K. Kuehn, A. Drlica-Wagner, K. Bechtol, A. K. Vivas, R. P. van der Marel, M. Wood, B. Yanny, V. Belokurov, P. Jethwa, D. B. Zucker, G. Lewis, R. Kron, D. L. Nidever, M. A. Sánchez-Conde, A. P. Ji, B. C. Conn, D. J. James, N. F. Martin, D. Martinez-Delgado, N. E. D. Noël, and MagLiteS Collaboration. Ships Passing in the Night: Spectroscopic Analysis of Two Ultra-faint Satellites in the Constellation Carina. , 857(2):145, Apr. 2018.

[155] Z.-Z. Li, Y.-Z. Qian, J. Han, T. S. Li, W. Wang, and Y. P. Jing. Constraining the Milky Way Mass Profile with Phase-space Distribution of Satellite Galaxies. , 894(1):10, May 2020.

[156] Z.-Z. Li, Y.-Z. Qian, J. Han, W. Wang, and Y. P. Jing. A Versatile and Accurate Method for Halo Mass Determination from Phase-space Distribution of Satellite Galaxies. , 886(1):69, Nov. 2019.

[157] L. Lindegren, J. Hernández, A. Bombrun, S. Klioner, U. Bastian, M. Ramos-Lerate, A. de Torres, H. Steidelmüller, C. Stephenson, D. Hobbs, U. Lammers, M. Biermann, R. Geyer, T. Hilger, D. Michalik, U. Stampa, P. J. McMillan, J. Castañeda, M. Clotet, G. Comoretto, M. Davidson, C. Fabricius, G. Gracia, N. C. Hambly, A. Hutton, A. Mora, J. Portell, F. van Leeuwen, U. Abbas, A. Abreu, M. Altmann, A. Andrei, E. Anglada, L. Balaguer-Núñez, C. Barache, U. Becciani, S. Bertone, L. Bianchi, S. Bouquillon, G. Bourda, T. Brüsemeister, B. Bucciarelli, D. Busonero, R. Buzzi, R. Cancelliere, T. Carlucci, P. Charlot, N. Cheek, M. Crosta, C. Crowley, J. de Bruijne, F. de Felice, R. Drimmel, P. Esquej, A. Fienga, E. Fraile,

M. Gai, N. Garralda, J. J. González-Vidal, R. Guerra, M. Hauser, W. Hofmann, B. Holl, S. Jordan, M. G. Lattanzi, H. Lenhardt, S. Liao, E. Licata, T. Lister, W. Löffler, J. Marchant, J. M. Martin-Fleitas, R. Messineo, F. Mignard, R. Morbidelli, E. Poggio, A. Riva, N. Rowell, E. Salguero, M. Sarasso, E. Sciacca, H. Siddiqui, R. L. Smart, A. Spagna, I. Steele, F. Taris, J. Torra, A. van Elteren, W. van Reeven, and A. Vecchiato. Gaia Data Release 2. The astrometric solution. , 616:A2, Aug. 2018.

[158] N. Lomb. Aboriginal astronomy – part one of the visions of space seminar in melbourne on thursday 22 september 2012, Dec 2018.

[159] N. Longeard, N. Martin, E. Starkenburg, R. A. Ibata, M. L. Collins, M. Geha, B. P. Laevens, R. Michael Rich, D. S. Aguado, A. Arentsen, R. G. Carlberg, P. Côté, V. Hill, P. Jablonka, J. I. Hernández, J. F. Navarro, R. Sánchez-Janssen, E. Tolstoy, K. A. Venn, and K. Youakim. Pristine dwarf galaxy survey - I. A detailed photometric and spectroscopic study of the very metal-poor Draco II satellite. *Monthly Notices of the Royal Astronomical Society*, 480(2):2609–2627, oct 2018.

[160] D. Lynden-Bell. Dwarf Galaxies and Globular Clusters in High Velocity Hydrogen Streams. *Monthly Notices of the Royal Astronomical Society*, 174(3):695–710, mar 1976.

[161] A. V. Macciò, X. Kang, F. Fontanot, R. S. Somerville, S. Koposov, and P. Monaco. Luminosity function and radial distribution of Milky Way satellites in a ΛCDM Universe. , 402(3):1995–2008, Mar. 2010.

[162] M. Magg, T. Hartwig, B. Agarwal, A. Frebel, S. C. O. Glover, B. F. Griffen, and R. S. Klessen. Predicting the locations of possible long-lived low-mass first stars: importance of satellite dwarf galaxies. , 473(4):5308–5323, Feb. 2018.

[163] H. B. Mann and D. R. Whitney. On a test of whether one of two random variables is stochastically larger than the other. *Ann. Math. Statist.*, 18(1):50–60, 03 1947.

[164] Y.-Y. Mao, M. Geha, R. H. Wechsler, B. Weiner, E. J. Tollerud, E. O. Nadler, and N. Kallivayalil. The SAGA Survey. II. Building a Statistical Sample of Satellite Systems around Milky Way-like Galaxies. *arXiv e-prints*, page arXiv:2008.12783, Aug. 2020.

[165] J. L. Marshall, T. Hansen, J. D. Simon, T. S. Li, R. A. Bernstein, K. Kuehn, A. B. Pace, D. L. DePoy, A. Palmese, A. Pieres, L. Strigari, A. Drlica-Wagner, K. Bechtol, C. Lidman, D. Q. Nagasawa, E. Bertin, D. Brooks, E. Buckley-Geer, D. L. Burke, A. Carnero Rosell, M. Carrasco Kind, J. Carretero, C. E. Cunha, C. B. D'Andrea, L. N. da Costa, J. De Vicente, S. Desai, P. Doel, T. F. Eifler, B. Flaugher, P. Fosalba, J. Frieman, J. García-Bellido, E. Gaztanaga, D. W. Gerdes, R. A. Gruendl, J. Gschwend, G. Gutierrez, W. G. Hartley, D. L. Hollowood, K. Honscheid, B. Hoyle, D. J. James, N. Kuropatkin, M. A. G. Maia, F. Menanteau, C. J. Miller, R. Miquel, A. A. Plazas, E. Sanchez, B. Santiago, V. Scarpine, M. Schubnell, S. Serrano, I. Sevilla-Noarbe, M. Smith, M. Soares-Santos, E. Suchyta, M. E. C. Swanson, G. Tarle, W. Wester, and DES Collaboration. Chemical Abundance Analysis of Tucana III, the Second r-process Enhanced Ultra-faint Dwarf Galaxy. , 882(2):177, Sept. 2019.

[166] N. F. Martin, R. A. Ibata, G. F. Lewis, A. McConnachie, A. Babul, N. F. Bate, E. Bernard, S. C. Chapman, M. M. L. Collins, A. R. Conn, D. Crnojević, M. A. Fardal, A. M. N. Ferguson, M. Irwin, A. D. Mackey, B. McMonigal, J. F. Navarro, and R. M. Rich. The PAndAS View of the Andromeda Satellite System. II. Detailed Properties of 23 M31 Dwarf Spheroidal Galaxies. , 833:167, Dec. 2016.

[167] N. F. Martin, A. W. McConnachie, M. Irwin, L. M. Widrow, A. M. N. Ferguson, R. A. Ibata, J. Dubinski, A. Babul, S. Chapman, M. Fardal, G. F. Lewis, J. Navarro, and R. M. Rich. PAndAS' CUBS: Discovery of Two New Dwarf Galaxies in the Surroundings of the Andromeda and Triangulum Galaxies. , 705:758–765, Nov. 2009.

[168] N. F. Martin, D. L. Nidever, G. Besla, K. Olsen, A. R. Walker, A. K. Vivas, R. A. Gruendl, C. C. Kaleida, R. R. Muñoz, R. D. Blum, A. Saha, B. C. Conn, E. F. Bell, Y.-H. Chu, M.-R. L. Cioni, T. J. L. de Boer, C. Gallart, S. Jin, A. Kunder, S. R. Majewski, D. Martinez-Delgado, A. Monachesi, M. Monelli, L. Monteagudo, N. E. D. Noël, E. W. Olszewski, G. S. Stringfellow, R. P. van der Marel, and D. Zaritsky. Hydra II: A Faint and Compact Milky Way Dwarf Galaxy Found in the Survey of the Magellanic Stellar History. , 804:L5, May 2015.

[169] N. F. Martin, D. R. Weisz, S. M. Albers, E. Bernard, M. L. M. Collins, A. E. Dolphin, A. M. N. Ferguson, R. A. Ibata, B. Laevens, G. F. Lewis, A. D. Mackey, A. McConnachie, R. M. Rich, and E. D. Skillman. A rogues gallery of Andromeda's dwarf galaxies I. A predominance of red horizontal branches. *ArXiv e-prints*, Apr. 2017.

[170] D. Massari and A. Helmi. With and without spectroscopy: Gaia DR2 proper motions of seven ultra-faint dwarf galaxies. , 620:A155, Dec. 2018.

[171] M. Mateo, J. I. Bailey, J. Crane, S. Shectman, I. Thompson, I. Roederer, B. Bigelow, and S. Gunnels. M2FS: the Michigan/Magellan Fiber System. In I. S. McLean, S. K. Ramsay, and H. Takami, editors, *Ground-based and Airborne Instrumentation for Astronomy IV*, volume 8446 of *Society of Photo-Optical Instrumentation Engineers (SPIE) Conference Series*, page 84464Y, Sept. 2012.

[172] A. W. McConnachie. The Observed Properties of Dwarf Galaxies in and around the Local Group. , 144:4, July 2012.

[173] A. W. McConnachie and K. A. Venn. Revised and New Proper Motions for Confirmed and Candidate Milky Way Dwarf Galaxies. , 160(3):124, Sept. 2020.

[174] A. W. McConnachie and K. A. Venn. Updated Proper Motions for Local Group Dwarf Galaxies Using Gaia Early Data Release 3. *Research Notes of the American Astronomical Society*, 4(12):229, Dec. 2020.

[175] A. McWilliam, G. Wallerstein, and M. Mottini. Chemistry of the Sagittarius Dwarf Galaxy: A Top-light Initial Mass Function, Outflows, and the R-process. , 778(2):149, Dec. 2013.

[176] G. E. Medina, R. R. Muñoz, A. K. Vivas, J. L. Carlin, F. Förster, J. Martínez, L. Galbany, S. González-Gaitán, M. Hamuy, T. de Jaeger, J. C. Maureira, and J. San Martín. Discovery of Distant RR Lyrae Stars in the Milky Way Using DECam. , 855(1):43, Mar. 2018.

[177] M. Metz, P. Kroupa, and N. I. Libeskind. The Orbital Poles of Milky Way Satellite Galaxies: A Rotationally Supported Disk of Satellites. *The Astrophysical Journal*, 680(1):287–294, jun 2008.

[178] G. Monari, B. Famaey, I. Carrillo, T. Piffl, M. Steinmetz, R. F. G. Wyse, F. Anders, C. Chiappini, and K. Janßen. The escape speed curve of the Galaxy obtained from Gaia DR2 implies a heavy Milky Way. , 616:L9, Aug. 2018.

[179] B. Moore. The dark matter crisis. In J. C. Wheeler and H. Martel, editors, *20th Texas Symposium on relativistic astrophysics*, volume 586 of *American Institute of Physics Conference Series*, pages 73–82, Oct. 2001.

[180] B. Moore, S. Ghigna, F. Governato, G. Lake, T. Quinn, J. Stadel, and P. Tozzi. Dark Matter Substructure within Galactic Halos. , 524(1):L19–L22, Oct. 1999.

[181] M. I. Moretti, M. Dall'ora, V. Ripepi, G. Clementini, L. D. Fabrizio, H. A. Smith, N. De Lee, C. Kuehn, M. Catelan, M. Marconi, I. Musella, T. C. Beers, and K. Kinemuchi. THE LEO IV DWARF SPHEROIDAL GALAXY: COLOR-MAGNITUDE DIAGRAM AND PULSATING STARS *. *The Astrophysical Journal*, 699:125–129, 2009.

[182] O. Müller, M. S. Pawlowski, H. Jerjen, and F. Lelli. A whirling plane of satellite galaxies around Centaurus A challenges cold dark matter cosmology. *Science*, 359(6375):534–537, feb 2018.

[183] I. Musella, V. Ripepi, G. Clementini, M. Dall'Ora, K. Kinemuchi, L. Di Fabrizio, C. Greco, M. Marconi, H. Smith, M. Radovich, and T. Beers. Pulsating Variable Stars in the Coma Berenices dwarf spheroidal galaxy. *Astrophysical Journal*, 695(1 PART 2):83–87, feb 2009.

[184] I. Musella, V. Ripepi, M. Marconi, G. Clementini, M. Dall'Ora, V. Scowcroft, M. I. Moretti, L. Di Fabrizio, C. Greco, G. Coppola, D. Bersier, M. Catelan, A. Grado, L. Limatola, H. A. Smith, and K. Kinemuchi. Stellar Archaeology in the Galactic halo with Ultra-Faint Dwarfs: VII. Hercules. *Astrophysical Journal*, 756(2):121, jun 2012.

[185] B. Mutlu-Pakdil, D. J. Sand, J. L. Carlin, K. Spekkens, N. Caldwell, D. Crnojević, A. K. Hughes, B. Willman, and D. Zaritsky. A Deeper Look at the New Milky Way Satellites: Sagittarius II, Reticulum II, Phoenix II, and Tucana III. , 863(1):25, Aug. 2018.

[186] D. Q. Nagasawa, J. L. Marshall, J. D. Simon, T. T. Hansen, T. S. Li, R. A. Bernstein, E. Balbinot, A. Drlica-Wagner, A. B. Pace, L. E. Strigari, C. M. Pellegrino, D. L. DePoy, N. B. Suntzeff, K. Bechtol, T. M. C. Abbott, F. B. Abdalla, S. Allam, J. Annis, A. Benoit-Lévy, E. Bertin, D. Brooks, A. Carnero Rosell, M. Carrasco Kind, J. Carretero, C. E. Cunha, C. B. D'Andrea, L. N. da Costa, C. Davis, S. Desai, P. Doel, T. F. Eifler, B. Flaugher, P. Fosalba, J. Frieman, J. García-Bellido, E. Gaztanaga, D. W. Gerdes, D. Gruen, R. A. Gruendl, J. Gschwend, G. Gutierrez, W. G. Hartley, K. Honscheid, D. J. James, T. Jeltema, E. Krause, K. Kuehn, S. Kuhlmann, N. Kuropatkin, M. March, R. Miquel, B. Nord, A. Roodman, E. Sanchez, B. Santiago, V. Scarpine, R. Schindler, M. Schubnell, I. Sevilla-Noarbe, M. Smith, R. C. Smith, M. Soares-Santos, F. Sobreira, E. Suchyta, G. Tarle, D. Thomas, D. L. Tucker, A. R. Walker, R. H. Wechsler, R. C. Wolf, and B. Yanny. Chemical Abundance

Analysis of Three α-Poor, Metal-Poor Stars in the Ultra-Faint Dwarf Galaxy Horologium I. *ArXiv e-prints*, Aug. 2017.

[187] E. National Academies of Sciences and Medicine. *Undergraduate Research Experiences for STEM Students: Successes, Challenges, and Opportunities*. The National Academies Press, Washington, DC, 2017.

[188] E. National Academies of Sciences and Medicine. *The Science of Effective Mentorship in STEMM*. The National Academies Press, Washington, DC, 2019.

[189] E. National Academies of Sciences and Medicine. *Promising Practices for Addressing the Underrepresentation of Women in Science, Engineering, and Medicine: Opening Doors*. The National Academies Press, Washington, DC, 2020.

[190] O. Newton, M. Cautun, A. Jenkins, C. S. Frenk, and J. C. Helly. The total satellite population of the Milky Way. , 479(3):2853–2870, Sept. 2018.

[191] J. E. Norris, T. C. Beers, and S. G. Ryan. Extremely Metal-poor Stars. VII. The Most Metal-poor Dwarf, CS 22876-032. , 540(1):456–467, Sept. 2000.

[192] J. E. Norris, R. F. G. Wyse, G. Gilmore, D. Yong, A. Frebel, M. I. Wilkinson, V. Belokurov, and D. B. Zucker. Chemical Enrichment in the Faintest Galaxies: The Carbon and Iron Abundance Spreads in the Boötes I Dwarf Spheroidal Galaxy and the Segue 1 System. , 723(2):1632–1650, Nov. 2010.

[193] J. Oñorbe, M. Boylan-Kolchin, J. S. Bullock, P. F. Hopkins, D. Kereš, C.-A. Faucher-Giguère, E. Quataert, and N. Murray. Forged in FIRE: cusps, cores and baryons in low-mass dwarf galaxies. , 454:2092–2106, Dec. 2015.

[194] P. Ocvirk, N. Gillet, P. R. Shapiro, D. Aubert, I. T. Iliev, R. Teyssier, G. Yepes, J.-H. Choi, D. Sullivan, A. Knebe, S. Gottlöber, A. D'Aloisio, H. Park, Y. Hoffman, and T. Stranex. Cosmic Dawn (CoDa): the First Radiation-Hydrodynamics Simulation of Reionization and Galaxy Formation in the Local Universe. , 463(2):1462–1485, Dec. 2016.

[195] S. Okamoto, N. Arimoto, Y. Yamada, and M. Onodera. A Suprime-Cam study of the stellar population of the Ursa Major I dwarf spheroidal galaxy. , 487:103–108, Aug. 2008.

[196] S. Okamoto, N. Arimoto, Y. Yamada, and M. Onodera. Stellar Populations and Structural Properties of Ultra Faint Dwarf Galaxies, Canes Venatici I, Boötes I, Canes Venatici II, and Leo IV. , 744:96, Jan. 2012.

[197] K. A. Oman, M. J. Hudson, and P. S. Behroozi. Disentangling satellite galaxy populations using orbit tracking in simulations. , 431:2307–2316, May 2013.

[198] A. B. Pace and T. S. Li. Proper motions of Milky Way Ultra-Faint satellites with ${Gaia}$ DR2 $$ DES DR1. *arXiv*, 875(1):77, jun 2018.

[199] E. Patel, G. Besla, K. Mandel, and S. T. Sohn. Estimating the Mass of the Milky Way Using the Ensemble of Classical Satellite Galaxies. , 857(2):78, Apr. 2018.

[200] E. Patel, N. Kallivayalil, N. Garavito-Camargo, G. Besla, D. R. Weisz, R. P. van der Marel, M. Boylan-Kolchin, M. S. Pawlowski, and F. A. Gómez. The Orbital Histories of Magellanic Satellites Using Gaia DR2 Proper Motions. *arXiv e-prints*, page arXiv:2001.01746, Jan. 2020.

[201] M. S. Pawlowski, B. Famaey, H. Jerjen, D. Merritt, P. Kroupa, J. Dabringhausen, F. Lüghausen, D. A. Forbes, G. Hensler, F. Hammer, M. Puech, S. Fouquet, H. Flores, and Y. Yang. Co-orbiting satellite galaxy structures are still in conflict with the distribution of primordial dwarf galaxies. *Monthly Notices of the Royal Astronomical Society*, 442(3):2362–2380, aug 2014.

[202] M. S. Pawlowski and P. Kroupa. The Milky Way's disc of classical satellite galaxies in light of Gaia DR2. *Monthly Notices of the Royal Astronomical Society*, 491(2):3042–3059, jan 2020.

[203] M. S. Pawlowski and S. S. McGaugh. Co-orbiting Planes of Sub-halos are Similarly Unlikely around Paired and Isolated Hosts. , 789(1):L24, July 2014.

[204] M. S. Pawlowski, J. Pflamm-Altenburg, and P. Kroupa. The VPOS: A vast polar structure of satellite galaxies, globular clusters and streams around the Milky Way. *Monthly Notices of the Royal Astronomical Society*, 423(2):1109–1126, jun 2012.

[205] F. Pedregosa, G. Varoquaux, A. Gramfort, V. Michel, B. Thirion, O. Grisel, M. Blondel, A. Müller, J. Nothman, G. Louppe, P. Prettenhofer, R. Weiss, V. Dubourg, J. Vanderplas, A. Passos, D. Cournapeau, M. Brucher, M. Perrot, and É. Duchesnay. Scikit-learn: Machine Learning in Python. *arXiv e-prints*, page arXiv:1201.0490, Jan. 2012.

[206] F. Pérez and B. E. Granger. IPython: a system for interactive scientific computing. *Computing in Science and Engineering*, 9(3):21–29, May 2007.

[207] C. Pfund. Studying the role and impact of mentoring on undergraduate research experience. *Paper commissioned for the committee on strengthening research experiences for undergraduate STEM students. National Academics of Sciences, Teaching, Engineering and Medicine Avaliable: http://nas. edu/STEM_undergraduate_Research_Mentoring. Accessed*, 30:07–18, 2016.

[208] S. Phelps, A. Nusser, and V. Desjacques. The Mass of the Milky Way and M31 Using the Method of Least Action. , 775(2):102, Oct. 2013.

[209] J. I. Phillips, C. Wheeler, M. C. Cooper, M. Boylan-Kolchin, J. S. Bullock, and E. Tollerud. The mass dependence of satellite quenching in Milky Way-like haloes. , 447:698–710, Feb. 2015.

[210] G. Pietrzy´nski, P. Pietrzy´nski, W. Gieren, O. Szewczyk, A. Walker, L. Rizzi, F. Bresolin, R.-P. Kudritzki, K. Nalewajko, J. Storm, M. Dall'ora, and V. Ivanov. THE ARAUCARIA PROJECT: THE DISTANCE TO THE SCULPTOR DWARF SPHEROIDAL GALAXY FROM INFRARED PHOTOMETRY OF RR LYRAE STARS *. *The Astronomical Journal*, 135, 2008.

[211] Planck Collaboration, P. A. R. Ade, N. Aghanim, M. Arnaud, M. Ashdown, J. Aumont, C. Baccigalupi, A. J. Banday, R. B. Barreiro, J. G. Bartlett, N. Bartolo, E. Battaner, R. Battye, K. Benabed, A. Benoît, A. Benoit-Lévy, J. P. Bernard, M. Bersanelli, P. Bielewicz, J. J. Bock, A. Bonaldi, L. Bonavera, J. R. Bond, J. Borrill, F. R. Bouchet, F. Boulanger, M. Bucher, C. Burigana, R. C. Butler, E. Calabrese, J. F. Cardoso, A. Catalano, A. Challinor, A. Chamballu, R. R. Chary, H. C. Chiang, J. Chluba, P. R. Christensen, S. Church, D. L. Clements, S. Colombi, L. P. L. Colombo, C. Combet, A. Coulais, B. P. Crill, A. Curto, F. Cuttaia, L. Danese, R. D. Davies, R. J. Davis, P. de Bernardis, A. de Rosa, G. de Zotti, J. Delabrouille, F. X. Désert, E. Di Valentino, C. Dickinson, J. M. Diego, K. Dolag, H. Dole, S. Donzelli, O. Doré, M. Douspis, A. Ducout, J. Dunkley, X. Dupac, G. Efstathiou, F. Elsner, T. A. Enßlin, H. K. Eriksen, M. Farhang, J. Fergusson, F. Finelli, O. Forni, M. Frailis, A. A. Fraisse, E. Franceschi, A. Frejsel, S. Galeotta, S. Galli, K. Ganga, C. Gauthier, M. Gerbino, T. Ghosh, M. Giard, Y. Giraud-Héraud, E. Giusarma, E. Gjerløw, J. González-Nuevo, K. M. Górski, S. Gratton, A. Gregorio, A. Gruppuso, J. E. Gudmundsson, J. Hamann, F. K. Hansen, D. Hanson, D. L. Harrison, G. Helou, S. Henrot-Versillé, C. Hernández-Monteagudo, D. Herranz, S. R. Hildebrand t, E. Hivon, M. Hobson, W. A. Holmes, A. Hornstrup, W. Hovest, Z. Huang, K. M. Huffenberger, G. Hurier, A. H. Jaffe, T. R. Jaffe, W. C. Jones, M. Juvela, E. Keihänen, R. Keskitalo, T. S. Kisner, R. Kneissl, J. Knoche, L. Knox, M. Kunz, H. Kurki-Suonio, G. Lagache, A. Lähteenmäki, J. M. Lamarre, A. Lasenby, M. Lattanzi, C. R. Lawrence, J. P. Leahy, R. Leonardi, J. Lesgourgues, F. Levrier, A. Lewis, M. Liguori, P. B. Lilje, M. Linden-Vørnle, M. López-Caniego, P. M. Lubin, J. F. Macías-Pérez, G. Maggio, D. Maino, N. Mandolesi, A. Mangilli, A. Marchini, M. Maris, P. G. Martin, M. Martinelli, E. Martínez-González, S. Masi, S. Matarrese, P. McGehee, P. R. Meinhold, A. Melchiorri, J. B. Melin, L. Mendes, A. Mennella, M. Migliaccio, M. Millea, S. Mitra, M. A. Miville-Deschênes, A. Moneti, L. Montier, G. Morgante, D. Mortlock, A. Moss, D. Munshi, J. A. Murphy, P. Naselsky, F. Nati, P. Natoli, C. B. Netterfield, H. U. Nørgaard-Nielsen, F. Noviello, D. Novikov, I. Novikov, C. A. Oxborrow, F. Paci, L. Pagano, F. Pajot, R. Paladini, D. Paoletti, B. Partridge, F. Pasian, G. Patanchon, T. J. Pearson, O. Perdereau, L. Perotto, F. Perrotta, V. Pettorino, F. Piacentini, M. Piat, E. Pierpaoli, D. Pietrobon, S. Plaszczynski, E. Pointecouteau, G. Polenta, L. Popa, G. W. Pratt, G. Prézeau, S. Prunet, J. L. Puget, J. P. Rachen, W. T. Reach, R. Rebolo, M. Reinecke, M. Remazeilles, C. Renault, A. Renzi, I. Ristorcelli, G. Rocha, C. Rosset, M. Rossetti, G. Roudier, B. Rouillé d'Orfeuil, M. Rowan-Robinson, J. A. Rubiño-Martín, B. Rusholme, N. Said, V. Salvatelli, L. Salvati, M. Sandri, D. Santos, M. Savelainen, G. Savini, D. Scott, M. D. Seiffert, P. Serra, E. P. S. Shellard, L. D. Spencer, M. Spinelli, V. Stolyarov, R. Stompor, R. Sudiwala, R. Sunyaev, D. Sutton, A. S. Suur-Uski, J. F. Sygnet, J. A. Tauber, L. Terenzi, L. Toffolatti, M. Tomasi, M. Tristram, T. Trombetti, M. Tucci, J. Tuovinen, M. Türler, G. Umana, L. Valenziano, J. Valiviita, F. Van Tent, P. Vielva, F. Villa, L. A. Wade, B. D. Wandelt, I. K. Wehus, M. White, S. D. M. White, A. Wilkinson, D. Yvon, A. Zacchei, and A. Zonca. Planck 2015 results. XIII. Cosmological parameters. , 594:A13, Sept. 2016.

[212] T. Quinn, N. Katz, and G. Efstathiou. Photoionization and the formation of dwarf galaxies. , 278:L49–L54, Feb. 1996.

[213] K. Rath, A. Peterfreund, and F. Bayliss. Programmatic mentoring: Providing mentoring as

a community, going beyond mentor/protégé pairs. *Understanding Interventions*, 9(2):6350, 2018.

[214] L. Rizzi, E. V. Held, I. Saviane, R. B. Tully, and M. Gullieuszik. The distance to the Fornax Dwarf Spheroidal Galaxy. *Monthly Notices of the Royal Astronomical Society*, 380(3):1255–1260, jul 2007.

[215] M. Rocha, A. H. G. Peter, and J. Bullock. Infall times for Milky Way satellites from their present-day kinematics. , 425:231–244, Sept. 2012.

[216] M. K. Rodriguez Wimberly, M. C. Cooper, D. C. Baxter, M. Boylan-Kolchin, J. S. Bullock, S. P. Fillingham, A. P. Ji, L. V. Sales, and J. D. Simon. Sizing from the Smallest Scales: The Mass of the Milky Way. *arXiv e-prints*, page arXiv:2109.00633, Sept. 2021.

[217] M. K. Rodriguez Wimberly, M. C. Cooper, S. P. Fillingham, M. Boylan-Kolchin, J. S. Bullock, and S. Garrison-Kimmel. The suppression of star formation on the smallest scales: what role does environment play? , 483(3):4031–4039, Mar. 2019.

[218] I. U. Roederer and E. N. Kirby. Detailed abundance analysis of the brightest star in Segue 2, the least massive galaxy. , 440(3):2665–2675, May 2014.

[219] I. U. Roederer, M. Mateo, I. Bailey, John I., Y. Song, E. F. Bell, J. D. Crane, S. Loebman, D. L. Nidever, E. W. Olszewski, S. A. Shectman, I. B. Thompson, M. Valluri, and M. G. Walker. Detailed Chemical Abundances in the r-process-rich Ultra-faint Dwarf Galaxy Reticulum 2. , 151(3):82, Mar. 2016.

[220] A. L. Rudolph. Cal-bridge: Creating pathways to the phd for underrepresented students in physics and astronomy. *Physics Today*, 72(10):50–57, 2019.

[221] A. L. Rudolph, K. Holley-Bockelmann, and J. Posselt. PhD bridge programmes as engines for access, diversity and inclusion. *Nature Astronomy*, 3:1080–1085, Dec. 2019.

[222] E. V. Ryan-Weber, A. Begum, T. Oosterloo, S. Pal, M. J. Irwin, V. Belokurov, N. W. Evans, and D. B. Zucker. The Local Group dwarf Leo T: HI on the brink of star formation. , 384:535–540, Feb. 2008.

[223] L. V. Sales, J. F. Navarro, N. Kallivayalil, and C. S. Frenk. Identifying true satellites of the Magellanic Clouds. , 465:1879–1888, Feb. 2017.

[224] J. Samuel, A. Wetzel, S. Chapman, E. Tollerud, P. F. Hopkins, M. Boylan-Kolchin, J. Bailin, and C.-A. Faucher-Giguère. Planes of satellites around Milky Way/M31-mass galaxies in the FIRE simulations and comparisons with the Local Group. *arXiv e-prints*, page arXiv:2010.08571, Oct. 2020.

[225] D. J. Sand, E. W. Olszewski, B. Willman, D. Zaritsky, A. Seth, J. Harris, S. Piatek, and A. Saha. The Star Formation History and Extended Structure of the Hercules Milky Way Satellite. , 704:898–914, Oct. 2009.

[226] D. J. Sand, A. Seth, E. W. Olszewski, B. Willman, D. Zaritsky, and N. Kallivayalil. A Deeper Look at Leo IV: Star Formation History and Extended Structure. , 718:530–542, July 2010.

[227] D. J. Sand, J. Strader, B. Willman, D. Zaritsky, B. McLeod, N. Caldwell, A. Seth, and E. Olszewski. Tidal Signatures in the Faintest Milky Way Satellites: The Detailed Properties of Leo V, Pisces II, and Canes Venatici II. , 756:79, Sept. 2012.

[228] I. M. E. Santos-Santos, A. Fattahi, L. V. Sales, and J. F. Navarro. Magellanic satellites in ΛCDM cosmological hydrodynamical simulations of the Local Group. , 504(3):4551–4567, July 2021.

[229] T. Sawala, P. Pihajoki, P. H. Johansson, C. S. Frenk, J. F. Navarro, K. A. Oman, and S. D. M. White. Shaken and stirred: the Milky Way's dark substructures. , 467:4383–4400, June 2017.

[230] S. Shao, M. Cautun, A. J. Deason, C. S. Frenk, and T. Theuns. Evolution of LMC/M33-mass dwarf galaxies in the EAGLE simulation. *Monthly Notices of the Royal Astronomical Society*, 479(1):284–296, sep 2018.

[231] S. Shao, M. Cautun, and C. S. Frenk. Evolution of galactic planes of satellites in the EAGLE simulation. *Monthly Notices of the Royal Astronomical Society*, 488(1):1166–1179, sep 2019.

[232] H. Shapley. A Stellar System of a New Type. *Harvard College Observatory Bulletin*, 908:1–11, Mar. 1938.

[233] H. Shapley. Two Stellar Systems of a New Kind. , 142(3598):715–716, Oct. 1938.

[234] J. D. Simon. Gaia Proper Motions and Orbits of the Ultra-faint Milky Way Satellites. , 863(1):89, Aug. 2018.

[235] J. D. Simon. The Faintest Dwarf Galaxies. , 57:375–415, Aug. 2019.

[236] J. D. Simon, A. Drlica-Wagner, T. S. Li, B. Nord, M. Geha, K. Bechtol, E. Balbinot, E. Buckley-Geer, H. Lin, J. Marshall, B. Santiago, L. Strigari, M. Wang, R. H. Wechsler, B. Yanny, T. Abbott, A. H. Bauer, G. M. Bernstein, E. Bertin, D. Brooks, D. L. Burke, D. Capozzi, A. Carnero Rosell, M. Carrasco Kind, C. B. D'Andrea, L. N. da Costa, D. L. DePoy, S. Desai, H. T. Diehl, S. Dodelson, C. E. Cunha, J. Estrada, A. E. Evrard, A. Fausti Neto, E. Fernandez, D. A. Finley, B. Flaugher, J. Frieman, E. Gaztanaga, D. Gerdes, D. Gruen, R. A. Gruendl, K. Honscheid, D. James, S. Kent, K. Kuehn, N. Kuropatkin, O. Lahav, M. A. G. Maia, M. March, P. Martini, C. J. Miller, R. Miquel, R. Ogando, A. K. Romer, A. Roodman, E. S. Rykoff, M. Sako, E. Sanchez, M. Schubnell, I. Sevilla, R. C. Smith, M. Soares-Santos, F. Sobreira, E. Suchyta, M. E. C. Swanson, G. Tarle, J. Thaler, D. Tucker, V. Vikram, A. R. Walker, W. Wester, and DES Collaboration. Stellar Kinematics and Metallicities in the Ultra-faint Dwarf Galaxy Reticulum II. , 808:95, July 2015.

[237] J. D. Simon, A. Frebel, A. McWilliam, E. N. Kirby, and I. B. Thompson. High-resolution Spectroscopy of Extremely Metal-poor Stars in the Least Evolved Galaxies: Leo IV. , 716(1):446–452, June 2010.

[238] J. D. Simon and M. Geha. The Kinematics of the Ultra-faint Milky Way Satellites: Solving the Missing Satellite Problem. , 670(1):313–331, Nov. 2007.

[239] J. D. Simon, T. S. Li, A. Drlica-Wagner, K. Bechtol, J. L. Marshall, D. J. James, M. Y. Wang, L. Strigari, E. Balbinot, K. Kuehn, A. R. Walker, T. M. C. Abbott, S. Allam, J. Annis, A. Benoit-Lévy, D. Brooks, E. Buckley-Geer, D. L. Burke, A. Carnero Rosell, M. Carrasco Kind, J. Carretero, C. E. Cunha, C. B. D'Andrea, L. N. da Costa, D. L. DePoy, S. Desai, P. Doel, E. Fernandez, B. Flaugher, J. Frieman, J. García-Bellido, E. Gaztanaga, D. A. Goldstein, D. Gruen, G. Gutierrez, N. Kuropatkin, M. A. G. Maia, P. Martini, F. Menanteau, C. J. Miller, R. Miquel, E. Neilsen, B. Nord, R. Ogando, A. A. Plazas, A. K. Romer, E. S. Rykoff, E. Sanchez, B. Santiago, V. Scarpine, M. Schubnell, I. Sevilla-Noarbe, R. C. Smith, F. Sobreira, E. Suchyta, M. E. C. Swanson, G. Tarle, L. Whiteway, B. Yanny, and DES Collaboration. Nearest Neighbor: The Low-mass Milky Way Satellite Tucana III. , 838:11, Mar. 2017.

[240] E. D. Skillman, M. Monelli, D. R. Weisz, S. L. Hidalgo, A. Aparicio, E. J. Bernard, M. Boylan-Kolchin, S. Cassisi, A. A. Cole, A. E. Dolphin, H. C. Ferguson, C. Gallart, M. J. Irwin, N. F. Martin, C. E. Martínez-Vázquez, L. Mayer, A. W. McConnachie, K. B. W. McQuinn, J. F. Navarro, and P. B. Stetson. The ISLAndS Project. II. The Lifetime Star Formation Histories of Six Andomeda dSphS. , 837:102, Mar. 2017.

[241] C. A. Sneden. *Carbon and Nitrogen Abundances in Metal-Poor Stars.* PhD thesis, THE UNIVERSITY OF TEXAS AT AUSTIN., Jan. 1973.

[242] J. S. Sobeck, R. P. Kraft, C. Sneden, G. W. Preston, J. J. Cowan, G. H. Smith, I. B. Thompson, S. A. Shectman, and G. S. Burley. The Abundances of Neutron-capture Species in the Very Metal-poor Globular Cluster M15: A Uniform Analysis of Red Giant Branch and Red Horizontal Branch Stars. , 141(6):175, June 2011.

[243] S. T. Sohn, G. Besla, R. P. van der Marel, M. Boylan-Kolchin, S. R. Majewski, and J. S. Bullock. The Space Motion of Leo I: Hubble Space Telescope Proper Motion and Implied Orbit. , 768(2):139, May 2013.

[244] J. M. Solanes, A. Manrique, C. García-Gómez, G. González-Casado, R. Giovanelli, and M. P. Haynes. The H I Content of Spirals. II. Gas Deficiency in Cluster Galaxies. , 548:97–113, Feb. 2001.

[245] R. S. Somerville. Can Photoionization Squelching Resolve the Substructure Crisis? , 572(1):L23–L26, June 2002.

[246] M. Spite, F. Spite, P. François, P. Bonifacio, E. Caffau, and S. Salvadori. A CEMP-no star in the ultra-faint dwarf galaxy Pisces II. , 617:A56, Sept. 2018.

[247] K. G. Stassun, A. Burger, and S. E. Lange. The fisk-vanderbilt masters-to-phd bridge program: A model for broadening participation of underrepresented groups in the physical sciences through effective partnerships with minority-serving institutions. *Journal of Geoscience Education*, 58(3):135–144, 2010.

[248] H. R. Tenenbaum, F. J. Crosby, and M. D. Gliner. Mentoring relationships in graduate school. *Journal of vocational behavior*, 59(3):326–341, 2001.

[249] L. S. Tenenbaum, M. K. Anderson, M. Jett, and D. L. Yourick. An innovative near-peer mentoring model for undergraduate and secondary students: Stem focus. *Innovative Higher Education*, 39(5):375–385, 2014.

[250] M. Teyssier, K. V. Johnston, and M. Kuhlen. Identifying Local Group field galaxies that have interacted with the Milky Way. , 426(3):1808–1818, Nov. 2012.

[251] A. A. Thoul and D. H. Weinberg. Hydrodynamic Simulations of Galaxy Formation. II. Photoionization and the Formation of Low-Mass Galaxies. , 465:608, July 1996.

[252] B. M. Tinsley. Stellar lifetimes and abundance ratios in chemical evolution. , 229:1046–1056, May 1979.

[253] E. J. Tollerud, M. Boylan-Kolchin, E. J. Barton, J. S. Bullock, and C. Q. Trinh. Small-scale Structure in the Sloan Digital Sky Survey and ΛCDM: Isolated $_*$ Galaxies with Bright Satellites. , 738(1):102, Sept. 2011.

[254] E. J. Tollerud, J. S. Bullock, L. E. Strigari, and B. Willman. Hundreds of Milky Way Satellites? Luminosity Bias in the Satellite Luminosity Function. , 688(1):277–289, Nov. 2008.

[255] E. J. Tollerud and J. E. G. Peek. Where Are All of the Gas-bearing Local Dwarf Galaxies? Quantifying Possible Impacts of Reionization. , 857(1):45, Apr. 2018.

[256] E. Tolstoy, K. A. Venn, M. Shetrone, F. Primas, V. Hill, A. Kaufer, and T. Szeifert. VLT/UVES Abundances in Four Nearby Dwarf Spheroidal Galaxies. II. Implications for Understanding Galaxy Evolution. , 125(2):707–726, Feb. 2003.

[257] G. Torrealba, V. Belokurov, S. E. Koposov, K. Bechtol, A. Drlica-Wagner, K. A. Olsen, A. K. Vivas, B. Yanny, P. Jethwa, A. R. Walker, T. S. Li, S. Allam, B. C. Conn, C. Gallart, R. A. Gruendl, D. J. James, M. D. Johnson, K. Kuehn, N. Kuropatkin, N. F. Martin, D. Martinez-Delgado, D. L. Nidever, N. E. Nöel, J. D. Simon, G. S. Stringfellow, and D. L. Tucker. Discovery of two neighbouring satellites in the Carina constellation with MagLiteS. *Monthly Notices of the Royal Astronomical Society*, 475(4):5085–5097, apr 2018.

[258] G. Torrealba, V. Belokurov, S. E. Koposov, T. S. Li, M. G. Walker, J. L. Sanders, A. Geringer-Sameth, D. B. Zucker, K. Kuehn, N. W. Evans, and W. Dehnen. The hidden giant: discovery of an enormous Galactic dwarf satellite in Gaia DR2. , 488(2):2743–2766, Sept. 2019.

[259] G. Torrealba, S. E. Koposov, V. Belokurov, and M. Irwin. The feeble giant: Discovery of a large and diffuse Milky Way dwarf galaxy in the constellation of Crater. *Monthly Notices of the Royal Astronomical Society*, 459(3):2370–2378, jul 2016.

[260] G. Torrealba, S. E. Koposov, V. Belokurov, M. Irwin, M. Collins, M. Spencer, R. Ibata, M. Mateo, A. Bonaca, and P. Jethwa. At the survey limits: discovery of the Aquarius 2 dwarf galaxy in the VST ATLAS and the SDSS data. *Monthly Notices of the Royal Astronomical Society*, 463(1):712–722, nov 2016.

[261] A. K. Vivas, K. Olsen, R. Blum, D. L. Nidever, A. R. Walker, N. F. Martin, G. Besla, C. Gallart, R. P. van der Marel, S. R. Majewski, C. C. Kaleida, R. R. Muñoz, A. Saha, B. C. Conn, and S. Jin. VARIABLE STARS IN THE FIELD OF THE HYDRA II ULTRA-FAINT DWARF GALAXY. *The Astronomical Journal*, 151(5):118, apr 2016.

[262] J. H. Waldeck, V. O. Orrego, T. G. Plax, and P. Kearney. Graduate student/faculty mentoring relationships: Who gets mentored, how it happens, and to what end. *Communication Quarterly*, 45(3):93–109, 1997.

[263] M. G. Walker, M. Mateo, E. W. Olszewski, S. Koposov, V. Belokurov, P. Jethwa, D. L. Nidever, V. Bonnivard, I. Bailey, John I., E. F. Bell, and S. R. Loebman. Magellan/M2FS Spectroscopy of Tucana 2 and Grus 1. , 819(1):53, Mar. 2016.

[264] S. M. Walsh, B. Willman, and H. Jerjen. The Invisibles: A Detection Algorithm to Trace the Faintest Milky Way Satellites. , 137(1):450–469, Jan. 2009.

[265] S. M. Walsh, B. Willman, D. Sand, J. Harris, A. Seth, D. Zaritsky, and H. Jerjen. Boötes II ReBoöted: An MMT/MegaCam Study of an Ultrafaint Milky Way Satellite. *The Astrophysical Journal*, 688(1):245–253, nov 2008.

[266] J. Wang, C. S. Frenk, and A. P. Cooper. The spatial distribution of galactic satellites in the Λ cold dark matter cosmology. , 429(2):1502–1513, Feb. 2013.

[267] L. L. Watkins, R. P. van der Marel, S. T. Sohn, and N. W. Evans. Evidence for an Intermediate-mass Milky Way from Gaia DR2 Halo Globular Cluster Motions. , 873(2):118, Mar. 2019.

[268] D. Webster, A. Frebel, and J. Bland-Hawthorn. Segue 1 – A Compressed Star Formation History before Reionization. , 818:80, Feb. 2016.

[269] C. Weidner, P. Kroupa, J. Pflamm-Altenburg, and A. Vazdekis. The galaxy-wide initial mass function of dwarf late-type to massive early-type galaxies. , 436(4):3309–3320, Dec. 2013.

[270] D. R. Weisz, A. E. Dolphin, E. D. Skillman, J. Holtzman, K. M. Gilbert, J. J. Dalcanton, and B. F. Williams. The Star Formation Histories of Local Group Dwarf Galaxies. I. Hubble Space Telescope/Wide Field Planetary Camera 2 Observations. , 789:147, July 2014.

[271] D. R. Weisz, A. E. Dolphin, E. D. Skillman, J. Holtzman, K. M. Gilbert, J. J. Dalcanton, and B. F. Williams. The Star Formation Histories of Local Group Dwarf Galaxies. II. Searching For Signatures of Reionization. , 789(2):148, July 2014.

[272] D. R. Weisz, S. E. Koposov, A. E. Dolphin, V. Belokurov, M. Gieles, M. L. Mateo, E. W. Olszewski, A. Sills, and M. G. Walker. A Hubble Space Telescope Study of the Enigmatic Milky Way Halo Globular Cluster Crater*. , 822(1):32, May 2016.

[273] D. R. Weisz, D. B. Zucker, A. E. Dolphin, N. F. Martin, J. T. A. de Jong, J. A. Holtzman, J. J. Dalcanton, K. M. Gilbert, B. F. Williams, E. F. Bell, V. Belokurov, and N. Wyn Evans. The Star Formation History of Leo T from Hubble Space Telescope Imaging. , 748:88, Apr. 2012.

[274] A. R. Wetzel, A. J. Deason, and S. Garrison-Kimmel. Satellite Dwarf Galaxies in a Hierarchical Universe: Infall Histories, Group Preprocessing, and Reionization. , 807:49, July 2015.

[275] A. R. Wetzel, J. L. Tinker, C. Conroy, and F. C. van den Bosch. Galaxy evolution in groups and clusters: satellite star formation histories and quenching time-scales in a hierarchical Universe. , 432:336–358, June 2013.

[276] A. R. Wetzel, E. J. Tollerud, and D. R. Weisz. Rapid Environmental Quenching of Satellite Dwarf Galaxies in the Local Group. , 808:L27, July 2015.

[277] C. Wheeler, J. Oñorbe, J. S. Bullock, M. Boylan-Kolchin, O. D. Elbert, S. Garrison-Kimmel, P. F. Hopkins, and D. Kereš. Sweating the small stuff: simulating dwarf galaxies, ultra-faint dwarf galaxies, and their own tiny satellites. , 453:1305–1316, Oct. 2015.

[278] C. Wheeler, J. I. Phillips, M. C. Cooper, M. Boylan-Kolchin, and J. S. Bullock. The surprising inefficiency of dwarf satellite quenching. , 442:1396–1404, Aug. 2014.

[279] B. Willman, M. R. Blanton, A. A. West, J. J. Dalcanton, D. W. Hogg, D. P. Schneider, N. Wherry, B. Yanny, and J. Brinkmann. A New Milky Way Companion: Unusual Globular Cluster or Extreme Dwarf Satellite? , 129:2692–2700, June 2005.

[280] B. Willman, J. J. Dalcanton, D. Martinez-Delgado, A. A. West, M. R. Blanton, D. W. Hogg, J. C. Barentine, H. J. Brewington, M. Harvanek, S. J. Kleinman, J. Krzesinski, D. Long, E. H. Neilsen, Jr., A. Nitta, and S. A. Snedden. A New Milky Way Dwarf Galaxy in Ursa Major. , 626:L85–L88, June 2005.

[281] B. Willman, F. Governato, J. J. Dalcanton, D. Reed, and T. Quinn. The observed and predicted spatial distribution of Milky Way satellite galaxies. , 353(2):639–646, Sept. 2004.

[282] J. H. Wise, V. G. Demchenko, M. T. Halicek, M. L. Norman, M. J. Turk, T. Abel, and B. D. Smith. The birth of a galaxy - III. Propelling reionization with the faintest galaxies. , 442(3):2560–2579, Aug. 2014.

[283] A. C. Wright, A. M. Brooks, D. R. Weisz, and C. R. Christensen. Reignition of star formation in dwarf galaxies. , 482(1):1176–1189, Jan. 2019.

[284] B. Yniguez, S. Garrison-Kimmel, M. Boylan-Kolchin, and J. S. Bullock. On the stark difference in satellite distributions around the Milky Way and Andromeda. , 439(1):73–82, Mar. 2014.

[285] D. G. York et al. The Sloan Digital Sky Survey: Technical Summary. , 120:1579–1587, Sept. 2000.

[286] C. Yozin and K. Bekki. Local ultra faint dwarves as a product of Galactic processing during a Magellanic group infall. , 453:2302–2307, Nov. 2015.

[287] D. B. Zucker, V. Belokurov, N. W. Evans, J. T. Kleyna, M. J. Irwin, M. I. Wilkinson, M. Fellhauer, D. M. Bramich, G. Gilmore, H. J. Newberg, B. Yanny, J. A. Smith, P. C. Hewett, E. F. Bell, H.-W. Rix, O. Y. Gnedin, S. Vidrih, R. F. G. Wyse, B. Willman, E. K. Grebel, D. P. Schneider, T. C. Beers, A. Y. Kniazev, J. C. Barentine, H. Brewington, J. Brinkmann, M. Harvanek, S. J. Kleinman, J. Krzesinski, D. Long, A. Nitta, and S. A. Snedden. A Curious Milky Way Satellite in Ursa Major. , 650:L41–L44, Oct. 2006.

[288] D. B. Zucker, V. Belokurov, N. W. Evans, M. I. Wilkinson, M. J. Irwin, T. Sivarani, S. Hodgkin, D. M. Bramich, J. M. Irwin, G. Gilmore, B. Willman, S. Vidrih, M. Fellhauer, P. C. Hewett, T. C. Beers, E. F. Bell, E. K. Grebel, D. P. Schneider, H. J. Newberg, R. F. G. Wyse, C. M. Rockosi, B. Yanny, R. Lupton, J. A. Smith, J. C. Barentine, H. Brewington, J. Brinkmann, M. Harvanek, S. J. Kleinman, J. Krzesinski, D. Long, A. Nitta, and S. A. Snedden. A New Milky Way Dwarf Satellite in Canes Venatici. , 643:L103–L106, June 2006.